A Review on Removal of Elemental Mercury from Flue Gas Using Advanced Oxidation Process: Chemistry and Process

Yangxian Liu*, [a] and Yusuf G. Adewuyi*, [b]

a. School of Energy and Power Engineering, Jiangsu University, Zhenjiang, Jiangsu 212013, China

b. Chemical, Biological and Bioengineering Department, North Carolina Agricultural and Technical State University, Greensboro, North Carolina 27411, USA

*Corresponding authors. Tel.: +86 51188743612; fax: +86 51188745824. E-mail: liuyx1984@126.com (Y.X. Liu).

Tel.: (336) 334-7564 or (336) 285 3651. Fax: (336) 334-7904. E-mail: adewuyi@ncat.edu. (Y.G. Adewuyi)

ABSTRACT: Mercury emission from combustion sources has become a great public concern due to its hazards for human health and ecosystem. Although a large number of Hg^0 removal technologies already have been developed, none of them can obtain large-scale applications due to various technical and economic issues. Therefore, more efforts are needed to develop cost-effective Hg^0 removal technologies. Advanced oxidation technologies (AOTs) are defined as those technologies that can generate mainly the hydroxyl radical (·OH) with high oxidation potential and other reactive oxygen species including superoxide anion radical ($O_2^{\cdot-}$), hydrogen peroxide (H_2O_2) and singlet oxygen, by various environmentally benign physical or chemical processes. In the past two decades, AOTs have gained an extensive attention research and successful applications in water treatment and soil remediation, as well as in flue gas purification for multipollutant treatment. In recent years, an increasing attention has been paid to the removal of Hg^0 in flue gas using AOTs due to the excellent prospects of this technology. To date, the four main AOTs for removing Hg^0 in flue gas include plasma AOTs, TiO_2 photocatalytic AOTs, photochemical AOTs and activated oxidant AOTs. While these AOTs have shown excellent prospects for removing Hg^0 in flue gas, a number of technical issues need to be resolved before they are amenable

to industrial applications. This article provides the first comprehensive review of the progress and recent developments of these four AOTs for removing Hg^0 in flue gas, with emphasis on the chemistry and processes involved. The effects of the main flue gas components and process parameters on Hg^0 removal using these AOTs are summarized. The reaction products, mechanism, kinetics, reactor types and process flow systems, and impacts on of Hg^0 removal are also comprehensively reviewed, with insights into the challenges for large-scale applications. This review is intended to advance our understanding and outline directions for future developments of this research field.

Keywords: Hg^0 removal; advanced oxidation technologies (AOTs); plasma; TiO_2 photocatalytic; photochemical; activated oxidant

Contents

1. Introduction

1.1 An overview of technologies for Hg^0 removal from flue gas

Mercury emission from combustion sources such as coal-fired boilers, municipal waste combustors and medical waste incinerators, which accounts for more than 90% of all anthropogenic mercury emissions, has become a great public concern due to its high toxicity, environmental persistency, bioaccumulation and detrimental effects on human health and ecosystem (Yang et al.2011; Stolle et al. 2014; Reddy et al.2012). Depending on combustion conditions and flue gas chemistry, mercury exists in three forms in typical flue gas: elemental mercury (Hg^0), oxidized mercury (Hg^{2+}) and particulate-bound mercury (Hg^p) (Cheng et al.2014; Chi et al. 2009). Both Hg^{2+} and Hg^p are easy to remove from flue gas using conventional air pollution control devices.

For example, Hg^{2+} can be removed with high efficiency using existing wet flue gas desulfurization (WFGD) equipments due to its high water-solubility. Hg^p can be easily captured from flue gas, along with fly ash particles, in electrostatic precipitators (ESPs) and/or baghouses (Rodríguez-Pérez et al. 2013; Wang et al. 2014a). However, Hg^0 is very difficult to remove from flue gas by existing air pollution control devices (APCD) because of its high volatility at room temperature and low solubility in water (Rodríguez-Pérez et al. 2013; Wang et al. 2014a). Therefore, developing effective Hg^0 control methods is currently an important area of research focus and need in the field of energy and environmental protection. Over the past few decades, a number of both dry and wet Hg^0 control technologies, including adsorption removal (Yang et al. 2007; Zheng et al. 2012; Chiu et al. 2014; Klasson et al. 2014; Tan et al. 2012; Zhao et al. 2010; Fuente-Cuesta et al. 2012; De et al. 2013; Than et al. 2011; Rupp et al. 2014; Shu et al. 2011; Ren et al. 2006; Shen et al. 2014), catalytic oxidation (Gao et al. 2013; Xu et al. 2014; Zhao et al. 2014a; Wiatros-Motyka et al. 2013; Li et al. 2013; Zhang et al. 2014a; Chen et al. 2014; Hou et al. 2014; Li et al. 2014; Xu et al. 2015; Zhang et al. 2014b), advanced oxidation (An et al. 2014a; Wang et al. 2010; Shan et al. 2009; Zhou et al. 2011; Tan et al. 2010; Fang et al. 2013; Granite et al. 2002; Liu et al. 2014a; Xu et al. 2008; Liu et al. 2014b; Lu et al. 2007; Zhao et al. 2014a; Zhao et al. 2014b; Martinez et al. 2007) and traditional chemical oxidation technologies (Wang et al. 2007; Fang et al. 2012; Hutson et al. 2008; Zhao et al. 2013; Zhao et al. 2013; Barnea et al. 2013; Cheng et al. 2014; Liu et al. 2010a; Stergaršek et al. 2010; Vaart et al. 2011), have been developed. The detailed classification of Hg^0 removal technologies from flue gas is further described in Figure 1.

Adsorption removal technologies can effectively remove Hg^0 in flue gas by initially converting Hg^0 to Hg^p, which is subsequently captured by existing ESPs and/or baghouses (Yang et al. 2007). At present, the exploration and development of high performance and inexpensive adsorbents are the key research initiatives and directions in this field (Yang et al. 2007). As shown in Figure 1, a large number of adsorbents, including modified and

111 supported adsorbents have been developed and reported in the literature to remove Hg^0 in flue gas in the past two
112 decades (Yang et al. 2007; Zheng et al. 2012; Chiu et al. 2014; Klasson et al. 2014; Tan et al. 2012; Zhao et al.
113 2010; Fuente-Cuesta et al. 2012; De et al. 2013; Tan et al. 2011; Rupp et al. 2014; Shu et al. 2013; Ren et al. 2006;
114 Shen et al. 2014). Some researchers have also published several detailed and in-depth reviews on the subject. For
115 example, Yang et al. 2007, Reddy et al.2012 and Liu et al.2008 reviewed the recent development of adsorbents for
116 capturing mercury in coal-fired boiler flue gas. Hower et al. 2010, Ahmaruzzaman et al. 2010 and Wilcox et
117 al.2012 reported mercury capture by fly ash in coal-fired power plants. Pavlish et al.2003 published an overview
118 and reported on recent developments in mercury control technologies for coal-fired power plants. Zheng et al.
119 2012 provided a general review of mercury removal technologies from flue gas from cement production
120 processes.

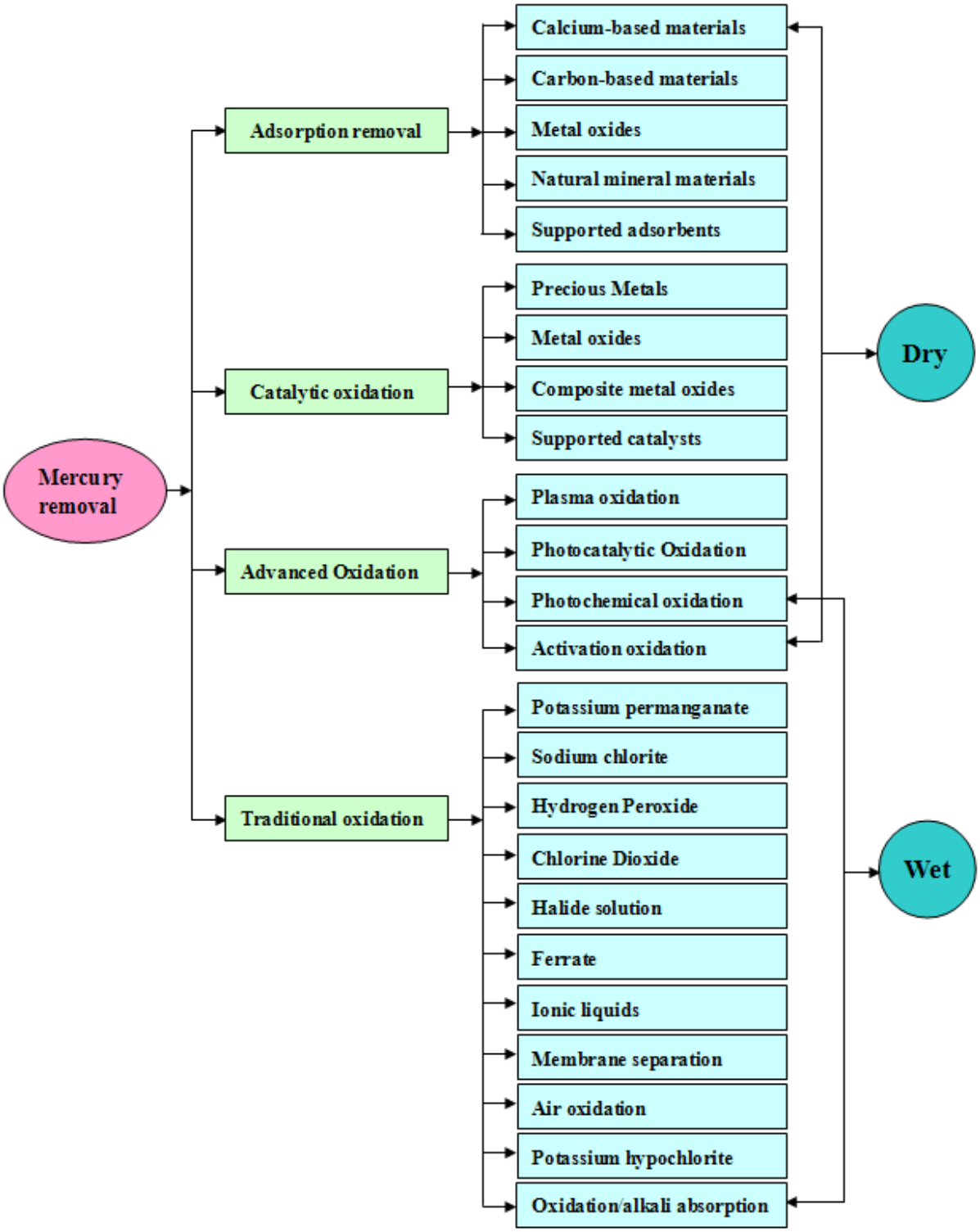

Figure 1. The detailed classification of Hg^0 from flue gas removal technology

In recent years, catalytic oxidation removal technologies of Hg^0 from flue gas has also received a great deal of attention because it can take full advantage of existing selective catalytic reduction (SCR) denitration catalysts

126 to oxidize Hg^0 to Hg^{2+} in a simplified and low cost process (Gao et al. 2013; Xu et al. 2014). Work in this area
127 currently focuses on the development of cost-effective and highly reliable catalysts. A large number of mercury
128 oxidation catalysts, mainly including precious metals, metal oxides, composite metal oxides and their modified or
129 supported catalysts, had been developed to remove Hg^0 in flue gas (Gao et al. 2013; Xu et al. 2014; Zhao et al.
130 2014a; Wiatros-Motyka et al. 2013; Li et al. 2013; Zhang et al. 2014a; Chen et al. 2014; Hou et al. 2014; Li et al.
131 2014; Xu et al. 2015), and are reported in recent comprehensive reviews. Wilcox et al.2012, Dranga et al.2012,
132 Reddy et al.2012 and Presto et al.2006 respectively reviewed the new developments in Hg^0 oxidation catalysts.
133 Adsorption and catalytic oxidation technologies have shown good prospects in laboratory studies, but the catalysts
134 still require further improvements for use in future industrial applications due to their low stability and reliability,
135 lack of effective regeneration method, and high costs of application. In addition, traditional chemical oxidation
136 and separation methods such as $KMnO_4$, $NaClO_2$, O_3, ClO_2, KClO, ferrate; and ionic liquids, air, halide and
137 membrane separations have been used to remove gaseous Hg^0 in various reactor types (Wang et al. 2007; Fang et
138 al. 2012; Hutson et al. 2008; Zhao et a.l 2013a; Zhao et a.l 2013b; Barnea et al. 2013; Cheng et al. 2014; Liu et al.
139 2013; Stergaršek et al. 2010; Vaart et al. 2011). Besides, some oxidants are also added to common calcium-based
140 and urea-based wet flue gas desulfurization (WFGD) equipment to enhance removal of Hg^0 in flue gas (Presto et
141 al. 2006; Fang et al. 2014; Zhong 1008; Zhao et al. 2008). However, these technologies are still unable to obtain
142 commercial applications due to a variety of unsolved problems such as high cost, secondary pollution of products
143 or low removal efficiency (Liu et al. 2014a; Liu et al. 2014c). Therefore, more research efforts are needed to
144 develop more cost-effective technologies for Hg^0 removal from flue gas, which are capable of large-scale
145 applications.

146 **1.2 An overview of advanced oxidation technologies (AOTs)**

147 Advanced oxidation technologies (AOTs) are defined as those technologies that can generate hydroxyl

148 radicals (·OH) by various physical or chemical methods (Liu et al. 2011a). The redox potentials of some common
149 oxidants under acidic conditions are summarized in Table 1. It can be seen from Table 1 that ·OH is a very strong
150 oxidant (second only to fluorine) in nature and therefore, capable of almost complete oxidation of most pollutants
151 in nature (Liu et al. 2011a; Serpone et al. 2010; Josepha et al. 2009; Ayoub et al. 2010; Feng et al. 2013; Sharma
152 et al. 2012). Hence, the oxidation reaction processes induced by ·OH has almost no secondary pollutants since the
153 final decomposition products of ·OH are O_2 and H_2O (Liu et al. 2011a; Serpone et al. 2010; Josepha et al. 2009;
154 Ayoub et al. 2010; Feng et al. 2013; Sharma et al. 2012).

155 **Table 1.** Redox potentials of several common oxidants under acidic conditions (Liu et al. 2011a; Portland et al.
156 1934).

Category	F_2	·OH	$SO_4{\cdot}^-$	$\cdot O_2^-$	K_2FeO_4	$K_2S_2O_8$	O_3	·O	H_2O_2
Potential (V)	2.87	2.80	2.67	2.21	2.20	2.08	2.08	2.05	1.76
Category	$KMnO_4$	$NaClO_2$	$HO_2{\cdot}$	NaClO	$NaClO_3$	Cl_2	KCr_2O_7	O_2	ClO_2
Potential (V)	1.70	1.64	1.51	1.49	1.47	1.36	1.36	1.23	1.19

157

158 In the past few decades, AOTs first have gained a very wide research and application in the field of water
159 treatment and soil remediation, and a large number of related reviews have been published (Serpone et al. 2010;
160 Josepha et al. 2009; Ayoub et al. 2010; Feng et al. 2013; Sharma et al. 2012; Oller et al. 2011; Antonopoulou et al.
161 2014; Vallejo et al. 2015; Asghar et al. 2014; Ribeiroa et al. 2015; Bokare et al. 2014; Tisa et al. 2014; Bagal et al.
162 2014; Matilainena et al. 2010; Babuponnusami et al. 2014; Gultekin et al. 2007; Klavarioti et al. 2009; Sillanpääa
163 et al. 2011; Wols et al. 2012). Some common AOTs are summarized in Figure 2. Furthermore, with growing air
164 pollution concerns, an increasing attention also has been paid to flue gas purification technologies using AOTs,
165 which are capable of individual or simultaneous removals of SO_2, NO_x, Hg^0, H_2S and VOCs from flue gas (An et
166 al. 2014a; Wang et al. 2010; Tan et al. 2010; Fang et al. 2013; Granite et al. 2002; Liu et al. 2014a; Xu et al. 2008;

Liu et al. 2014b; Zhao et al. 2014d; Martinez et al. 2007; Kim et al. 2004; Chen et al. 2009; Liu et al. 2014a; Liu et al. 2010a; Yu et al. 2013; Xu et al. 2014; Huang et al. 2012). Recent reports (An et al. 2014a; Wang et al. 2010; Tan et al. 2010; Fang et al. 2013; Granite et al. 2002; Liu et al. 2014a; Zhao et al. 2014b; Martinez et al. 2007; Wang et al. 2007; Liu et al. 2010) have demonstrated that AOTs have excellent prospects for multi-pollutant flue gas cleanup. Existing AOTs with great prospects for removing Hg^0 in flue gas fall into four main catagories: (1) Plasma AOTs; (2) TiO_2 photocatalytic AOTs; (3) Photochemical AOTs; and (4) Activated oxidant AOTs (An et al. 2014a; Wang et al. 2010; Tan et al. 2010; Fang et al. 2013; Granite et al. 2002; Liu et al. 2014a; Liu et al. 2014b; Lu et al. 2007; Zhao et al. 2014a; Zhao et al. 2014b; Martinez et al. 2007; Wang et al. 2007). While these AOTs have shown excellent prospects for removing Hg^0 in flue gas, there are still a number of technical issues to be resolved before they are ready for large-scale industrial applications. This article provides the first comprehensive review of the major research progress on these four AOTs for removing Hg^0 in flue gas, and the effects of major flue gas components, and process parameters on Hg^0 removal are summarized. The reaction products and mechanism, kinetics, reactor types and process flow of Hg^0 removal using these four AOTs are comprehensively reviewed and discussed. Finally, some unresolved issues and challenges, and future research directions of Hg^0 removal using the AOTs of interest are addressed. This review should provide useful insights and serve as a meaningful guidance for the future developments of these technologies.

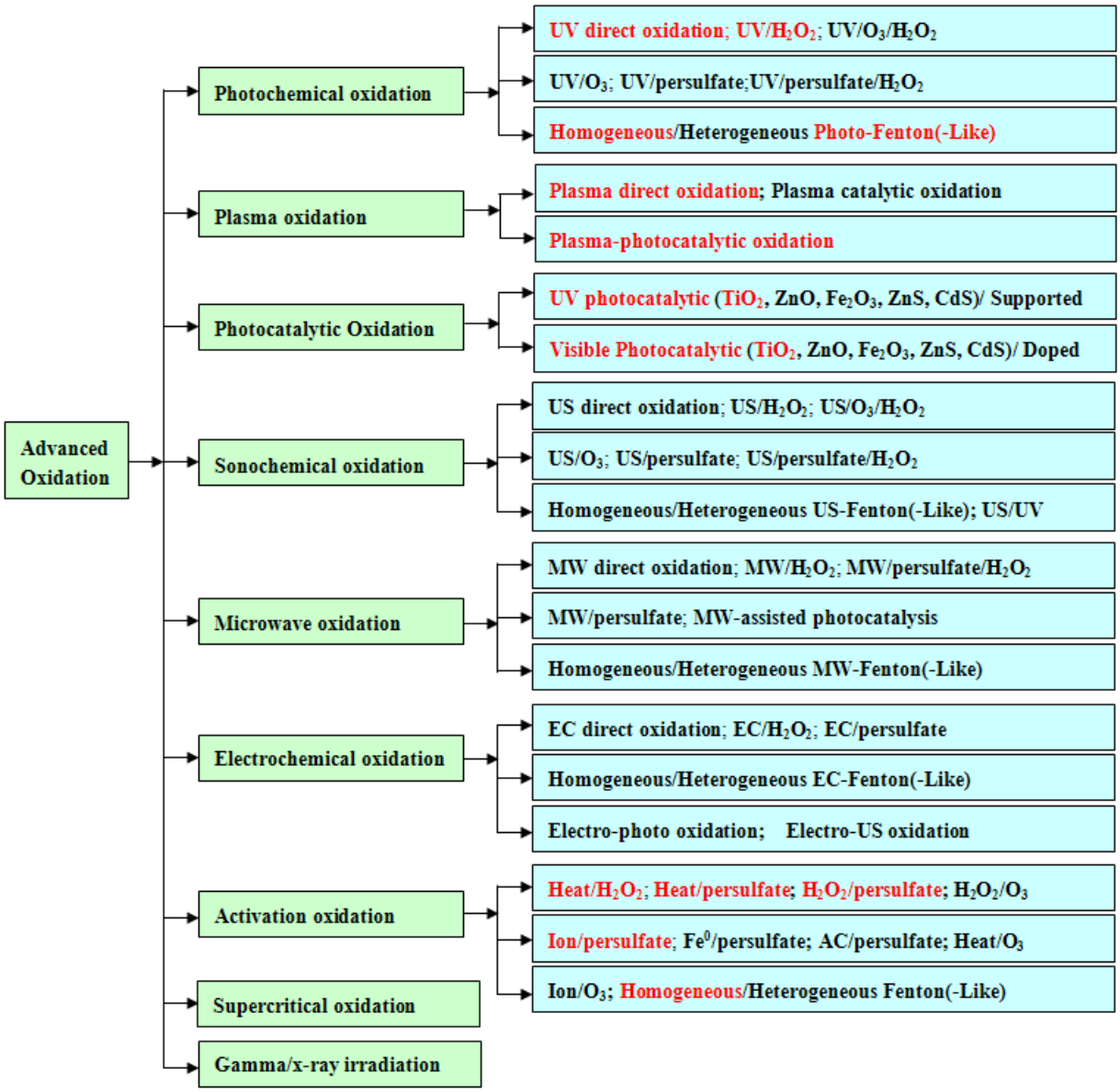

Figure 2. Common AOTs in the field of water treatment, soil remediation and flue gas purification

2. Plasma AOTs for removing Hg^0 in flue gas

2.1 Overview of plasma AOTs for removing Hg^0 in flue gas

Plasma is an ionized gas which is in its fourth state unlike the other three states of matters (solid, liquid and gas). It consists of electrons, ions, radicals and neutrals which are in fundamental and excited states. From a macroscopic point of view, plasma is electrically neutral (Bogaerts et al. 2002; Chang et al. 2002). Plasma can be artificially generated by several methods such as gas discharge, ray irradiation, photoionization and thermal

ionization. In these methods, gas discharge is recognized as the most effective way, and has been widely used in scientific research and industrial applications (Bogaerts et al. 2002; Chang et al. 2002). Depending on the differences in the generating methods, plasma can of several types, but generally can be divided into thermal equilibrium state plasma (or high-temperature plasma) and non-thermal equilibrium state plasma (or low-temperature plasma) based on the state of thermodynamic equilibrium (or particle temperature) (Bogaerts et al. 2002; Chang et al. 2002; Tendero et al. 2006; Kogelschatz et al. 2004; McAdams et al. 2001; Li et al. 2014a). Of the two, non-thermal equilibrium state plasma (NTP) can be further divided into two types consisting of thermal plasma (or quasi-equilibrium plasma) and cold plasma (or non quasi-equilibrium plasma) (Bogaerts et al. 2002; Chang et al. 2002; Tendero et al. 2006; Kogelschatz et al. 2004; McAdams et al. 2001; Li et al. 2014a). Specific classification of plasma technology is further summarized in Figure 3.

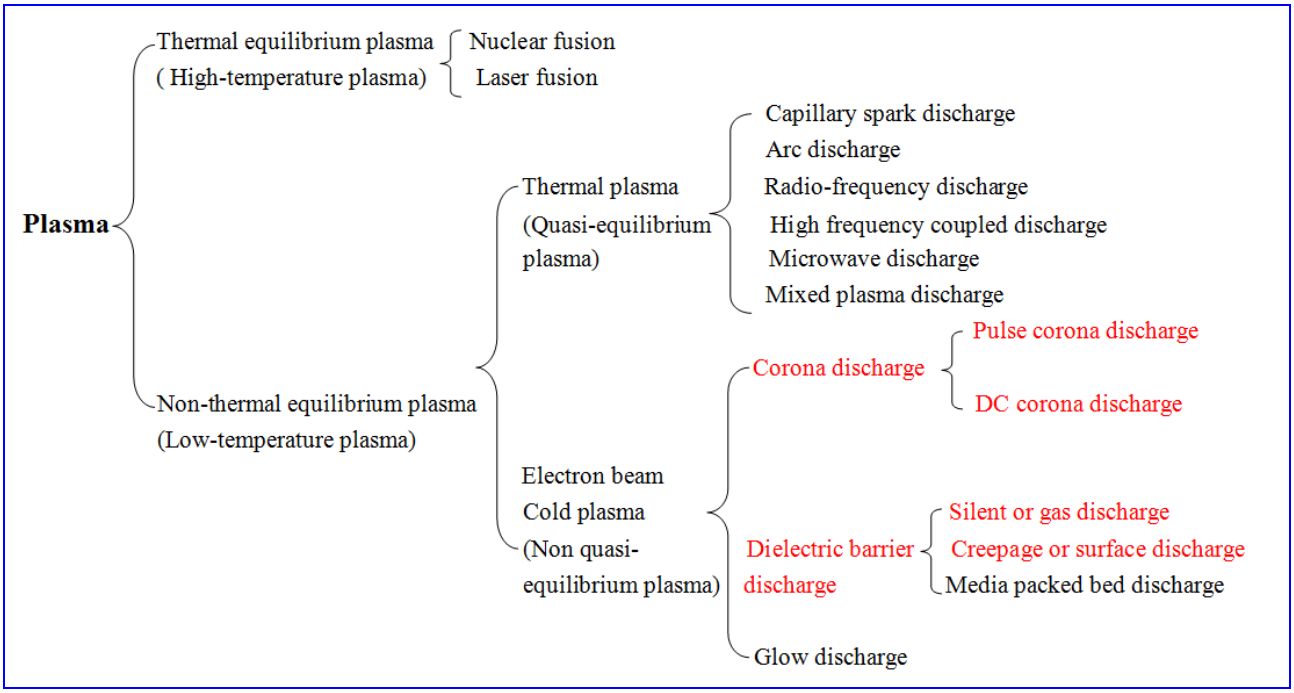

Figure 3. Specific classification of plasma technology.

Among these techniques, the cold plasma, especially electron beam, corona discharge plasma and dielectric barrier discharge plasma, has been extensively studied and applied in flue gas purification (McAdams et al. 2001;

206 Li et al. 2014a). The electron beam method was the first used for flue gas purification. In 1970s, Kawamura et al.
207 1979, 1980, 1981 used electron beam irradiation to remove SO_2 and NO_x from flue gas in a pilot plant facility
208 with processing capacity of 10000 Nm^3/h, In the few decades following, other world-wide investigators have
209 carried out relevant research, and established more pilot plants and demonstration projects (Frank et al. 1995;
210 Chmielewski et al. 1992; Chmielewski et al. 2007; Norman et al. 1992; Chmielewski et al. 2003; Basfar et al.
211 2008; Licki et al. 2003). These studies have demonstrated that electron beam irradiation could remove SO_2 and
212 NO_x in flue gas with efficiencies of more than 95% and 80%, respectively (Frank et al. 1995; Chmielewski et al.
213 1992; Chmielewski et al. 2007; Norman et al. 1992; Chmielewski et al. 2003). The electron beam irradiation can
214 obtain high removal efficiencies of pollutants, but it also has several deficiencies such as high energy consumption
215 and costs, short life of electron gun as well as complex system, which limit its commercial applications
216 (Kogelschatz er al. 2003; Park et al. 1999; Yan et al. 1999). Many researchers subsequently developed corona
217 discharge plasma and dielectric barrier discharge plasma to remove SO_2, NO_x, VOCs, etc. in flue gas, and
218 obtained good results (Kogelschatz er al. 2003; Park et al. 1999; Yan et al. 1999; Tas et al.1997; Takaki et al.
219 1999; Chang et al. 1992; Penetrante et al. 1996; Ma et al. 2002; Sun et al. 1996; Dhali et al. 1991; Evans et al.
220 1991; Koutsospyros et al. 2005; Mok et al. 2002; Yoshida et al. 2009; Mok et al. 1999). Compared to electron
221 beam radiation, corona discharge plasma and dielectric barrier discharge plasma have lower energy consumption
222 and more reliable equipment, and are hence, recognized as more promising flue gas purification technologies
223 (Mok et al. 1999; Chang et al. 2003). In the past two decades, a large number of studies related to removals of SO_2,
224 NO_x, H_2S and VOCs in flue gas using corona discharge plasma and dielectric barrier discharge plasma have been
225 reported (Kogelschatz er al. 2003; Park et al. 1999; Yan et al. 1999; Tas et al.1997; Takaki et al. 1999; Chang et al.
226 1992; Penetrante et al. 1996; Ma et al. 2002; Sun et al. 1996; Dhali et al. 1991; Evans et al. 1991; Koutsospyros et
227 al. 2005; Mok et al. 2002; Yoshida et al. 2009; Mok et al. 1999; Mok et al. 1999; Chang et al. 2003). In addition,

228 Masuda et al. 1987, Urabe et al. 1988 and Helfritch et al 1996 and 1998 successfully reported for the first time,
229 the use of pulse-corona discharge plasma for the oxidative removal of Hg^0 in flue gas. Based on these studies, Hg^0
230 removal technologies using various plasma discharge processes were further developed by many researchers, and
231 some other plasma discharge processes such as dielectric barrier discharge (DBD), including typical DBD, surface
232 discharge and packed-bed discharge, as well as DC corona discharge were also used for removal of Hg^0 in flue gas
233 (Liang et al. 2002; Xu et al. 2009; Wang et al. 2009; Ko et al. 2008a; Ko et al. 2008b; Ko et al. 2008c; Byun et al.
234 2008; Byun et al. 2011a; Chen et al. 2006; Jeong et al. 2007; Byun et al. 2011b; Bo et al. 2009; Tang et al. 2008;
235 Wang et al. 2011; Lin et al.2011; Yang et al. 2012a; Yang et al.2014b; An et al. 2014b; Wu et al. 1996).

236 **2.2 Effects of process parameters on Hg^0 removal using non-thermal plasma**

237 Related studies (Liang et al. 2002; Mannava et al. 2004; Xu et al. 2009; Wang et al. 2009; Ko et al. 2008a;
238 Ko et al. 2008b; Ko et al. 2008c; Byun et al. 2008; Byun et al. 2011a; Chen et al. 2006; Jeong et al. 2007; Byun et
239 al. 2011b; Bo et al. 2009; Tang et al. 2008; Wang et al. 2011; Lin et al.2011; Yang et al. 2012a; Yang et al.2014a;
240 An et al. 2014a; Wu et al. 1996) have reported that oxidation process of Hg^0 in flue gas using non-thermal plasma
241 is affected by various process parameters. To better understand and grasp the key process parameters of Hg^0
242 oxidation using non-thermal plasma, in the next sections, the effects of several process parameters on Hg^0
243 oxidation using non-thermal plasma will be reviewed and discussed.

244 **2.2.1 Effects of supplied voltage or specific energy density**

245 Corona discharge plasma and dielectric barrier discharge (DBD) plasma are often generated artificially by
246 gas discharge (Tendero et al. 2006; Kogelschatz et al. 2004), thus energy input is regarded as a key parameter for
247 plasma discharge process. Supplied voltage (SV) and specific energy density (SED), as two important indicators,
248 are often used to characterize the number of input energy. In plasma discharge process, various active species,
249 including ·OH, O_3, ·O, etc., are generated by high-energy electrons impacting with flue gas components (N_2, O_2,

250 H_2O and CO_2) (Chang et al.2002; Tendero et al.2006; Kogelschatz et al.2004; McAdams et al.2011; Li et al.
251 2014). Relevant studies (An et al.2014a; Byun et al.2008; Yang et al.2012a; Yang et al.2012b) showed that
252 removal of Hg^0 in flue gas was mainly achieved by oxidations of these active substances such as ·OH, O_3 and ·O
253 produced by plasma discharge process. With increasing SV or SED, the number of generated high-energy
254 electrons will increase, which also will raise the yield of these active substances (An et al.2014a; Byun et al.2008;
255 Yang et al.2012a; Yang et al.2012b), thereby promoting removal of Hg^0. Wang et al 2010, Jeong et al. 2007 and
256 Lin et al. 2010 investigated the effects of SV on Hg^0 oxidation using DBD plasma, and all of them found that Hg^0
257 removal efficiency dramatically increased with increasing SV. Wang et al. 2011 studied the effects of SV on Hg^0
258 oxidation using different discharge modes, including positive pulsed corona discharge, negative/positive DC
259 discharge and 12 kHz AC discharge, and their results showed that under different discharge modes, Hg^0 removal
260 efficiencies still increase with increasing SV. Yang et al.2012a also obtained similar results using a combined
261 plasma-TiO_2 photocatalysis process.

262 Furthermore, the effects of SED on Hg^0 removal are also studied by several researchers. Chen et al.2006 and
263 Ko et al.2008 investigated the effects of SED on Hg^0 oxidation in a DBD reactor, and their results showed that
264 with increasing SED, Hg^0 conversion greatly increased. The effects of SED on Hg^0 oxidation using positive
265 pulsed corona discharge and negative/positive DC discharge were also tested by Ko et al.2008 and Wang et
266 al.2011, respectively, and their results indicated that with increasing SED, Hg^0 conversion greatly increased. An et
267 al. 2014a and 2014b also studied the effects of SED on Hg^0 oxidation in a surface discharge plasma (SDP) reactor
268 and a SDP reactor inserted in simulated flue duct, respectively, and they also found that Hg^0 conversion rate
269 greatly increased with increasing SED. Based on the above results, it can be seen that there is a positive
270 relationship between SV/SED and Hg^0 oxidation efficiency. However, it is also noteworthy that increasing SV or
271 SED can effectively raise Hg^0 oxidation efficiency, but the power consumption of the system also increases

accordingly. Therefore, it is necessary to maintain an optimal value between Hg^0 oxidation efficiency and system power consumption in future industrial application.

2.2.2 Effect of pulse frequency

Pulse frequency is an important parameter for pulse discharge plasma process. Xu et al.2009 studied the effects of pulse frequency on Hg^0 oxidation efficiency in a positive DC reactor, and their results indicated that Hg^0 oxidation efficiency increased almost linearly with increasing pulse frequency. Liang et al.2002 also found that Hg^0 removal efficiencies increased with increasing pulse frequency in a prototype electrostatic precipitators (ESPs). Masuda et al.1987 also observed a similar trend in Hg^0 removal efficiency using a pulse discharge process. In a pulse discharge plasma system, the relationship between the total discharge energy of system and pulse frequency can be described by the following equation (1) (Bo et al. 2009),

$$SED = \frac{\tau \cdot f \cdot P_0}{V} \quad (1)$$

where SED is the specific energy density of system, J/L; τ is the residence time, s; f is the pulse frequency, Hz; P_0 is the input energy of single pulse, W; and V is the gas flow rate, L/s.

It can be seen from the equation (1) that with increase of pulse frequency, the SED will increase, thus the yield of active species (·OH, O_3, O·, etc.) will increase as well. Hg^0 oxidation efficiency primarily depends on the yield of these active species, and as a result, it increases with increasing pulse frequency.

2.2.3 Effects of discharge polarity, power supply and reactor structure

Related studies (An et al.2014a; Wang et al.2009; Bo et al.2009; Wang et al. 2011; An et al.2014b) reported that different discharge polarities and power supplies will result in different yields and concentration distributions of active substances and electrons in plasma reactor, and even under the same discharge polarity and power supply, the yield and concentration distribution of active substances and electrons also have significant differences with the changes of the plasma reactor structure. As we mentioned earlier, Hg^0 oxidation mainly depends on the yield

294 of active substances in plasma discharge process, thus it is very necessary to discuss the effects of discharge
295 polarity, power supply and plasma reactor structure on Hg^0 oxidation.

296 **(1) Discharge polarity and power supply**

297 Wang et al. 2009 studied the effects of power supply modes on Hg^0 oxidation in a link tooth wheel-cylinder
298 reactor energized by different high voltage power supplies. The results showed that Hg^0 oxidation efficiency and
299 O_3 production of negative DC corona discharge were much higher than those of positive DC corona and AC
300 corona discharge with the same supplied voltages. O_3 has been widely considered to be one of the most effective
301 active substances for Hg^0 oxidation in plasma discharge process (An et al.2014a; Liang et al.2002; Wang et al.
302 2009; Byun et al. 2011a; Byun et al. 2011b; Wang et al. 2011; An et al.2014b), thus the authors inferred that this
303 difference in Hg^0 oxidation efficiency may be attributed to the different O_3 production under different power
304 supply modes. Liang et al. 2002 also studied the effects of three power supply modes, including positive DC
305 corona discharge, negative DC corona discharge and pulse corona discharge, on Hg^0 oxidation in prototype
306 electrostatic precipitators (ESPs), and their results showed that the order of Hg^0 oxidation efficiency was negative
307 DC corona energization > positive DC corona energization > pure pulse corona energization. The results of
308 Masuda et al.1987 ndicated that for Hg^0 oxidation, there was no performance difference between positive and
309 negative polarity for the temperature up to 200℃, but at 300℃ and higher, the negative polarity performed better.
310 Byun et al. 2011b also examined the effect of polarity on Hg^0 oxidation via a pulsed corona discharge (PCD)
311 reactor, and found that the positive PCD showed a higher Hg^0 oxidation than the negative one at the same applied
312 voltage, but there was no difference in Hg^0 oxidation at the same SED.

313 It is obvious from these studies that, there is a contradiction on the effects of positive and negative polarities
314 on Hg^0 oxidation between the results of Liang et al. and other investigators. The results of Byun et al. 2011a
315 showed that Hg^0 oxidation efficiency increased from 10% to 70% with increasing the reaction time at a fixed SED

316 by the autocatalytic role of Hg^{2+}, as an active site, attached to the reactor surface. Therefore, Byun et al.2011a
317 suggested that the results of Liang et al. might have not considered the effect of surface catalytic reaction of Hg^{2+}
318 on Hg^0 removal, thereby resulting in this difference. Wang et al.2011 investigated the effects of discharge polarity
319 (positive and negative DC corona discharge) under the same SED on Hg^0 oxidation and O_3 formation, and they
320 found that the outlet concentration of O_3 and Hg^0 oxidation efficiency using positive DC corona discharge were
321 significantly higher than those using negative DC corona discharge at a fixed SED. Wang et al.2011 urther
322 investigated the reasons for this difference by photographing the images of positive and negative DC corona
323 discharge at same conditions as shown in Figure 4.

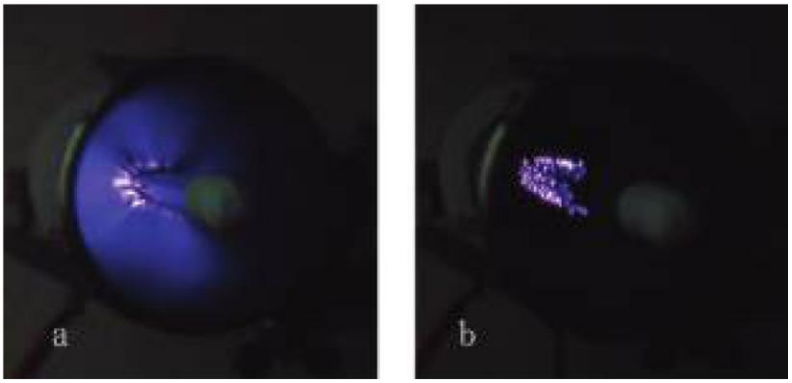

324

325 **Figure 4.** Images of positive DC corona discharge (a) and negative DC corona discharge (b) (Wang et al. 2011).

326 It can be observed from Figure 4 that positive DC corona discharge shows a brilliant and uniform streamer
327 corona across the entire inter-electrode space, while only the glow corona can be observed in the vicinity of
328 discharge tooth tine for negative DC discharge with the same applied voltage. The streamer corona discharge
329 exhibits higher chemical activity than the glow corona discharge due to a relatively larger ionized region
330 (Gasparik et al. 2000). Therefore, this difference between positive and negative polarities was mainly attributed to
331 the relatively higher chemical activity of positive polarity as compared to the negative one. Besides, an optical
332 spectrum measurement by Jani et al.1999 lso indicated that the average electron-energy induced by positive
333 discharge was obviously higher than that by negative discharge for the same energy consumption. Under a

positive discharge mode, the stronger electric-field intensity will increase the yields of high-energy electrons, which also will enhance the dissociation of O_2 and H_2O to produce more active substances, thereby showing a better Hg^0 oxidation.

(2) Reactor structure

Wang et al.2011 studied the effects of discharge tooth wheel number on Hg^0 oxidation in a link tooth wheel-cylinder reactor using a negative DC corona discharge, and they found that increasing the number of discharge tooth wheels resulted in a higher Hg^0 oxidation. The authors speculated that this result may be attributed to the fact that a specific injection energy, corresponding to the yield of high energy electrons and active substances, was proportional to the number of tooth wheels. Thus Hg^0 oxidation was enhanced by increasing the number of tooth wheels. Xu et al.2009 studied the effects of the electrode number on Hg^0 oxidation using a positive pulsed corona discharge, and they found that Hg^0 oxidation efficiency increased approximately linearly with increasing electrode number. They hypothesized that increasing electrode number could extend the length of pulsed corona discharge area, producing more high-energy electrons and active substances in plasma reactor, and thereby enhancing Hg^0 oxidation.

Liang et al.2002 tested the performance of a two-stage discharge mode for Hg^0 removal in a prototype electrostatic precipitators (ESPs) (the first stage (upstream) was supplied with pulse voltage to oxidize Hg^0 by plasma reactions, while the second stage with DC voltage was used to generate a high drift field.), and the results showed that Hg^0 oxidation efficiency using this kind of two-stage energization mode was higher than that under positive DC corona energization and pulse corona energization, but lower than that under negative DC corona energization. An et al.2014a developed a non-thermal plasma (NTP) injection approach to oxidize Hg^0 in flue gas. In their studies, a surface discharge plasma (SDP) reactor was inserted in a simulated flue duct, and was used to generate and inject active species into simulated flue gas. The differences of “injection approach”, also called

356 “indirect oxidation”, and “direct oxidation” in Hg^0 oxidation efficiency and energy consumption were evaluated
357 by the authors, and the results indicated that the “injection approach” or “indirect oxidation” has higher Hg^0
358 removal efficiency and lower energy consumption than “direct oxidation” under the same conditions.

359 **2.2.4 Effects of residence time**

360 Residence time is an important parameter for chemical reaction and reactor design. Jeong et al.2007 studied
361 the effects of residence time on Hg^0 oxidation using a DBD reactor under different voltages. The results indicated
362 that Hg^0 oxidation was significantly enhanced with increasing residence time. Xu et al.2009 found that Hg^0
363 oxidation efficiency significantly increased with increasing residence time (below 6s), but almost remained
364 constant when residence time exceeded 6s in a positive DC reactor. Appropriately increasing residence time will
365 raise the probabilities of collision between active substances and contaminant molecules, thereby enhancing the
366 reaction process. However, an excessive residence time is unnecessary because, not only will it not further
367 increase Hg^0 removal efficiency, but also will result in an excessive large reactor volume and high costs.

368 **2.2.5 Effects of Hg^0 inlet concentration**

369 Hg^0 inlet concentration often changes from a few $\mu g/m^3$ to a few hundred $\mu g/m^3$ depending on the different
370 fuels and combustion conditions. Jeong et al.2007 tested the effects of Hg^0 inlet concentration on Hg^0 oxidation in
371 a DBD reactor, and they found that increasing Hg^0 inlet concentration was not conducive to Hg^0 oxidation. Xu et
372 al.2009 and An et al.2014b also obtained similar results in a positive DC reactor and a SDP reactor, respectively.
373 However, Liang et al.2002 btained the opposite results, which indicated that Hg^0 oxidation efficiencies
374 significantly increased with increasing Hg^0 inlet concentration under four kinds of discharge modes, including
375 positive DC corona discharge, negative DC corona discharge, pulse corona discharge as well as the combination
376 of pulse corona discharge and negative DC corona discharge, in a prototype electrostatic precipitators (ESPs).

377 **2.3 Effects of flue gas components on Hg^0 removal using non-thermal plasma**

The results of Granite et al.2002 showed that the untreated typical coal-fired flue gas from a coal-fired utility burning a low-sulfur eastern bituminous coal is often a complex mixture of several gas components, which typically consists of 5-7% H_2O, 3-4% O_2, 15-16% CO_2, 1 ppb total Hg, 20 ppm CO, 10 ppm hydrocarbons, 100 ppm HCl, 800 ppm SO_2, 10ppm SO_3, 500ppm NO_x, and the balance N_2. These flue gas components are found to have obvious impact on plasma discharge process (mainly affecting the yield and concentration distribution of active substances and electrons as well as energy utilization efficiency of the system), thereby further interfering with the oxidation of Hg^0 in flue gas as reported by several investigators (An et al.2014a; Wang et al.2010; Liang et al.2002; Wang et al.2009; Byun et al.2011a; Byun et al. 2011b; Wang et al.2011; An et al. 2014b).

2.3.1 Effects of O_2

O_2 is one of the main component in coal-fired flue gas, and is often considered as the important precursor of the active substances such as ·O and O_3 in most of advanced oxidation reactions. Thus its content often has a significant impact on Hg^0 oxidation using non-thermal plasma. The effects of O_2 on Hg^0 oxidation in a DBD reactor were investigated by Wang et al. 2010 and Lin et al.2010 respectively, and their results showed that Hg^0 oxidation was greatly strengthened with increasing O_2 concentration. An et al. 2014a also tested the effects of O_2 concentration on Hg^0 oxidation in a SDP reactor inserted in simulated flue duct, and the results indicated that Hg^0 oxidation was also promoted by adding O_2. Yang et al. 2012a also obtained similar results in a combined plasma-TiO_2 photocatalysis reactor. The generation of active species such as O_3, ·O, ·OH, etc. in non-thermal plasma discharge process via high-energy electrons impacting on O_2 molecules in the flue gas can be described by reactions (2)-(6) (An et al. 2014a; Wang et al. 2010; Lin et al. 2010).

$$O_2(g) + e \rightarrow \cdot O(^3P)(g) + \cdot O(^1D)(g) + e \quad (2)$$

$$O_2(g) + e \rightarrow \cdot O(^3P)(g) + \cdot O(^3D)(g) + e \quad (3)$$

$$O_2(g) + \cdot O(g) \rightarrow O_3(g) \quad (4)$$

$$Hg(g) + O_3(g) \rightarrow HgO(g) + O_2(g) \quad (5)$$

$$Hg(g) + \cdot O(g) \rightarrow HgO(g) \quad (6)$$

It is obvious from these reactions that increase in O_2 levels in flue gas leads to increased generation of active species and enhances Hg^0 oxidation.

2.3.2 Effects of H_2O

In advanced oxidation reactions, H_2O is often the precursor of ·OH radical in various reactions (An et al. 2014a; Wang et al. 2010). Wang et al. 2010 found that Hg^0 oxidation was increased by adding single H_2O in a DBD reactor. An et al. 2014a investigated the effects of H_2O in a SDP reactor inserted in simulated flue duct, and their results showed that adding 4% and 6% H_2O made Hg^0 oxidation efficiency increased from 81% to 86% and 89%, respectively. Lin et al.2010 and Yang et al. 2012a and 2012b also obtained similar positive results in a DBD reactor and a combined plasma-TiO_2 photocatalysis reactor, respectively. ·OH will be generated in plasma discharge process through high-energy electrons impacting on H_2O molecules, and it is an effective Hg^0 oxidant in a variety of advanced oxidation reactions (An et al. 2014a; Wang et al. 2010; Lin et al.2010; Yang et al. 2012a). The related process can be described by reactions (7)-(11) (An et al. 2014a; Wang et al. 2010; Lin et al.2010; Yang et al. 2012a).

$$H_2O(g) + e \rightarrow \cdot OH(g) + \cdot H(g) + e \quad (7)$$

$$Hg(g) + \cdot OH(g) \rightarrow HgOH(g) \quad (8)$$

$$HgOH(g) + \cdot OH(g) \rightarrow Hg(OH)_2(g) \quad (9)$$

$$HgOH(g) + O_2(g) \rightarrow HgO(g) + HO_2 \cdot (g) \quad (10)$$

$$Hg(OH)_2(g) \rightarrow HgO(g) + H_2O(g) \quad (11)$$

However, the results of An et al.2014b indicated that H_2O inhibited Hg^0 oxidation in a SDP reactor. An et al.2014b showed that H_2O inhibition of O_3 generation was responsible for the antagonistic effect of H_2O on Hg^0

oxidation. The results of Ko et al. 2008 found that Hg^0 oxidation was hardly affected by H_2O in a DBD reactor. The authors speculated that the hydroxides of mercury were very likely to re-decompose back to Hg^0 at high temperature because they were very unstable even at room temperature. The results of Goodsite et al. 2004 which were based on quantum chemical calculations showed that the lifetime of HgOH is only 280μs at 25℃, consistent with the speculation of Ko et al. 2008.

2.3.3 Effects of HCl

During the combustion process, chlorine always exists in coal or waste materials, and eventually will be converted into the gaseous HCl (Li et al. 2003). Although HCl has a low concentration (about 100 ppm) in flue gas, it has a significant impact on Hg^0 oxidation using non-thermal plasma (An et al. 2014a; Wang et al. 2010). The results of Wang et al. 2010 in a DBD reactor showed that with 30 ppm of HCl added into the gas stream, Hg^0 conversion rate gradually increased from 43.2% to 70.6% within 30 min, and with further increase from from 30 ppm to 60 ppm, Hg^0 conversion rate dramatically increased from 70.6% to 96.8% just within 15 min. Ko et al. 2008 and 2009 studied the effects of HCl on Hg^0 oxidation in a DBD reactor and a pulsed corona discharge (PCD) reactor, and their results showed that Hg^0 oxidation was promoted by adding HCl in two plasma reactors. An et al. 2014a and Yang et al. 2012a obtained similar results in a SDP reactor inserted in simulated flue duct and a combined plasma-TiO_2 photocatalysis reactor, respectively. Other researchers (An et al. 2014a; Wang et al. 2010; Li et al. 2003) studied the mechanism of HCl effects on Hg^0 oxidation, and suggested that the additional formation of Cl· and HOCl was the main reason for the enhanced oxidation of Hg^0 through the following series of elementary reactions (12)-(24).

$$HCl(g) + e \rightarrow \cdot H(g) + Cl \cdot (g) + e \quad (12)$$

$$HCl(g) + \cdot OH(g) \rightarrow H_2O(g) + Cl \cdot (g) \quad (13)$$

$$Cl \cdot (g) + \cdot OH(g) \rightarrow HOCl(g) \quad (14)$$

444 $$Cl\cdot(g)+\cdot OH(g)\rightarrow HOCl(g) \quad (15)$$

445 $$Cl\cdot(g)+Hg^{0}(g)\rightarrow HgCl(g) \quad (16)$$

446 $$HOCl(g)+Hg^{0}(g)\rightarrow HgCl(g)+\cdot OH(g) \quad (17)$$

447 $$HOCl(g)+Hg^{0}(g)\rightarrow HgO(g)+HCl(g) \quad (18)$$

448 $$HgCl(g)+Cl\cdot(g)\rightarrow HgCl_{2}(g) \quad (19)$$

449 $$Cl\cdot(g)+Cl\cdot(g)\rightarrow Cl_{2}(g) \quad (20)$$

450 $$Cl_{2}(g)+H_{2}O(g)\rightarrow HOCl(g)+HCl(g) \quad (21)$$

451 $$Cl_{2}(g)+Hg^{0}(g)\rightarrow HgCl(g)+Cl\cdot(g) \quad (22)$$

452 $$HgCl(g)+Cl_{2}(g)\rightarrow HgCl_{2}(g)+Cl\cdot(g) \quad (23)$$

453 $$Cl_{2}(g)+Hg^{0}(g)\rightarrow HgCl_{2}(g) \quad (24)$$

454 **2.3.4 Effects of SO_2**

455 SO_2 is a major environmental concern because of its detrimental effects (e.g., acid rains) (Wang et al. 2007;
456 Hutson et al. 2008). In future industrial applications using non-thermal plasma process, it will be advantageous to
457 simultaneously remove SO_2, NO and Hg^0 in the flue gas using a single reactor. Hence, investigating the
458 interaction between these pollutants is a valuable contribution to this goal. Wang et al. 2010 examined the effect of
459 SO_2 on Hg^0 oxidation in a DBD reactor, and the results indicated that Hg^0 oxidation efficiency greatly declined
460 with increasing SO_2 concentration. SO_2 often competes with Hg^0 for active species such as $\cdot O$, O_3 and $\cdot OH$
461 through reactions (25)-(27) (An et al. 2014a; Wang et al. 2010), hindering Hg^0 conversion.

462 $$SO_{2}(g)+\cdot O(g)\rightarrow SO_{3}(g) \quad (25)$$

463 $$SO_{2}(g)+O_{3}(g)\rightarrow SO_{3}(g)+O_{2}(g) \quad (26)$$

464 $$SO_{2}(g)+\cdot OH(g)+M\rightarrow OHSO_{2}(g)+M \quad (27)$$

465 On the other hand, Wang et al. 2009 showed that Hg^0 oxidation efficiency increased with addition of SO_2 in a

negative DC reactor. The product HgO of Hg^0 oxidation will be consumed by $OHSO_2$(g) produced in reaction (27) as shown in reactions (28) and (29), which promote Hg^0 oxidation by changing the chemical equilibrium of Hg^0 oxidized by ·O and O_3 (Wang et al. 2009).

$$OHSO_2(g) + O_2(g) \rightarrow SO_3(g) + HO_2 \cdot (g) \quad (28)$$

$$HgO(g) + SO_3(g) \rightarrow HgSO_4(g) \quad (29)$$

Also, An et al. 2014a and 2014b showed that increasing SO_2 concentration had little effects on Hg^0 oxidation in a SDP reactor and a SDP reactor inserted in simulated flue duct, respectively. The authors suggested that both ·O and O_3 were the main oxidizers of Hg^0 removal, while ·OH was the main oxidizer of SO_2 removal. Therefore, the consumption of ·O and O_3 by reacting with SO_2 is very minor due to the low reaction rates, and as a result, SO_2 has little effects on Hg^0 oxidation. Hence, it should be noted that SO_2 shows very complex effects on Hg^0 oxidation using different plasma reactors, and require further mechanistic studies.

2.2.5 Effects of NO

The effects of NO on Hg^0 oxidation using plasma discharge processes as studied by several researchers show consistent results. Wang et al. 2010 investigated the effects of NO on Hg^0 oxidation in a DBD reactor, and found Hg^0 oxidation greatly diminished by the presence of NO. Wang et al. 2009 also showed that Hg^0 oxidation efficiency greatly decreased with increased NO concentration in a negative DC corona discharge reactor. An et al. 2014a and 2014b and Ko et al. 2008 also obtained similar results in a SDP reactor, a SDP reactor inserted in simulated flue duct as well as a typical DBD reactor, respectively. The authors hypothesized that the observed results are likely attributed to the fact that NO can consume active oxidants in competition with Hg^0, and hence, reducing its conversion as in reactions (30)-(33) (An et al. 2014a; Wang et al. 2010; Ko et al. 2008; An et al. 2014b).

$$NO(g) + \cdot O(g) \rightarrow NO_2(g) \quad (30)$$

$$NO(g) + O_3(g) \rightarrow NO_2(g) + O_2(g) \quad (31)$$

$$NO(g) + \cdot OH(g) \rightarrow HNO_2(g) \quad (32)$$

$$NO_2(g) + \cdot OH(g) \rightarrow HNO_3(g) \quad (33)$$

Wang et al. 2009 demonstrated the validity of these reactions in a study which simultaneously detected NO and O_3 in the exhaust gas and showed O_3 concentration significantly decreased while NO_2 dramatically increased from the oxidation of NO.

2.3.6 Effects of CO_2

In the typical coal-fired flue gas from a coal-fired utility burning a low-sulfur eastern bituminous coal, the volume fraction of CO_2 is up to 15-16% (Granite et al. 2002), which is the second largest component after N_2. Related results confirmed (Wang et al. 2009; Lin et al. 2010) that the high-energy electrons from plasma discharge process can effectively decompose CO_2 by breaking the molecular bond in CO_2. Hence, studying the impact of CO_2 on Hg^0 oxidation is essential for future applications of this technology. Wang et al. 2009 tudied the effect of CO_2 on Hg^0 removal in a negative DC corona reactor, and their results indicated that CO_2 greatly weakened Hg^0 oxidation. For example, at 10 kV of supplied voltage, Hg^0 oxidation efficiency roughly decreased from 67.8% to 17.5% with the addition of 12% CO_2. The results of Lin et al. 2010 also indicated that with the additions of 4.5% and 7.5% CO_2 into $N_2/O_2/Hg^0$ gas stream, Hg^0 oxidation efficiency reduced from 97.4% to 96.6% and 89.7%, respectively. Chen et al. 2006 suggested that $\cdot O$ will be generated by the electron-impact dissociation of CO_2 in plasma discharge process through reaction (34), which will provide more active species, $\cdot O$ for Hg^0 oxidation.

$$CO_2(g) + e \rightarrow CO(g) + \cdot O(g) + e \quad (34)$$

However, some other investigators have also argued that although the electron-impact dissociation of CO_2 created more $\cdot O$, it was negligible since the dissociation rate of CO_2 was 4-5 orders of magnitude lower than that of O_2. This dissociation of CO_2 consumed a lot of high-energy electrons and meanwhile, strengthened the reducing

510 atmosphere by generating the reducing gas CO (Wang et al. 2009; Lin et al. 2010), which was not conducive to
511 Hg^0 oxidation. Based on the existing results, the latter view seems closer to the experimental results to date.

512 **2.3.7 Synergistic effects of mixing gas components**

513 As mentioned earlier, the components of actual coal-fired flue gas are very complex, thus studying the
514 influence of any single fuel gas component on Hg^0 oxidation is not adequate for future developments of these
515 potential technologies for eventual industrial applications. Some researchers preliminarily studied the effects of
516 multi-components on Hg^0 oxidation using plasma discharge process. Chen et al. 2006 tested the effects of single
517 H_2O, coexisting O_2 and H_2O as well as coexisting CO_2, O_2 and H_2O on Hg^0 oxidation using a DBD process. The
518 results showed that on the average only 18% Hg^0 average conversion was achieved by adding single H_2O, but Hg^0
519 obtained a complete conversion with the joint addition of O_2 and H_2O, and a 80% conversion with the joint
520 addition of CO_2, O_2 and H_2O, respectively, indicating the synergetic effects of presence of these multi-components.
521 The results of Wang et al. 2010 showed that compared to the positive effect of adding single H_2O or O_2, there was
522 a more complex effect on Hg^0 oxidation in a DBD reactor with the joint addition of O_2 and H_2O. For example,
523 Hg^0 oxidation rate had a significant increase followed by a quick decline with continuously increase of H_2O
524 content in the presence of O_2. The authors suggested that adding a small amount of H_2O could improve Hg^0
525 oxidation by generating more $\cdot OH$. However, when the excess H_2O was added, the excess H_2O also consumed O_3
526 and $\cdot O$ by competing with Hg^0 through reactions (35)-(38). The active species, O_3 and $\cdot O$, are considered as more
527 effective active substances than $\cdot OH$ for Hg^0 oxidation (An et al. 2014a; Wang et al. 2010). Hence, the addition of
528 excess H_2O resulted in the remarkable decrease in Hg^0 conversion.

529 $$H_2O(g) + O_3(g) \rightarrow H_2O_2(g) + O_2(g) \quad (35)$$

530 $$H_2O_2(g) \rightarrow \cdot OH(g) + \cdot OH(g) \quad (36)$$

531 $$O_3(g) + \cdot OH(g) \rightarrow HO_2 \cdot (g) + O_2(g) \quad (37)$$

$$\cdot OH(g) + \cdot O(g) \rightarrow O_2(g) + \cdot H(g) \quad (38)$$

Ko et al. 2008 nvestigated the synergistic influence of HCl and H_2O on Hg^0 oxidation using a DBD process, and their results showed that only adding H_2O almost had no effect on Hg^0 oxidation, but when HCl was also added to the flue gas stream, the addition of H_2O clearly accelerated Hg^0 oxidation. Related results (An et al. 2014a; Wang et al. 2010; Lin et al. 2010; Yang et al. 2012a; Yang et al. 2012b) demonstrated that ·OH could be generated in plasma discharge process by high-energy electrons impacting on the H_2O molecules. The Cl_2 present in flue gas could also react with ·OH to generate the new reactive intermediates, HOCl and Cl·, according to the following reaction (39).

$$Cl_2(g) + \cdot OH(g) \leftrightarrow Cl \cdot (g) + HOCl(g) \quad (39)$$

The generated Cl· and HOCl are important reactive intermediates for enhancing Hg^0 oxidation to produce HgCl by reactions (40) and (41) (An et al. 2014a; Lin et al. 2010; Yang et al. 2012; ; Yang et al. 2012b).

$$Hg^0(g) + Cl \cdot (g) + M \rightarrow HgCl(g) + M \quad (40)$$

$$Hg^0(g) + HOCl(g) \rightarrow HgCl(g) + \cdot OH(g) \quad (41)$$

An et al. 2014a also investigated the synergistic effects of mixed gas components, including O_2, H_2O, HCl, NO and SO_2, on Hg^0 oxidation in a SDP reactor inserted in simulated flue duct, and their results showed that adding O_2 alone resulted in the highest Hg^0 oxidation efficiency but was greatly reduced in the presence of mixed gas components of O_2, H_2O, NO and SO_2. However, when 20 ppm HCl was also added to in the mixed gas components, Hg^0 oxidation efficiency singnificantly increased, but was still lower than that of adding single O_2 alone. The results of Lin et al. 2010 found that compared to a single component such as O_2 or H_2O, Hg^0 oxidation efficiency using a DBD discharge process declined by of 20% on the average in $HCl/N_2/CO_2/O_2/H_2O$ complex atmosphere. Wang et al. 2010 evaluated the synergistic effects of coexisting SO_2/NO and CO_2/O_2 gas streams on Hg^0 oxidation using positive and negative DC corona discharge process, and their results indicated that Hg^0

554 oxidation was enhanced by adding SO_2 alone, but the degree of enhancement was significantly reduced by further
555 addition of NO into the gas stream. The authors speculated that the results were likely to be attributed to the fact
556 that O_2 was the main source of O_3 and ·O, thus increasing its concentrations was beneficial to Hg^0 oxidation (An
557 et al. 2014a; Wang et al. 2011). However, NO is an efficient scavenger of O_3 and ·O (An et al. 2014a; Wang et al.
558 2011; Lin et al. 2010), thus increasing its concentrations was detrimental to Hg^0 oxidation. To prove this theory,
559 the authors further measured the O_3 concentration along with Hg^0 oxidation efficiency, and found that both
560 increased with the increase of O_2/CO_2 ratio (Wang et al. 2011). In addition to these studies, the effects of some
561 other flue gas components such as various particulate matters, VOCs, NO_2, CO, H_2S, alkali metal salts, etc., and
562 their mechanisms on Hg^0 oxidation using plasma discharge process require further in-depth evaluations.

563 **2.4 Products and mechanism of Hg^0 removal using non-thermal plasma**

564 **2.4.1 Products of Hg^0 removal using non-thermal plasma**

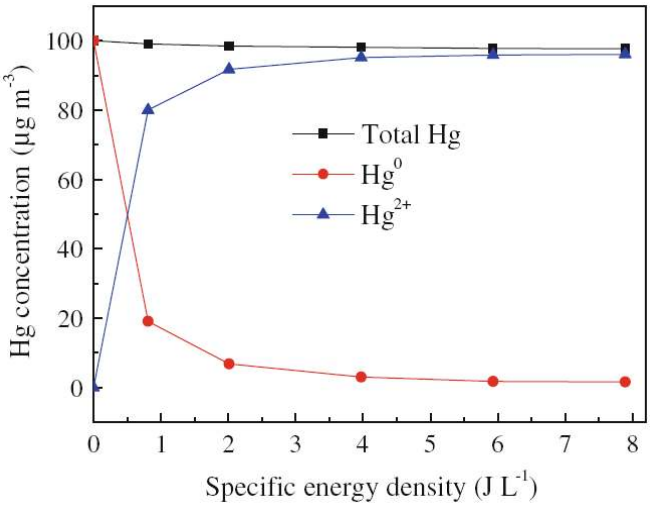

565

566 **Figure 5.** Content changes of different mercury components (An et al. 2014a).

567 An et al. 2014a and 2014b etermined the gaseous and solid products of Hg^0 oxidation in a SDP reactor and a
568 SDP reactor inserted in simulated flue duct using a mercury analyzer, X-ray photoelectron spectroscopy (XPS),
569 electronic probe microanalysis (EPMA) and energy dispersive spectroscopy (EDS). The results showed that the
570 concentration of Hg^0 in flue gas exhibited a dramatic decrease, while the concentration of oxidized Hg in flue gas

increased greatly. The total Hg concentration slightly decreased due to the accumulation of mercury species in the form of yellow deposits on the internal surface of the simulated flue duct. The changes in contents of different mercury species are depicted in Figure 5. The elements and elemental oxidation states of the deposited mercury species on the internal surface of simulated flue duct were determined by XPS, and the results are shown in Figure 6. It can be seen that the presence of Hg 4f was detected, and two typical peaks at 106.99 and 103.00 eV for Hg $4f_{5/2}$ and Hg $4f_{7/2}$, respectively, suggested that Hg was possibly combined with oxygen (He et al. 2011). The authors (An et al. 2014a and 2014b) calculated the elemental contents and Hg/O atomic ratio by the normalized peak areas of the Si 2p, Hg 4f and O 1s core level spectra, and they found that for the deposited mercury species, the atom ratio of O and Hg on the surface was observed to be approximately 1.01, suggesting that the deposited mercury species predominantly existed in the form of HgO. Also, using EPMA, the authors (An et al. 2014a and 2014b) found the atomic ratio of O and Hg to be approximately 0.996 and 1.05, respectively, consistent with XPS results.

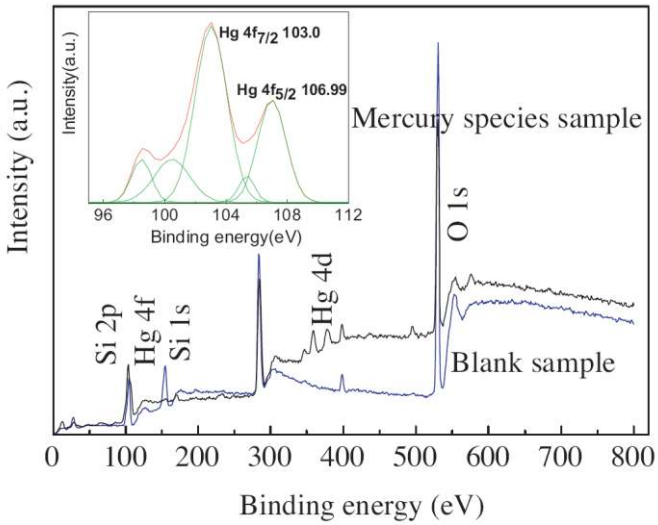

Figure 6. XPS spectra of deposited mercury species for NTP injection (An et al. 2014a).

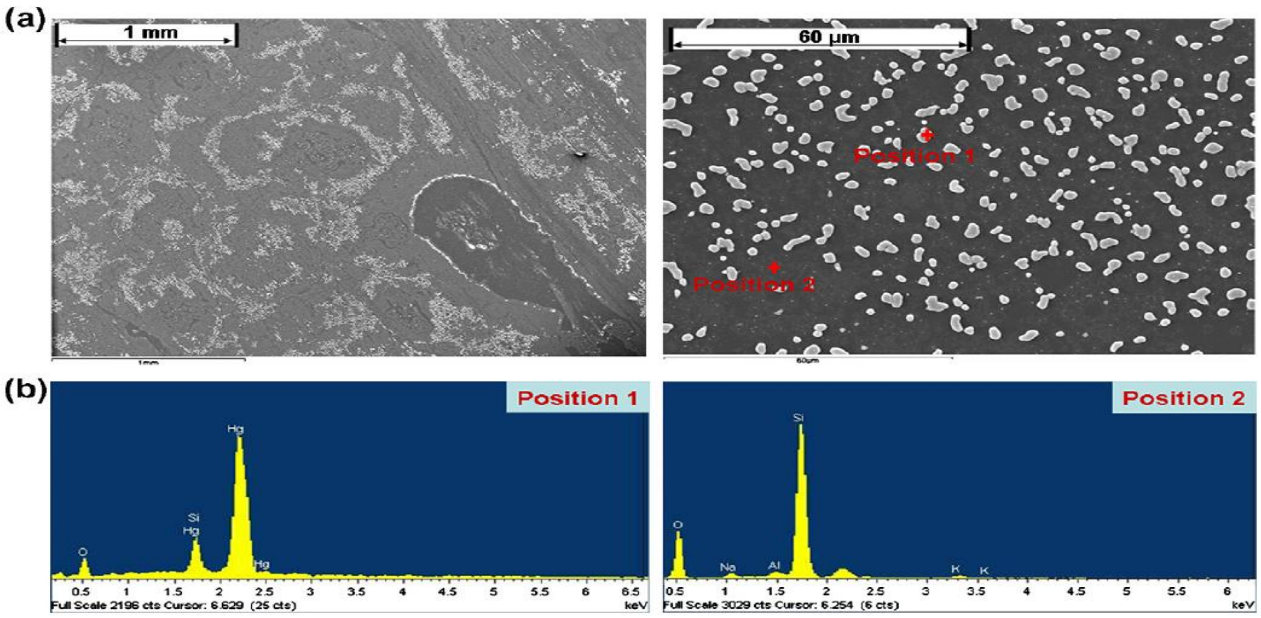

585

586 **Figure 7.** SEM-EDS analysis of the reactor (quartz) surface after using DBD reactor for 2 months without

587 cleaning procedure. (a) SEM images and (b) EDS spectra obtained at two positions 1 and 2 (Byun et al. 2011a).

588 Byun et al. 2011a also analyzed the deposited mercury species on the reactor surfaces of Hg^0 removal in a

589 DBD reactor by scanning electron microscopy (SEM)-energy dispersive spectroscopy (EDS) and temperature-

590 programmed desorption and dissociation (TPDD). They continuously operated the DBD reactor for two months

591 without cleaning it and then found out yellow stains accumulated on the reactor surfaces. The authors analyzed the

592 properties of the reactor surfaces by using SEM-EDS, and the results are shown in Figure 7 (a) and (b). It can be

593 seen that the yellow stains were conglomerated like islands on the reactor surfaces. For further comparison, two

594 groups of parallel analyses, including a Position 1 with yellow stains and a Position 2 without yellow stains, were

595 conducted, and the results are shown in Figure 7 (b). It is obvious that no Hg peak was detected at Position 1 but

596 was detected at Position 2. In addition, the TPDD results showed new peak in TPDD spectra observed in the

597 region of 260-380℃, attributable to HgO_3(s), which was subsequently decomposed to more stable HgO(s) at

598 higher temperature.

599 **2.4.2 Mechanism of Hg^0 removal using non-thermal plasma**

600 Relevant results (Bogaerts et al. 2002; Chang et al. 2002; Tendero et al. 2002; Kogelschatz et al. 2004;

601 McAdams et al. 2001; Li et al. 2014) showed that non-thermal plasma discharge process can produce a large
602 number of high-energy particles with high activity such as electrons, ions, free radicals and molecules under
603 excited states. These high-energy particles can directly destroy the molecular bonds of background gases and
604 gaseous pollutants. In the dissociation process of gas molecules, some active species such as ·OH, ·O, O_3, etc. are
605 generated. These reactive oxygen species can effectively oxidize and degrade various pollutants. The plasma
606 removal process for SO_2, NO_x, H_2S and VOCs mainly includes two reaction pathways, namely, the dissociations
607 of pollutants by high-energy electrons followed by the oxidations by reactive species (Bogaerts et al. 2002; Chang
608 et al. 2002; Tendero et al. 2002; Kogelschatz et al. 2004; McAdams et al. 2001; Li et al. 2014). However,
609 elementary mercury (Hg^0) is mainly removed by direct oxidations rather than by dissociation (An et al. 2014a;
610 Wang et al. 2010; Byun et al. 2011a; An et al. 2014b). Therefore, to date, research on Hg^0 removal mechanism has
611 focused on determining Hg^0 oxidation pathways (An et al. 2014a; Byun et al. 2011a; Yang et al. 2012a; An et al.
612 2014b).

613 An et al. 2014a investigated the reaction mechanism of Hg^0 removal in a SDP reactor inserted in simulated
614 flue duct using comparative studies, mercury mass balance and byproducts analysis using XPS and EPMA, and
615 they found that the pathways for Hg^0 removal include oxidations by several active substances (·OH, ·O, O_3,
616 Cl· and HOCl) as well as excitations from UV-light generated by corona discharge with oxidation by O_3 playing
617 the dominant role. Byun et al. 2011a also investigated the reaction mechanism of Hg^0 removal in a DBD reactor,
618 and they found that the pathways of Hg^0 removal in the DBD reactor mainly included gas-phase oxidations active
619 oxidants (·OH, ·O, O_3, etc., with O_3 playing a pivotal role) and surface-induced reactions. It was also shown that
620 mercury species deposited on the reactor surfaces acted as active sites and provided extra ·O to oxidize the
621 adsorbed Hg^0 on the surfaces, resulting in an acceleration of Hg^0 removal as the oxidation process of Hg^0
622 proceeded. The reaction mechanism of Hg^0 removal in a DBD (SDP also belongs to DBD) reactor involving

623 oxidants (·OH, ·O, Cl^-, HOCl, O_3, etc., with O_3 a major oxidation pathway), UV-induced excitations and surface

624 reaction, is further described in Figure 8.

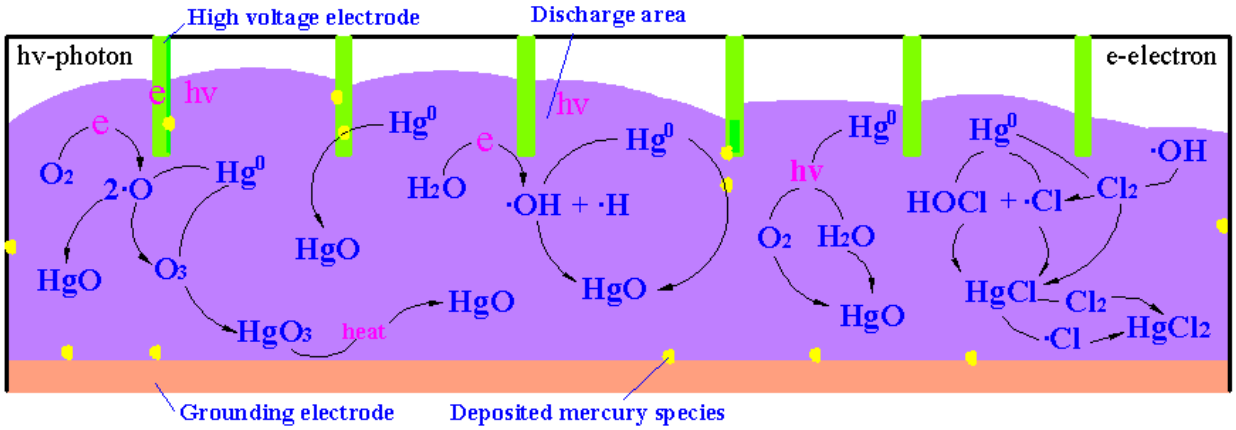

625

626 **Figure 8.** Schematic of Hg^0 removal mechanism using DBD process.

627 It is worth noting that some potential factors may result in the changes of Hg^0 removal pathways in different

628 non-thermal plasma reactors involving several aspects. (1) Different plasma reactors, flue gas compositions or

629 operating conditions will lead to potential differences in the yields and concentration distributions of active

630 substances such as ·OH, ·O, O_3, Cl· and HOCl (An et al. 2014a; Liang et al. 2002; Xu et al. 2009; Wang et al.

631 2009; Byun et al. 2011a; Bo et al. 2009; Wang et al. 2011; An et al. 2014b), which may result in different

632 pathways of Hg^0 removal; (2) Due to the differences in the inner contact surface of reactor, different plasma

633 reactors may result in the differences in surface-induced catalytic reactions (Byun et al. 2011a); (3) Different

634 plasma reactors have different hydrodynamics as well as heat and mass transfer characteristics (Bo et al. 2009),

635 which also will change the reaction pathways as well as the final forms and contents of the Hg^0 removal products.

636 These observations suggest complex reaction mechanisms, and require more efforts on comparative studies in the

637 future.

638 **2.5 Kinetics of Hg^0 removal using non-thermal plasma**

639 To date, the kinetic studies of Hg^0 removal using non-thermal plasma are rare. Zhou et al. 2009 developed a

640 kinetic mechanistic model of Hg^0 removal, consisting of 30 elementary reactions, in $NO/O_2/N_2$ gas stream using a

DBD reactor. The model equations were solved by collision reaction cross section method, and the results successfully used to predict the concentration distribution of radicals and Hg^0 in the reactor.

2.6 Non-thermal plasma reactor and process flow of Hg^0 removal

2.6.1 Non-thermal plasma reactor

As previously discussed the non-thermal plasma reactor types for Hg^0 oxidation mainly include corona discharge and dielectric barrier discharge. Corona discharge is initiated by partial breakdown of a gas gap in a strong inhomogeneous electric field (Bogaerts et al. 2002; Chang et al. 2002; Tendero et al. 2002; Kogelschatz et al. 2004; McAdams et al. 2001; Li et al. 2014). The active ionization region is restricted to a small volume around the corona electrodes with a small radius of curvature. A passive zone of low conductivity connects the active zone to the opposite electrode and stabilizes the low current discharge (Bogaerts et al. 2002; Chang et al. 2002; Tendero et al. 2002; Kogelschatz et al. 2004; McAdams et al. 2001; Li et al. 2014). The charge carriers in this drift region can be used to charge solid particles and droplets or to induce the formation of chemically reactive species. The corona discharge plasma reactors mainly include three types, namely, needle-plate, wire-plate and wire-cylinder (Bogaerts et al. 2002; Chang et al. 2002; Tendero et al. 2002; Kogelschatz et al. 2004; McAdams et al. 2001; Li et al. 2014). The structure and principle of the three typical corona discharge plasma reactors are shown in Figure 9. The corona discharge plasma reactor with wire-cylinder structure is used widely for Hg^0 oxidation in laboratory studies because of its simple structure and good sealing. The corona discharge plasma reactor with wire-plate structure has better adaptability for flue gas treatment volume, richer industrial design experience and more systematic theoretical foundation because plasma reactor first evolves from electrostatic precipitator (ESP), which widely uses wire-plate structure, and hence, more adaptable for industrial applications (Wu et al. 2006; Lin et al. 2002). Compared with the corona discharge plasma reactor with wire-cylinder and wire-plate structures, the corona discharge plasma reactor with needle-plate structure has a smaller and more

663 inhomogeneous discharge region (Wu et al. 2006; Lin et al. 2002). Thus, reports using the corona discharge

664 plasma reactor with needle-plate structure for Hg^0 oxidation are rare.

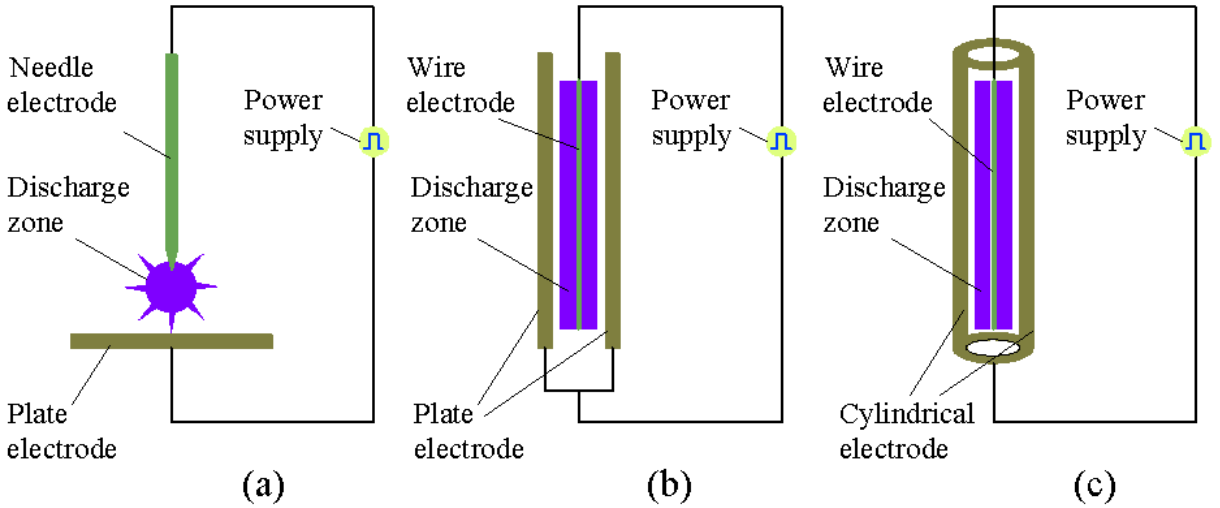

665

666 **Figure 9.** Structure and principle of corona discharge plasma reactors: (a) needle-plate; (b) wire-plate; (c)

667 wire-cylinder.

668 The corona discharge has large discharge space and low onset voltage, but has low electron density and small

669 discharge area. Compared to the corona discharge, the dielectric barrier discharge (DBD) can generate higher

670 electron density as well as more high energy active species that are needed in chemical reactions (Zhou et al.

671 2013). DBD, also referred to silent discharge, is another main way of generating non-thermal plasma at

672 atmospheric pressure. The electrode configuration is characterized by the presence of at least one dielectric barrier

673 or insulator in the current path in addition to the gas gap used for discharge initiation (Tendero et al. 2002;

674 Kogelschatz et al. 2004; McAdams et al. 2001). The discharge is maintained by a large number of short-lived

675 localized current filaments called microdischarges in gases. At least one of these electrodes is covered by a

676 dielectric layer or insulator. To ensure stable plasma discharge operation, the gap which separates the electrodes is

677 limited to a few millimeters wide (Tendero et al. 2002; McAdams et al. 2001).

678

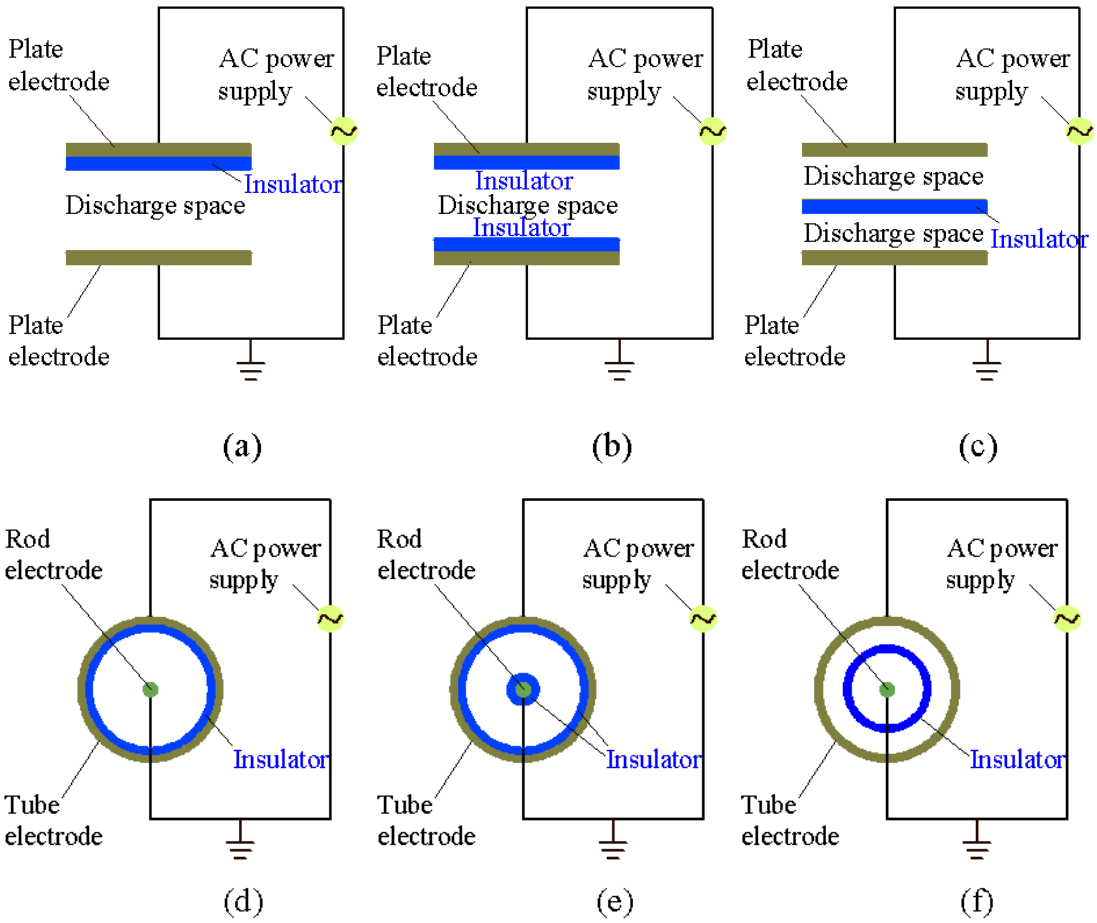

679

680 **Figure 10.** Schematic diagram of specific configuration of several DBD reactors: (a) plate type with a insulator;
681 (b) plate type with two insulator; (c) plate type with a suspended insulator; (d) cylinder type with a insulator; (b)
682 cylinder type with two insulator; (c) cylinder type with a suspended insulator.

683 Recently, DBD has received extensive attention in the field of flue gas mercury control due to its high
684 removal efficiency and environmental compatibility (Kogelschatz et al. 2004; Li et al. 2014). Based on the
685 differences in reactor geometry, DBD can be divided into four types, namely, typical DBD, surface discharge,
686 coplanar discharge and packed-bed discharge. The typical DBD reactor often consists of two plane-parallel metal
687 electrodes with one or two insulators (Kogelschatz et al. 2004; Li et al. 2014). Also, some DBD reactors with
688 rod-tube electrodes have been recently developed for oxidation of Hg^0 in flue gas (Ko et al. 2008; Byun et al.
689 2011; Chen et al. 2006). Depending on the different placed locations and numbers of insulators, these
690 plane-parallel or rod-tube DBD reactors may be further subdivided into three types (Tendero et al. 2002;

691 Kogelschatz et al. 2004; McAdams et al. 2001; Li et al. 2014): (a) an insulator adhered to the high voltage
692 electrode; (b) two insulators respectively adhered to the high voltage electrode and ground electrode; (c) an
693 insulator suspended in the space between the two electrodes. The schematic diagram of configuration of these
694 DBD reactors is depicted in Figure 10.

695 As shown Figure 10, the discharge process of these DBD reactors occurs in the space between the two
696 electrodes. However, An et al. 2014a and 2014b and Yang et al. 2012a recently reported studies using surface
697 discharge plasma (SDP) and packed-bed discharge plasma (PDDP) reactors for oxidation of Hg^0 in flue gas,
698 respectively. The schematic diagram of typical SDP and PDDP reactors are shown in Figure 11. It can be seen
699 from Figure 11 that although both of the SDP and PDDP also belong to the category of the typical DBD, there is
700 some significant differences between them. The discharge process of the SDP occurs mainly at the electrode
701 surface, while the discharge process of the PDDP occurs in the interspaces between fillers, not the common gas
702 space between two electrodes. SDP reactors have aroused considerable interest because of their unique features
703 and characteristics. For example, they are easily manufactured than other DBD reactors, and result in a decrease in
704 the breakdown voltages, and hence better energy efficiency (Malik et al. 2011). Moreover, the flue gas resistance
705 in SDP reactors is much less than those in other DBD reactors due to its much larger electrode gap (An et al.
706 2014a and 2014b). An et al. 2014b recently reported the application of SDP reactor for Hg^0 oxidation, comparing
707 Hg^0 removal efficiency and energy yield in different plasma reactors, as summarized in Table 2. As can be
708 observed from Table 2 the concentric cylinder discharge (CCD) reactor and wire-plate reactor showed lower Hg^0
709 oxidation efficiency and energy yield compared to SDP reactor. Hg^0 oxidation efficiencies obtained by
710 wire-cylinder reactor were comparable with those of SDP reactor, but the energy yields were far lower than that of
711 SDP reactor. Thus, SDP is a more cost-effective method for oxidizing Hg^0 in flue gas.

712 **Table 2.** Comparison of Hg^0 removal efficiency and energy yield in different plasma reactors (An et al. 2014b).

Reactor type	Gas flow ($L\ min^{-1}$)	Hg^0 concentration ($\mu g\ m^{-3}$)	SED ($J\ L^{-1}$)	Oxidation efficiency (%)	Energy yield ($\mu g\ kJ^{-1}$)
CCD reactor	2.5	300	23.7	59	7.5
Wire-plate reactor	2.0	50	18.0	80	2.2
Wire-cylinder reactor	6.0	110	894.0	98	0.1
			80.0	98	1.3
SDP reactor	4.5	110	7.9	98	13.7

713

714 The major characteristic of PDDP reactors is the presence of contact points between pellets and pellets/
715 electrodes (Chen et al. 2008). Because of the short distance near these contact points, the electric field strength is
716 significantly higher than the mean value in the reactor (Chen et al. 2008). The fact that PDDP reactor could
717 achieve higher electric fields has been confirmed in various simulation studies. Chen et al. 2008 reviewed the
718 current progress in PDDP reactor for ozone generation and abatement of air pollutants, mainly including NO_x,
719 VOCs and greenhouse gases. Yang et al. 2012b measured the spectrum of dielectric barrier discharge process at
720 atmospheric pressure in a coaxial reactor, and found that the typical spectrum of N_2 molecule under dielectric
721 barrier discharge was identified in wavelength range of 200-400nm, which covered the most UV-light
722 wavelengths that are suitable for photocatalytic activity. Based on the theories of photocatalysis and PDDP reactor,
723 Yang et al. 2012a recently developed a PDDP reactor, also called combined plasma-photocatalysis reactor, for
724 oxidation of Hg^0 in flue gas by filling TiO_2 in a typical DBD reactor. Compared with the typical DBD process,
725 Hg^0 oxidation efficiency increased by 18.7-26.3 % with the addition of TiO_2 photocatalyst in this kind of
726 combined plasma-photocatalysis reactor.

727 Liu et al. 2015d developed a plasma–catalyst reactor which was used for the adsorption of elemental mercury
728 at low temperatures. SiO_2, TiO_2 and SiO_2/TiO_2 supported transitionmetal oxide catalysts were packed in the
729 plasma discharge zone for adsorption enhancement. The results showed that the plasma–catalyst system displayed

730 a much higher Hg^0 adsorption efficiency than a catalyst only or plasma only system, and a synergistic function
731 between the plasma and catalyst occurred in the plasma–catalyst system. Huang et al. 2016 developed a novel
732 discharge activation reactor and tested removal performance for Hg^0 in simulated flue gas. The results showed that
733 the novel discharge activation reactor could improve the generation of reactive chemical species, such as Cl· or
734 Cl_2, which facilitated the mercury removal.
735

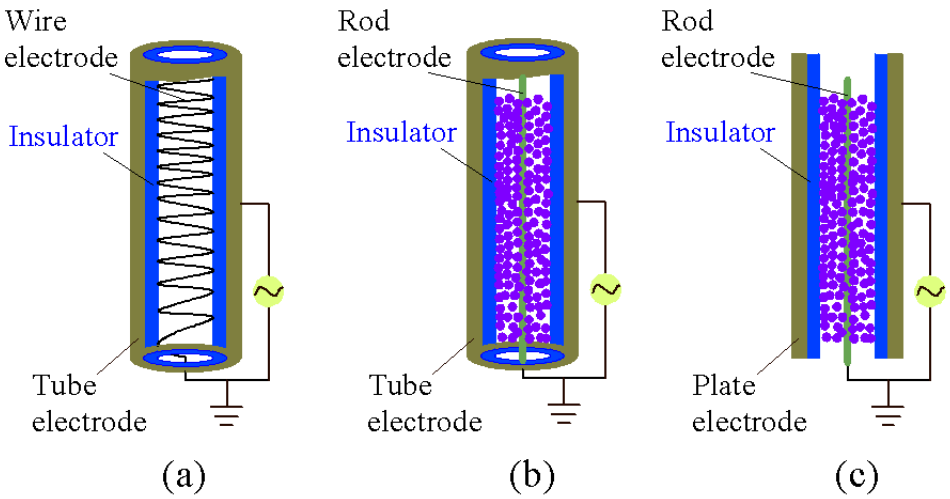

736
737 **Figure 11.** Schematic diagram of surface discharge plasma reactor (a) and packed-bed plasma reactor: (b)
738 cylindrical style and (c) plate style.

739 Related studies (An et al. 2014a; An et al. 2014b; Wu et al. 2006; Lin et al. 2002) showed that the high
740 energy consumption is one of the main obstacles for the commercial applications of flue gas purification using
741 non-thermal plasma. In order to reduce the energy consumption of non-thermal plasma process for flue gas
742 mercury removal, an “indirect oxidation” plasma reactor based on plasma discharge was developed for flue gas
743 purification by several researchers (An et al. 2014a; Wu et al. 2006; Lin et al. 2002). For this kind of plasma
744 reactor, the removal process of contaminants mainly includes two steps: (1) Active substances were first produced
745 by plasma discharge of oxygen-enriched gas stream; (2) Active substances produced were injected into the flue
746 gas stream to oxidize contaminants. This type of plasma reactor consists of two common structures, which are

747 respectively depicted in Figure 12 (a) and (b).

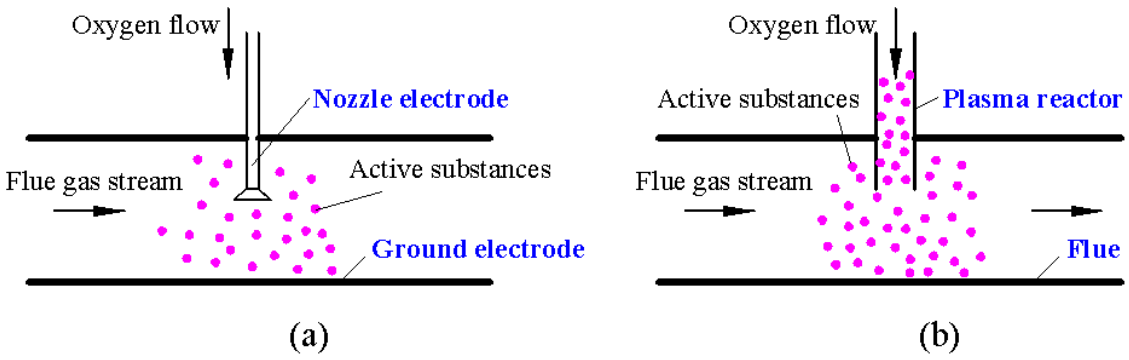

748

749 **Figure 12.** Schematic diagram of "indirect oxidation" plasma reactors: (a) nozzle electrode type and (b) SDP type.

750 It can be seen from the Figure 12 (a) and (b) that the two "indirect oxidation" plasma reactors have the
751 similar principle, but different structures. The former is an integral plasma reactor. The nozzle for injecting active
752 substances itself is also a high-voltage electrode, while the shell of container is the ground electrode. Compared to
753 the former, the latter consists of a plasma reactor which can is easily be retrofitted into the existing boilers to
754 remove Hg^0 in the flue gas by combination with traditional WFGD devices. In a comparative study, An et al.
755 2014a investigated the performance and energy consumption of Hg^0 removal using "indirect oxidation" in the
756 latter reactor. The results indicated that for the same Hg^0 oxidation efficiency, the energy yield of "indirect
757 oxidation" was approximately 7.5 times higher than that of the "direct oxidation", where the polluted flue gas
758 directly flows through the discharge space of the plasma reactor. The energy yields under different SEDs for
759 "indirect oxidation" and "direct oxidation' are listed in Table 3.

760 **Table 3.** Comparison of energy yields under different SEDs for "indirect oxidation" and "direct oxidation" (An et
761 al. 2014a).

SED ($J \cdot L^{-1}$)	Energy yields (μg/kJ)	
	"indirect oxidation"	"direct oxidation"
2.0	27.8	3.7

3.0	24.6	3.3
3.9	20.5	2.7

762

763 **2.6.2 Process flow of Hg^0 removal using non-thermal plasma**

764 Due to the very low concentrations of mercury in flue gas and the huge amount of flue gas, using an
765 independent device to control mercury emission is considered to be an uneconomical method (Wang et al. 2007;
766 Hutson et al. 2008; Su et al. 2013; Adewuyi et al. 2013; Ding et al. 2014; Obradović et al. 2011). Simultaneous
767 removal of multi-pollutants has been recognized as a cost-effective control strategy and has showed very good
768 prospects for development (Wang et al. 2007; Hutson et al. 2008; Su et al. 2013; Adewuyi et al. 2013; Ding et al.
769 2014; Obradović et al. 2011). Currently, the representative process flows of mercury removal using non-thermal
770 plasma involve two strategies. One is the simultaneous removal of Hg^0, NO_x and SO_2 in a single non-thermal
771 plasma reactor using injecting ammonia with schematic diagram shown in Figure 13 (a). According to this
772 strategy, NH_4NO_3, $(NH_4)_2SO_4$ and Hg^{2+} will be first produced from the oxidations of NO_x, SO_2 and Hg^0 as well as
773 the neutralization of NH_3, which finally will form mercury-containing aerosols, and further collected in the back
774 dust collector, generally being electrostatic precipitator (ESP) and/or baghouses. The other strategy is the
775 simultaneous removal of Hg^0, NO_x and SO_2 using a combination of plasma oxidation and WFGD device
776 absorption shown in the Figure 13 (b). For this strategy, the gaseous NO_2, HNO_2, HNO_3, SO_3, H_2SO_4 and Hg^{2+}
777 will be first produced from the oxidations of NO_x, SO_2 and Hg^0 in flue gas, and then will be further absorbed in
778 the back WFGD device. These two strategies can effectively remove NO_x, SO_2 and Hg^0 in flue gas, but both of
779 them are not able to recover mercury resources, which may result in a new mercury secondary pollution in the
780 process and products.

781 This problem may be effectively solved by moving the oxidation process to the front of ESP. Related studies

782 have reported (Yang et al. 2007; Hower et al. 2010; Ahmaruzzaman et al. 2010) that coal-fired fly ash is an
783 effective sorbent for gaseous Hg^{2+}. If the flue gas containing $NO_2/HNO_2/ HNO_3/SO_3/H_2SO_4/Hg^{2+}$ firstly flows
784 through ESP, Hg^{2+} will be captured by coal-fired fly ash through adsorption. The mercury resources may be
785 recovered by high-temperature desorption using flue gas heat or other methods in an additional desorption tower.
786 The remaining $NO_2/HNO_2/HNO_3/SO_3/H_2SO_4$ in flue gas could then be converted into NH_4NO_3 and $(NH_4)_2SO_4$
787 with the injection of NH_3 in the back container or flue. However, it is worth noting that this kind of arrangement
788 also has inherently significant deficiencies. For example, untreated flue gas contains large amounts of particulate
789 matters and corrosive substances such as acid gases and alkali metal vapor, which could have detrimental effects
790 on the electrodes in the plasma reactor, including eroding and wearing them out, and accumulation of particulate
791 matter blocking the small discharge space between the electrodes. It is interesting that “flue injection” or “indirect
792 oxidation” method, which has been mentioned in the previous Section 2.4-(1), may provide a potential solution to
793 this problem. The related process flow is illustrated in the Figure 13 (c) and (d), indicating that the electrodes in
794 plasma reactor does have direct contact with the dust-containing/corrosive substances in the flue gas. This kind of
795 arrangement strategy would effectively avoid the clogging, scouring and corrosion problems of the electrodes and
796 discharge spaces. An et al. 2014a have tested the performance and energy consumption of this process, and they
797 found that with 80% Hg^0 removal efficiency, the energy consumption of this kind of “flue injection” or “indirect
798 oxidation” method was lower than that of several common “direct oxidation” methods, with very good prospects
799 for industrial applications.

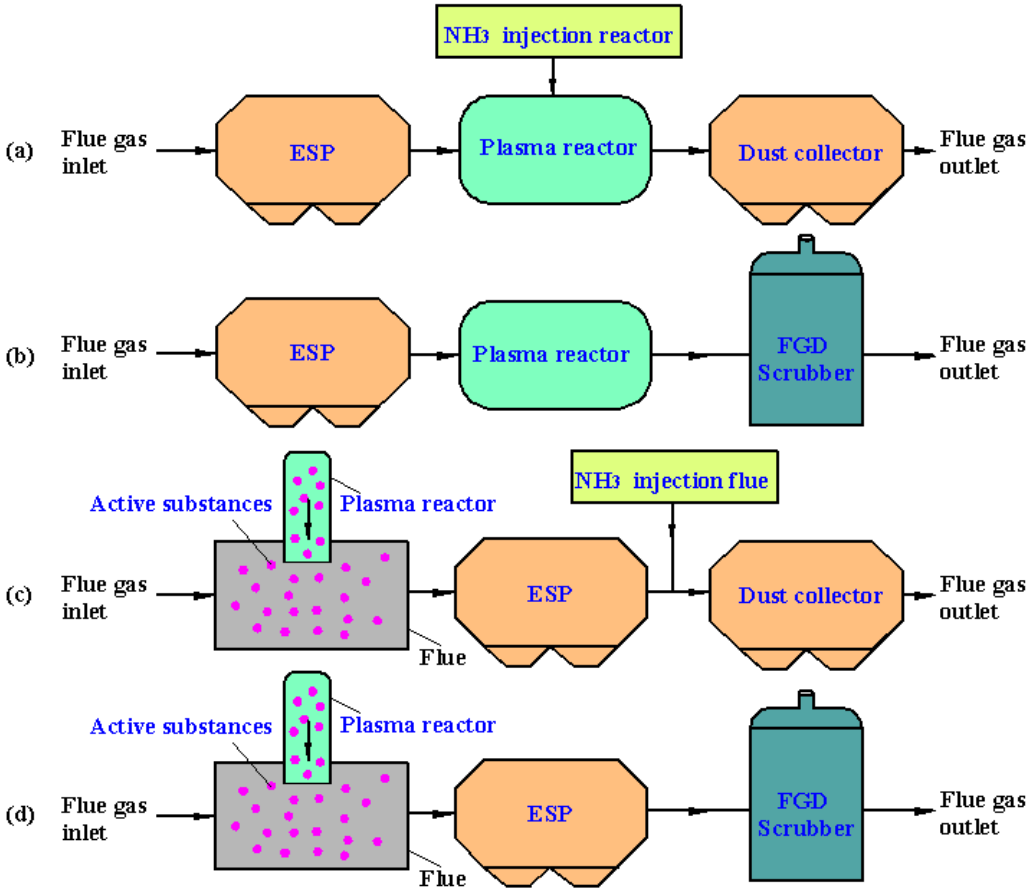

800

801 **Figure 13.** Several potential process flows of mercury removal using non-thermal plasma: (a) Typical plasma
802 removal process; (b) Typical plasma "direct oxidation" & wet scrubbing; (c) SDP plasma "indirect oxidation" &
803 dust; (d) SDP plasma "indirect oxidation" & wet scrubbing.

804

805 ## 3. TiO_2 photocatalytic AOTs for removing Hg^0 in flue gas

806 ### 3.1 Overview of TiO_2 photocatalytic AOTs for removing Hg^0 in flue gas

807 In the past few decades, photocatalytic technologies, as one of AOTs, have received more and more attention
808 because of its broad developmental prospects in the field of energy conversion and environmental protection
809 (Hashimoto et al. 2005; Meng et al. 2007; Thiruvenkatachari et al. 2008; Biswas et al. 1988; Lee et al. 2010;
810 Daghrir et al. 2013; Kumar et al. 2011; Fujishima et al. 1972). To date, many kinds of photocatalysts have been
811 developed, which are summarized in Table 4, but among these photocatalysts, TiO_2 is not only the most popular

812 but also the most promising because of its high activity and stability, low cost as well as nontoxicity (Hashimoto
813 et al. 2005; Meng et al. 2007; Thiruvenkatachari et al. 2008; Biswas et al. 1988; Lee et al. 2010; Daghrir et al.
814 2013; Kumar et al. 2011; Fujishima et al. 1972).

815 **Table 4.** Common semiconductors used in photocatalysis (Daghrir et al. 2013; Kumar et al. 2011, Qi et al. 2016;).

Photocatalysts	band gap (eV)	Valence band (V vs NHE)	Conduction band (V vs NHE)
TiO_2	3.2	+3.1	-0.1
ZnO	3.2	+3.0	-0.2
ZnS	3.7	+1.4	-2.3
SnO_2	3.8	+4.1	+0.3
WO_3	2.8	+3.0	+0.4
CdSe	2.5	+1.6	-0.1
CdS	2.5	+2.1	-0.4
$BiOIO_3$	3.1	+4.1	-0.97

816

817 In 1972, Fujishima and Honda (1972) successfully achieved UV-light induced water cleavage by using a
818 TiO_2 photoanode in combination with a Pt counter electrode immersed in an aqueous electrolytic solution. Since
819 then, this great discovery has led to a powerful and long-lasting research boom for TiO_2 photocatalytic technology
820 all over the world. TiO_2 photocatalytic technology has been widely studied and applied in the field of wastewater,
821 air pollution purification as well as energy conversion (Hashimoto et al. 2005; Meng et al. 2007;
822 Thiruvenkatachari et al. 2008; Biswas et al. 1988; Lee et al. 2010; Daghrir et al. 2013; Kumar et al. 2011;
823 Fujishima et al. 1972). In 1971, Kaluza and Boehm 1971 applied titania as a thin film on a glass slide with a drop
824 of Hg^0, and yellow color (mercury oxide) was observed after 1.5 h under UV irradiation in the range of 390-410

825 nm, demonstrating the feasibility of mercury removal using TiO_2 photocatalytic AOTs. Wu, Lee and Biswas et al.
826 1998 and 2001 made important contribution in utilizing TiO_2 photocatalytic technology for oxidation of Hg^0 in
827 flue gas with good results. Since then, a number of such studies have been conducted world-wide involving the
828 use of pure TiO_2, composite TiO_2, and other doped or coupled TiO_2 with other materials, which have been
829 developed (Worathanakul et al. 2008; Suriyawong et al. 2009; Wang et al. 2011; Lee et al. 2004; Lee et al. 2005;
830 Tsai et al. 2011; His et al. 2012; Pitoniak er al. 2005; Yuan et al. 2011; Jeon et al. 2008; Granite et al. 2008; Chen
831 et al. 2007; Hong et al. 2005; Zhou et al. 2008; Zhuang et al. 2014; Chen et al. 2014). The effectiveness of these
832 materials for Hg removal, details of the mechanisms, kinetics and processes involved, and recent progress on
833 these technologies will be examined in the next sections.

834 **3.2 Pure TiO_2**

835 TiO_2 photocatalytic AOTs have been extensively studied in the field of wastewater treatment and flue gas
836 purification because of its very strong oxidizing and environmentally friendly feature (Chen et al. 2007; Zhou et al.
837 2008; Zhuang et al. 2014; Chen et al. 2014; Seery et al. 2007; Grabowska et al. 2010; Dozzi et al. 2012; Binitha et
838 al. 2009). Wu and Lee 1998 developed in situ-generated TiO_2 photocatalyst with ultraviolet (UV) irradiation to
839 capture Hg^0 in flue gas, and obtained a 96% Hg^0 capture efficiency, which confirmed the feasibility of Hg^0
840 removal from flue gas using TiO_2 AOTs, and spurred further research and developmental studies. Lee and Biswas
841 2001 used three common sorbents (TiO_2, SiO_2 and CaO) to contrast their Hg^0 capture capabilities in an entrained
842 flow reactor, and the results showed that TiO_2 in the presence of UV irradiation was most effective for Hg^0 capture,
843 resulting in a greater than 98% Hg^0 capture efficiency. CaO particles only had a 33% Hg^0 capture efficiency, while
844 SiO_2 was completely ineffective for Hg^0 capture. Worathanakul et al. 2008 evaluated the performance of
845 commercially available (four types of iron oxide, TiO_2, titania pillared clay) and in-house synthesized (magnetite
846 and SUZ-4 zeolite) sorbents for Hg^0 capture in a differential bed reactor, and they found that TiO_2 showed the

847 greatest potential for capturing Hg^0 with UV irradiation due to the high capture efficiency.

848 Related studies (Linsebigler et al. 1995; Kwon et al. 2008) verified that TiO_2 from different synthesis
849 methods often had different Hg^0 removal performances. Suriyawong et al. 2009 tested the performance of Hg^0
850 capture by nano-structured TiO_2 with different synthesis methods under UV irradiation, and they found that the
851 pre-synthesized nano-structured TiO_2 demonstrated the highest Hg^0 capture efficiency because of its larger surface
852 area and higher proportion of anatase to rutile, followed by in-situ generated and commercial TiO_2 (Degussa, P25).
853 Wang et al. 2011 prepared a novel titania nanotube (TNT) with vast surface area and high porosity by
854 hydrothermal method to remove Hg^0 in flue gas, and their results showed that the TNT exhibited an excellent Hg^0
855 removal efficiency. In addition, Lee et al. 2004 and 2005 tested the removal performance of Hg^0 using various
856 light sources, and they found that Hg^0 removal was significantly affected by different light sources. Tsai and His
857 2011 and 2012 synthesized oxygen-vacant titanium dioxide (TiO_{2-x}) nanoparticles using N_2/Ar/He and He/Ar
858 thermal plasma as two heating sources and evaluated their photocatalytic activity for capturing gaseous Hg^0. The
859 results showed that both TiO_{2-x} nanoparticles demonstrated good photocatalytic activity for capturing Hg^0 under
860 UV-light and visible-light because of the formation of oxygen-vacant sites. Granite et al. 2008 used commercially
861 available self-cleaning windows (titania-coated glass) to sequester mercury from oxygen-nitrogen mixtures in a
862 specially designed photo-reactor, and verified the possibility of removing mercury using the self-cleaning
863 windows. Wu et al. 2015b synthesized TiO_2 hollow sphere by hydrothermal method, and studied the the removal
864 performance of gaseous elemental mercury under UV light. The results showed that the mercury removal
865 efficiency reached up to 82.75%.

866 **3.3 Composite of TiO_2 with other materials**

867 TiO_2 powders with UV irradiation have proven to be an effective mercury sorbent/catalyst in the laboratory
868 (Wu et al. 1998; Lee et al. 2001). However, TiO_2 powders were easily washed away with the flue gas stream and

869 also lightly agglomerate together to form larger clusters due to the presence of water vapor in coal-fired flue gas
870 (Hashimoto et al. 2005; Thiruvenkatachari et al. 2008). reover, pure TiO_2 powders have a very low adsorption
871 capacity for gaseous pollutants, which is not conducive to photocatalytic reaction because the adsorption process
872 is often the rate-controlling step (Hashimoto et al. 2005; Thiruvenkatachari et al. 2008; Lee et al. 2001). Therefore,
873 to avoid the loss and agglomeration of TiO_2 powders and to provide stronger adsorption capacity, TiO_2 powders
874 typically need to be coated on a variety of support materials with larger specific surface area and stronger
875 adsorption capacity, also referred to as the carriers, to be more adaptable for future industrial applications.
876 Common TiO_2 support materials or carriers include reactor walls, glass beads, metal oxides, carbon-based
877 materials, zeolites, silicone, natural mineral materials, and even some organic materials (Hashimoto et al. 2005;
878 Meng et al. 2007; Thiruvenkatachari et al. 2008; Biswas et al. 1998).

879 Nanostructured silica gel has excellent adsorption capacity and good light transmission, and is one of the
880 most common sorbents/carriers (Hashimoto et al. 2005; Thiruvenkatachari et al. 2008). Pitoniak et al. 2003, 2004
881 and 2005 developed SiO_2-TiO_2 composites using a sol-gel method to remove Hg^0 from flue gas with UV
882 irradiation. The results showed that the composites achieved a more than 99% Hg^0 removal efficiency due to the
883 synergistic adsorption and photocatalytic oxidation roles of the catalyzer and carrier. Yuan et al. 2011 and 2012
884 prepared a TiO_2-aluminum silicate fiber nanocomposite by sol-gel method to capture Hg^0 in flue gas under UV
885 irradiation, and obtained a 84% Hg^0 removal efficiency. Jeon et al. 2008 developed several nanotitanosilicates by
886 three different carrier gases (air, N_2, and Ar) in a diffusion flame reactor, and achieved a 88% Hg^0 capture
887 efficiency. Wu et al. 2015a prepared a low cost CuO/TiO_2 photocatalysts and test the removal performance of
888 gaseous elemental mercury under UV light and visible light (both xenon lamp and LED), respectively. The results
889 showed that the CuO/TiO_2 photocatalysts were highly efficient in oxidizing Hg^0, reaching above 70% in all cases
890 under UV light, peaking at 57.8% with 1.25 wt.% CuO under visible light and peaking at about 60% with 1.25

891 wt.% CuO under LED light.

892 Activated carbon fiber (ACF) is a promising sorbent/carrier due to its huge surface area, developed gap
893 structure and good thermal conductivity (Hashimoto et al. 2005; Thiruvenkatachari et al. 2008). Hsi et al. 2012
894 developed a TiO_{2-x}/ACF composite via a N_2/Ar/He thermal plasma system, and also achieved an efficient Hg^0
895 removal with UV irradiation. Biomass coke is the byproduct from gasification process of biomass materials, and
896 has been widely studied for flue gas purification because of its good pore structure and surface properties as well
897 as low cost and wide sources (De et al. 2013; Tan et al. 2011). Tan et al. 2010 prepared a novel char /nano-TiO_2
898 photocatalyst by sol-gel method to remove Hg^0 in flue gas, and obtained a 86% Hg^0 removal efficiency in the
899 presence of 10% oxygen. Fly ash, generated during coal combustion, is an industrial by-product, and has been
900 proven to be an effective and potential mercury sorbent because of its low costs and huge reserves (Yang et al.
901 2007; Hower et al. 2010; Ahmaruzzaman et al. 2010). Fang et al. 2013 developed a TiO_2 /coal fly ash by
902 impregnation method to capture Hg^0 in flue gas, and achieved a 63.8% Hg^0 conversion. Shen et al. 2016 prepared
903 the WO_3/TiO_2 photocatalysts by sol-gel synthesis, which are immobilized on the surfaces of glass beads. The
904 authors studied the photo-oxidation efficiencies of elemental mercury at high temperatures, and the results showed
905 that the photo-oxidation efficiency of Hg^0 was greatly enhanced by WO_3 dopant at a high temperature of 160
906 Celsius. The improvement was due to the modification of WO_3 that enlarged the band gap energy of TiO_2 and
907 effectively promoted the separation of photo-induced electrons and holes.

908 **3.4 Doped or coupled TiO_2 using other materials**

909 Although TiO_2 has been recognized as a promising photocatalyst, the large band gap and the fast
910 recombination of photogenerated electron-hole pairs limit its further development (Daghrir et al. 2013). Results of
911 related studies (Kumar et al. 2011) suggest that TiO_2 could only be activated in the UV irradiation region with a
912 lower than 387 nm wavelength due to its large band gap (3.2 eV for anatase and brookite, 3.0 eV for rutile). The

fact that it can only absorb less than 5% of solar energy (solar light consists of 5% UV, 43% visible, and 52% harvesting infrared light) (Daghrir et al. 2013; Kumar et al. 2011), which has prevented its large-scale applications for free solar energy with huge reserves (Daghrir et al. 2013). A large number of studies (Hashimoto et al. 2005; Meng et al. 2007; Thiruvenkatachari et al. 2008; Biswas et al 1998; Lee et al. 2010; Daghrir et al. 2013) have shown that the former problem of charge carriers recombination can be overcome by modifying the electronic band structure of TiO_2 using various strategies including coupling with a narrow band gap semiconductor, cation/anion doping, co-doping with two or more, surface sensitization by organic dyes or metal complexes, and noble or poor metal deposition. The latter can be improved by changing the surface properties of TiO_2 by fluorination or sulfation, or by adding suitable electron acceptors besides molecular oxygen in the reaction mediums (Hashimoto et al. 2005; Meng et al. 2007; Thiruvenkatachari et al. 2008; Biswas et al 1998; Lee et al. 2010; Daghrir et al. 2013). Some common modified methods for TiO_2 are summarized in Figure 14.

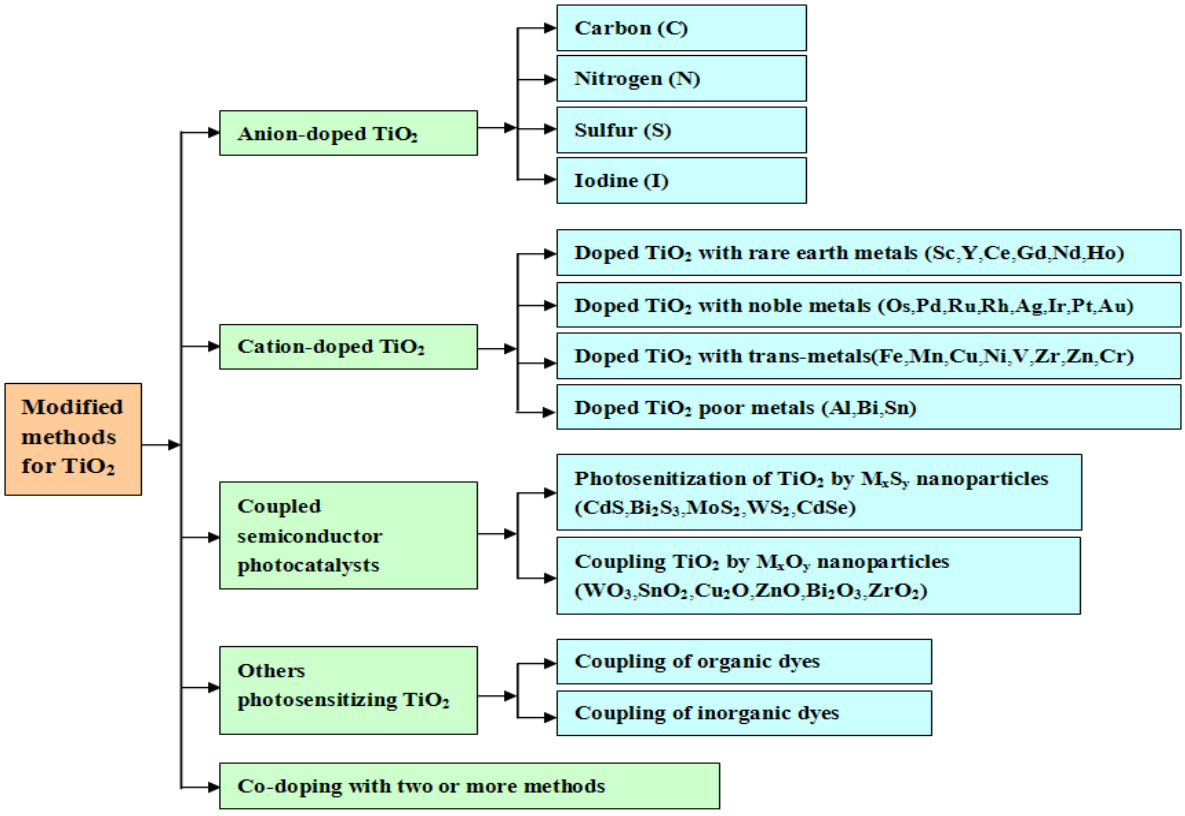

Figure 14. Some common modified methods for TiO_2.

3.4.1 Anion-doped TiO_2

A large number of doping methods recently have been used to extend the spectral response of TiO_2 into the visible region and to enhance its photocatalytic activity. Doping TiO_2 with anionic nonmetals such as carbon (C) (Chen et al. 2004; Ren et al. 2007), nitrogen (N) (Asahi et al. 2001; Burda et al. 2003; Diwald et al. 2004), sulfur (S) (Ohno et al. 2003; Umebayashi et al. 2002; Umebayashi et al. 2003), and iodine (I) (Hong et al. 2005) or co-doping with these anionic nonmetals (Chen et al. 2007; Zhou et al. 2008) have received an increasing attention. Related studies (Chen et al. 2004; Ren et al. 2007) showed that carbon doping of TiO_2 was an acceptable choice for improving the above problems. The substitution of C atoms in TiO_2 photocatlyst introduces new states (C 2p) close to the valence band edge of TiO_2 (O 2p). Accordingly, the conduction band edge shifts and narrows the band gap. The incorporation of C into TiO_2 may form carbonaceous species on the surface of photocatalyst, which has been reported to facilitate the absorption for visible light (Wu et al. 1998; Chen et al. 2007; Ren et al. 2007). Hsi et al. 2012 developed an oxygen-vacant TiO_{2-x}/activated carbon fiber composite via a N_2/Ar/He thermal plasma system, and achieved an effective removal of Hg^0 from flue gas under visible-light irradiation. Zhuang et al. 2014 synthesized a carbon-modified TiO_2 nanotubes (CTNTs) via a hydrothermal method to capture Hg^0 in flue gas under the irradiation of white light LED lamps, and they found that the catalyst exhibited a high visible-light photocatalytic performance for Hg^0 in flue gas, and achieved a 90% Hg^0 oxidation. Doping TiO_2 with nonmetals such as N element can effectively change the refraction index, hardness, electrical conductivity, elastic modulus, and the photocatalytic activity toward the visible light absorption (Daghrir et al. 2013; Kumar et al. 2011; Asahi et al. 2011; Burda et al. 2003; Diwald et al. 2004). Chen et al. 2014 prepared a N-doped TiO_2 nanoparticles that exhibited a narrow band gap by calcining a mixture of Degussa P-25 TiO_2 and NH_4Cl for Hg^0 removal in flue gas. XPS and UV/Vis diffuse reflectance spectra indicated that the molecular state N was incorporated into a TiO_2 lattice, causing an observable shift of the absorption edge to along wavelength of 441 nm. Moreover, the N-doped

948 TiO_2 nanoparticles not only have a high photocatalytic activity for Hg^0 capture but also can effectively resist the
949 competitive adsorption from moisture and negative photocatalytic effects caused by other flue gas components.

950 **3.4.2 Cation-doped TiO_2**

951 TiO_2 doped with cations such as noble metals (Seery et al. 2007; Grabowska et al. 2010; Dozzi et al. 2012;
952 Binitha et al. 2009), poor metals (Depero et al. 2000; Ji et al. 2009; Sui et al. 2010; Fresno et al. 2006), rare earth
953 metals (Stengl et al.2009; El-Bahy et al. 2009; Fan et al. 2006; Shi et al. 2009) and transition metals (Kment et al.
954 2010; Paola et al. 2002; Sun et al. 2009; Asilturk et al. 2009) or co-doped with these cations (Zhang et al. 2011a;
955 Hsieh et al. 2009) have been widely studied in many research fields including mercury capture, and the results
956 have shown that cations doping or co-doping TiO_2 broadened the light absorption range, increased the redox
957 potential of photogenerated free radicals, as well as strengthened the quantum efficiency by inhibiting the fast
958 recombination of photogenerated electron-hole pairs. Tsai et al. 2013 successfully prepared transition metal
959 Cu-doped TiO_2 nanoparticles via a single-step process using Cu powder and Degussa P-25 nanoparticles in a
960 non-transferred plasma torch system, and they found that the Cu-doped TiO_2 exhibited a good photocatalytic
961 activity for Hg^0 removal under visible-light irradiation. Dai et al. 2012 prepared Fe-doped TiO_2 nanocomposites
962 for Hg^0 removal by direct dissolution method, and obtained a higher Hg^0 conversion as compared to pure TiO_2.
963 Related studies (Kment et al. 2010; Paola et al. 2002) showed that doping TiO_2 with transition metals could
964 effectively tune the electronic structure and shift the light absorption region from the UV to the visible-light,
965 enhancing the photocatalytic activity. The shift of the absorption edge to the visible light region was mainly
966 caused by the charge-transfer transition between the d electrons of the transition metals and the conduction or
967 valence band of TiO_2 (Wu et al. 1998; Lee et al. 2001; Kment et al. 2010; Paola et al. 2002). The coping generated
968 a new electron state in the electronic structure of TiO_2, which was able to capture the excited electrons from TiO_2
969 valence band and prevented the recombination of charge carriers (Kment et al. 2010; Sun et al. 2009; Asilturk et al.

970 2011). Aluminum is one of the most abundant metals found in Earth's crust, and classified as poor metal. Tsai and
971 coworkers (2012) developed a Al-doped TiO_2 visible-light photocatalyst via a single step using vaporized Ti, Al,
972 and O_2 in a non-transferred plasma torch system. Results showed that the formed Al-doped TiO_2 nanoparticles
973 were a mixture of anatase and rutile phase and had a size between 10 and 105 nm, with the absorption spectra
974 shifting towards the visible light region. Hg^0 breakthrough tests revealed that the nanoparticles had an appreciable
975 Hg^0 removal under visible-light irradiation. The results of a related study (Depero et al. 2000), indicate doping
976 TiO_2 with Al hinders the phase transformation of TiO_2 from anatase to rutile by stabilizing the surface state and
977 inhibiting the grain growth of TiO_2 particles.

978 **3.4.3 Coupled TiO_2 with other semiconductors or metallic oxides**

979 Coupling with other semiconductors or metallic oxides with different energy levels is another effective
980 approach to extend the absorption wavelength range and to hinder the recombination of photogenerated charge
981 carriers (Daghrir et al. 2013; Kumar et al. 2011; Zhang et al. 2009). A large number of studies (Daghrir et al. 2013;
982 Kumar et al. 2011; Robert et al. 2007; Zhang et al. 2009; Hernàndez-Alons et al. 2009; Ilieva et al. 2012;
983 Bessekhouad et al. 2004; Kannaiyan et al. 2010; Shang et al. 2004; Ho et al. 2004; Coehoorn et al. 1987; Lo et al.
984 2004) have shown that an appropriate coupling between conduction band and valence band of two kinds of
985 semiconductors or metallic oxides often could achieve an effective transfer of charge carriers from one to another.
986 When the large band gap of TiO_2 is coupled with a small band gap semiconductor with more negative conduction
987 band level, the electron could be injected from the small band gap of the semiconductor used as a sensitizer to the
988 TiO_2, thereby promoting the separation between the photogenerated electron-holes (Robert et al. 2007; Zhang et al.
989 2009; Hernàndez-Alons et al. 2009; Ilieva et al. 2012; Bessekhouad et al. 2004; Kannaiyan et al. 2010; Shang et al.
990 2004; Ho et al. 2004; Coehoorn et al. 1987; Lo et al. 2004). Yuan et al. 2012a, 2012b and 2012c prepared several
991 coupled TiO_2 nanofibers with semiconductors and metal oxides, including CuO, In_2O_3, V_2O_5, WO_3 and Ag_2O, by

992 an electrospinning method, and tested them for Hg^0 removal from flue gas under dark, visible light and UV
993 irradiation, respectively. The results indicated that, compared to pure TiO_2, the UV-vis absorption intensities of
994 coupled TiO_2 nanofibers significantly increased and the absorption bandwidth also expanded, especially for
995 Ag_2O-TiO_2 and V_2O_5-TiO_2. WO_3-doped TiO_2 exhibited the highest Hg^0 removal efficiency of 100% under UV
996 irradiation. Doping V_2O_5 into TiO_2 enhanced Hg^0 removal efficiency greatly from 6% to 63% under visible light
997 irradiation.

998 **3.5 Effects of flue gas components on Hg^0 removal using TiO_2 photocatalytic AOTs**

999 Coal-fired flue gas is a complex mixture containing fly ash particles, moisture, CO, and many acid gases
1000 (Granite et al. 2002). Therefore, studying the influences of several flue gas components, including H_2O, O_2, SO_2
1001 and NO, on TiO_2 photocatalytic removal of Hg^0 in flue gas deserves important consideration.

1002 **3.5.1 Effects of H_2O**

1003 Pitoniak et al. 2003 studied the effects of relative humidity on Hg^0 capture using SiO_2-TiO_2 composite with
1004 UV irradiation, and they found that the relative humidity impeded Hg^0 adsorption, thereby decreasing Hg^0
1005 removal efficiency. Based on the results of Pitoniak et al. 2003, Li et al. 2006, 2007 and 2008 further investigated
1006 the role of moisture on Hg^0 removal as well as the corresponding mechanism, and they found that water vapor
1007 dramatically suppressed both Hg^0 adsorption and photocatalytic oxidation because of the significant reemission of
1008 captured Hg^0 on the nanocomposite. This phenomenon was ascribed to the repellant effect of the adsorbed water
1009 vapor to the captured Hg^0 on TiO_2 surface because of the super-hydrophilic properties of TiO_2 surface (Li et al.
1010 2006, 2007 and 2008). Tsai et al. 2011 and 2012a and Hsi et al. 2012 also found that the presence of moisture had
1011 a negative impact on Hg^0 removal using two kinds of oxygen-vacant TiO_{2-x} nanoparticles and TiO_{2-x}/ACF
1012 composite with UV and visible light irradiation, respectively; and verified these results to be due to the reemission
1013 of Hg species from these photocatalysts surface due the competitive adsorption for the active sites between Hg

1014 species and H_2O. Tsai et al. 2012b and 2013, Chen et al. 2014 and Cho et al. 2012 also obtained the similar results
1015 in studying the photocatalytic removal of Hg^0 using Cu-doped, Al-doped, N-doped TiO_2 and pure TiO_2
1016 nanoparticles with UV, visible light and household fluorescent lighting irradiation. The results suggest that
1017 moisture could suppress Hg^0 removal using pure or doped TiO_2 photocatalytic AOTs due to the reemission of Hg
1018 species from TiO_2 surface. A typical coal-fired flue gas often contains 5%-7% H_2O (Granite et al. 2002), therefore,
1019 the need to suppress the negative effects of H_2O is an important research issue. Related studies (Chen et al. 2014;
1020 Tsai et al. 2012b) have verified that doped TiO_2 with metal or non-metallic materials was one of the effective
1021 methods for suppressing the reemission of captured Hg^0 on catalyst surface. Tsai et al. 2012b prepared Cu-doped
1022 TiO_2 nanoparticles, and found it to effectively suppress Hg reemission from TiO_2 surface. Chen et al. 2014
1023 prepared N-doped TiO_2 nanoparticles for Hg^0 removal and showed that the reemission of adsorbed Hg on TiO_2
1024 surface caused by H_2O competition for active sites was markedly inhibited by N modification, possibly due to the
1025 strong bonding between Hg, N, and O groups.

1026 **3.5.2 Effects of O_2**

1027 The results of Hsi (2012) and Tsai (2011 and 2012a) using two kinds of oxygen-vacant TiO_{2-x} nanoparticles
1028 and a kind of TiO_{2-x}/ACF composite with UV and visible light irradiation, respectively, showed that the presence
1029 of O_2 enhanced Hg^0 removal. Tsai et al. 2013 found that Hg capture was enhanced with increasing O_2
1030 concentration using Cu-doped TiO_2 photocatalyst under visible-light irradiation. The results of Yuan et al. 2012a
1031 and 2012b indicated that O_2 exhibited a promotional effect on Hg^0 removal using TiO_2-aluminum silicate fiber
1032 under UV irradiation. Chen et al. 2014 also obtained similar results in studying the photocatalytic removal of Hg^0
1033 using N-doped TiO_2 under UV and visible-light irradiation. Related results (His et al. 2012; Yuan et al. 2012d; Li
1034 et al. 2006) also showed that the promotional effect of O_2 on photocatalytic removal of Hg^0 was mainly attributed
1035 to the formation of lattice oxygen and the enhancement of catalytic oxidation.

3.5.3 Effects of SO_2

Li et al. 2007 and 2008 studied the effect of SO_2 on Hg^0 removal using SiO_2-TiO_2 composite with UV irradiation showed that SO_2 promoted the oxidation of Hg^0 to Hg^{2+}, resulting in a higher Hg^0 removal efficiency. Yuan et al. 2012a, 2012d and 2012e also tested the effects of SO_2 on Hg^0 removal using TiO_2-aluminum silicate fiber with UV irradiation, and also found that SO_2 had a promotional effect on Hg^0 oxidation. The results of Chen et al. 2014 using N-doped TiO_2 under UV and visible-light irradiation, showed that SO_2 had a negative impact Hg^0 removal Lee et al. 2004 and Cho et al. 2012 also obtained similar negative results in studying TiO_2 photocatalytic removal of Hg^0 using UV and household fluorescent lighting irradiation, respectively. However, Zhuang et al. 2014 obtained a more complex result which showed that low concentrations of SO_2 had almost no effect on Hg^0 oxidation, but high concentrations of SO_2 reduced Hg^0 oxidation when using carbon modified TiO_2 nanotubes under irradiation of visible-light LED. The multiple effects of SO_2 on photocatalytic removal of Hg^0 are attributed mainly to two factors. On the one hand, the presence of appropriate SO_2 may enhance Hg^{2+} transform into more stable $HgSO_4$, which can effectively suppress Hg reemission from the TiO_2 surface (Yuan et al. 2012b; Li et al. 2007; Li et al. 2008; Yuan et al. 2012e). However, on the other hand, the presence of excess SO_2 may substantially consume $O_2^{-}\cdot$ and $\cdot OH$ and occupy the active sites on TiO_2 surface by competing with Hg^0 (Suriyawong et al. 2009; Zhuang et al. 2014; Chen et al. 2014; Cho et al. 2012), thereby reducing removal of Hg^0. The impact of SO_2 on Hg^0 oxidation will show different results depending on the experimental conditions and reaction systems.

3.5.4 Effects of NO

Li et al. 2007 and 2008 examined the effects of NO on Hg^0 removal using SiO_2-TiO_2 composite with UV irradiation, and showed that NO had a dramatic inhibitory effect on Hg^0 removal. Also, Yuan et al. 2012a and 2012e, Chen et al. 2014, Zhuang et al. 2014 and Cho et al. 2012 found that NO inhibited Hg^0 removal using

1058 TiO_2-aluminum silicate fiber, N-doped TiO_2, carbon modified TiO_2 nanotubes and TiO_2-coated glass beads under
1059 UV-light, visible-light, visible-light LED and household fluorescent lighting irradiation, respectively. Other
1060 researchers (Zhuang et al. 2014; Chen et al. 2014; Li et al. 2007 and 2008; Cho et al. 2012; Yuan et al. 2012e)
1061 suggested that the negative effect of NO on photocatalytic removal of Hg^0 should be attributed to NO occupying
1062 the adsorption sites on TiO_2 surface and consuming $O_2^{-}\cdot$ and $\cdot OH$ free radicals by competing with Hg^0.

1063 **3.5.5 Effects of other components such as HCl and NO_2**

1064 HCl and NO_2 are also widely present in the actual coal-fired flue gas (Granite et al. 2002), and have been
1065 shown to have significant impacts on Hg^0 oxidation in other combustion chemistry fields (Hou et al. 2014; Tan et
1066 al. 2010; Ko et al. 2008). Cho et al. 2012 studied the effects of HCl on the photocatalytic removal of Hg^0 using
1067 TiO_2-coated glass beads under household fluorescent lighting irradiation, and they found that Hg^0 removal
1068 efficiency slightly decreased with increasing HCl concentration from 30 ppm to 120 ppm. The results of Chen et
1069 al. 2014 indicated that HCl also had a negative impact on Hg^0 removal using N-doped TiO_2 under UV and
1070 visible-light irradiation. Li et al. 2007 and 2008 examined the effects of HCl and NO_2 on Hg^0 removal using
1071 SiO_2-TiO_2 composite with UV irradiation and determined that NO_2 had no significant effect on Hg^0 removal,
1072 while HCl promoted Hg^0 removal. The dual effects of HCl were attributed mainly to two phenomena (Chen et al.
1073 2014; Li et al. 2007 and 2008; Cho et al. 2012): (1) HCl can occupy the adsorption sites on TiO_2 surface and
1074 consume $O_2^{-}\cdot$ and $\cdot OH$ free radicals; (2) HCl can effectively promote the heterogeneous catalytic oxidation of Hg^0,
1075 which has been widely reported by in many studies (Hou et al. 2014; Tan et al. 2010; Ko et al. 2008).

1076 **3.6 Effects of process parameters on Hg^0 removal using TiO_2 photocatalytic AOTs**

1077 **3.6.1 Effects of calcination temperature**

1078 Calcination temperature often has a significant influence on physical and chemical properties of adsorbent/
1079 catalyst, as widely reported in the field of catalysis and adsorption (Yang et al. 2007; Gao et al. 2011). Lee and his

1080 group (2006) examined the effects of calcination temperature for the photocatalytic activity and the ability of in
1081 situ generated TiO_2 to capture Hg^0 under UV irradiation. The results showed that Hg^0 capture efficiencies for TiO_2
1082 particles generated at 500℃, 650℃, 750℃, 850℃ and 1000℃ were 3.3%, 14.2%, 25.3%, 41.4%, and 62.5%,
1083 respectively. It was found that Hg^0 capture efficiency increased with increasing calcination temperature. It was
1084 suggested that, with increasing calcination temperature, the overall TiO_2 aggregate size increased, which made
1085 TiO_2 become more open-structured, resulting in easier access to Hg^0 and UV light, and subsequently leading to an
1086 improved Hg^0 capture (Lee et al. 2006). It has also been demonstrated that the anatase phase in TiO_2 was the
1087 preferred crystalline for photocatalytic reaction because of its more excellent photocatalytic capability as
1088 compared to rutile phase (Lee et al. 2010; Kumar et al. 2011). Yuang et al. 2012d and 2012e tested the effects of
1089 calcination temperature on photocatalytic activity of TiO_2-aluminum silicate fiber for capturing Hg^0 in flue gas
1090 under UV irradiation by detecting the changes in anatase and rutile contents. It was observed that the anatase was
1091 the exclusive phase of TiO_2 at calcination temperature below 500℃. However, the anatase phase turned gradually
1092 into the rutile phase when calcination temperature further increased, resulting a lower Hg^0 capture efficiency.
1093 Zhuang et al. 2014 also studied the effects of calcination temperature in the 200-500℃ range on Hg^0 removal
1094 using carbon modified titanium dioxide nanotubes under visible-light LED irradiation, and found that, the catalyst
1095 calcinated at 300℃ exhibited the best photocatalytic activity, with 90% Hg^0 oxidation capability in a long time
1096 light-on test. The superior activity of the catalyst calcinated at 300℃ was ascribed to the expanded light
1097 adsorption spectrum resulting from carbon doping, the high surface area and the well sustained structure of the
1098 nanotubes (Zhuang et al. 2014).

1099 Wang et al. 2011 tested the effects of calcination temperature in the 0-600℃ on Hg^0 removal using titania
1100 nanotubes (TNTs) under UV irradiation, and showed that the catalyst calcinated at 500℃ exhibited the best
1101 removal performance for Hg^0. The results of XRD patterns of the calcined TNTs showed that anatase crystals

were few in the original nanotubes, and could not be formed at 300℃, but were formed and enlarged at 400℃ and 500℃, enhancing photocatalytic activity. However, with further increase in calcination temperature to 600℃, the nanotubes were completely transformed to rodlike particles, indicating the sintering of tubes, greatly reducing photocatalytic activity. Yang et al. 2009 also tested the removal performance of Hg^0 using TiO_2-AC and TiO_2-fiber with UV irradiation at 500℃ and 700℃, found that the catalyst calcined at 500℃ has better Hg^0 removal performance than that at 700℃. The results of XRD, SEM and BET indicated that the anatase with higher activity was observed to be the only phase of TiO_2 at 500℃, while the mixture of anatase and rutile co-existed in TiO_2 at 700℃. In addition, increasing the heat treatment temperature promoted the growth of TiO_2 particles and agglomerates, destroying the nanostructures of the catalyst. The authors suggested (Yang et al. 2009) that the different results observed at 500℃ and 700℃ are attributable to the changes of the anatase phase contents and the properties of the nanostructures. Based on the above comments, it can be seen that calcination temperature has a very significant impact on the physical (surface and structural characteristics) and chemical (crystal type and proportion) properties of TiO_2, and typically there is an optimum value.

3.6.2 Effects of doping or coupling amount with other materials

Based on the results of prior studies (Wu et al. 1988; Lee et al. 2001; Chen et al. 2007; Asahi et al. 2001; Diwald et al. 2004; Zhang et al. 2011; Yuan et al. 2012d) and as indicated earlier, the doped TiO_2 using other materials can broaden the absorption range of light and enhance the quantum efficiency by inhibiting the fast recombination of the photogenerated electrons and holes. Related studies (Wu et al. 1988; Lee et al. 2001; Chen et al. 2007; Zhang et al. 2011; Yuan et al. 2012d) have demonstrated that the concentration of dopant substantially influenced the TiO_2 photocatalytic activity. Yuan et al. 2012b prepared TiO_2-WO_3 nanofibers by electrospinning method and examined the effects of doping content of WO_3 on Hg^0 capture. The results indicated that the UV-Vis absorption intensity, specific surface area and pore volume of TiO_2-WO_3 nanofibers significantly increased with

increasing WO_3 doping content, compared to the pure TiO_2. As a result, Hg^0 removal efficiency was also greatly improved by doping WO_3, up to 100% at a doping content of 7 wt% WO_3. Tsai et al. 2012 examined the effects of Al_2O_3/Ti mass ratios (0 to 0.5) on Hg^0 capture using Al-doped TiO_2 nanoparticles under visible-light (VL) irradiation, and their results indicated that the absorption spectra of the nanoparticles shifted towards the visible light region with doping Al, and showed a strong absorption in visible light range at the doping ratio of Al_2O_3/Ti = 0.5. Tsai et al. 2013 examined the effects of doping Cu content in the range of 0-5wt% Cu/(Cu+TiO_2) mass ratios on Hg^0 removal using Cu-doped TiO_2 nanoparticles under visible-light, and they found that the crystal structure of the formed nanoparticles primarily consisted of anatase and rutile, but the mass fraction of anatase decreased with increasing doping Cu content. The result of UV-Vis spectrum indicated that the absorption wavelength extended to the visible light range with the addition of Cu, and 5 wt% was found to be the optimal doping content. Pitoniak et al. 2003 tested the effects of TiO_2 loading mass on Hg^0 removal using SiO_2-TiO_2 composite, and they found that 13 wt% TiO_2 showed the best performance. Fang et al. 2010 examined the effects of TiO_2 loading mass using TiO_2/coal fly ash, indicating that the loading of 3% TiO_2 on coal fly ash achieved the highest Hg^0 removal efficiency.

3.6.3 Effects of light sources

Light source is regarded as one of three essential elements of a photocatalytic process (other two are photocatalyst and photoreactor), which not only affects photocatalytic efficiency, but also dominates energy consumption and cost of system (Worathanakul et al. 2008). Related studies (Worathanakul et al. 2008) showed that Hg^0 removal using TiO_2 photocatalysis was significantly affected by the light sources. Lee et al. 2004 investigated Hg^0 removal by TiO_2 photocatalysis using various light sources, including UV black light, UV sterilizing light, fluorescent light and the blue light, and their results showed that for the three types of commercially available TiO_2, more than 99% of initial Hg^0 was removed under all light sources tested except for

1146 the blue light which obtained only 85% Hg^0 removal efficiency. Yuan et al. 2012b and 2012d examined the effects
1147 of different light sources (visible light and UV light) using TiO_2-WO_3 nanofibers reported that Hg^0 removal
1148 efficiency was up to 99% with UV light, and only reached 16% with visible light. Chen et al. 2014 and Hsi et al.
1149 2012 also found that UV light had a better Hg^0 removal performance than visible light using N-doped TiO_2
1150 nanoparticles and TiO_{2-x}/ACF composites. It can be deduced from these results that UV light has a more favorable
1151 effect than the other light sources for photocatalytic removal of Hg^0 because of its greater quantum energy.
1152 However, it's also worth noting that the other light sources such as visible light, accounts for about 43% of all
1153 sunlight (Kumar et al. 2011), and thus has much greater application prospects as compared to the UV light, which
1154 accounts for 5% (Kumar et al. 2011).

1155 **3.6.4 Effects of operating temperature**

1156 Temperature often has an important impact for both chemical reaction and adsorption (Yang et al. 2007; Gao
1157 et al. 2013). Hsi et al. 2012 tested the effects of three operating temperatures, 25/50/100℃, on Hg^0 removal
1158 performance using oxygen-vacant TiO_{2-x} nanoparticles under UV and visible light irradiations, respectively, and
1159 their results indicated that Hg^0 removal performance at 50℃ was better than those at 25℃ and 100℃. Yuan et al.
1160 2012e also studied the effects of operating temperature on Hg^0 removal using TiO_2-aluminum silicate fiber with
1161 UV irradiation, and they found that with increasing temperature from 30℃ to 120℃, Hg^0 removal efficiency
1162 reduced from 93% to 79%. Chen et al. 2014 also found that increasing temperature decreased Hg^0 removal
1163 effciency using N-doped TiO_2 nanoparticles under dark, UV light and visible light. Results of other studies (Chen
1164 et al. 2014; Yuan et al. 2012d; Yuan et al. 2012e) showed that increasing temperature can promote the reaction rate
1165 of Hg^0 oxidation in accordance with Arrhenius equation, but will also negatively impact the adsorption process of
1166 involving Hg^0 because of its exothermic nature (Chen et al. 2014).

1167 **3.6.5 Effects of residence time**

1168 Residence time is a key parameter for photocatalytic process and the design of photocatalytic reactor.
1169 Pitoniak et al. 2003 tested the effects of residence time on Hg^0 removal using SiO_2-TiO_2 composite under UV
1170 irradiation, and they found that Hg^0 removal efficiency drastically with decreasing residence time. The results of
1171 Cho et al. 2012 showed that TiO_2 photocatalytic removal of Hg^0 using household fluorescent lighting was
1172 improved by increasing residence time. Zhuang et al. 2014 also studied the effects of residence time on Hg^0
1173 removal using C-modified TiO_2 nanotubes under visible-light LED irradiation, and their results indicated that with
1174 increasing residence time, the photocatalytic efficiency of Hg^0 greatly increased to nearly 90% within 4.5 s,
1175 beyond which there was no further enhancement. A decrease in residence time will reduce reaction time between
1176 Hg^0 and oxidants, resulting in more escape of Hg^0 from reactor. However, increasing residence time will require a
1177 larger reactor volume, resulting in higher investment and operating costs. The choice of a cost-effective residence
1178 time requires joint consideration of both factors.

1179 **3.6.6 Effects of other operating parameters**

1180 In addition to the effects of the operating parameters described previously, Pitoniak et al. 2003 also tested the
1181 impact of gas flow on Hg^0 removal using SiO_2-TiO_2 composite under UV irradiation, and it to drastically decrease
1182 efficiency with increasing gas flow. Lee et al. 2009 studied the effect of TiO_2 feed rate on Hg^0 capture under UV
1183 irradiation, and the results showed that with increasing TiO_2 feed rate, and hence a higher concentration of TiO_2
1184 and more availability of active sites, resulted in an increase in Hg^0 capture efficiency. In addition, Yuan et al.
1185 2012d and 2012e investigated the effect of UV intensity on Hg^0 removal using TiO_2-aluminum silicate fiber with
1186 UV irradiation, and the results indicated that UV irradiation was critical to the successful oxidation of Hg^0, and
1187 with the decrease of UV intensity, photocatalytic oxidation efficiency for Hg^0 evidently reduced due to the
1188 reduction of photoexcited active species. In addition, Hsi (2012) and Tsai (2011, 2012) synthesized oxygen-vacant
1189 TiO_{2-x} nanoparticles and TiO_{2-x}/ACF composite using N_2/Ar/He and He/Ar thermal plasma as two heating sources,

and they found that both of different applied plasma currents and atmospheres also have significant impacts on activity of these photocatalysts for Hg^0 removal.

3.7 Products, mechanism and kinetics of Hg^0 removal using TiO_2 photocatalytic AOTs

3.7.1 Products of Hg^0 removal using TiO_2 photocatalytic AOTs

The products of Hg^0 removal using TiO_2 photocatalytic oxidation are important information for the recovery of mercury resources and avoiding new secondary mercury contamination. Wu et al. 1998 determined the reaction products of Hg^0 removal by in situ-generated TiO_2 with UV irradiation using the combination of XRD and electron dispersive X-ray spectroscopy (EDS). The formation of HgO on the collected particles as determined by XRD is shown in Figure 15. In addition, Ti and Hg on the same particles were also further identified using EDS.

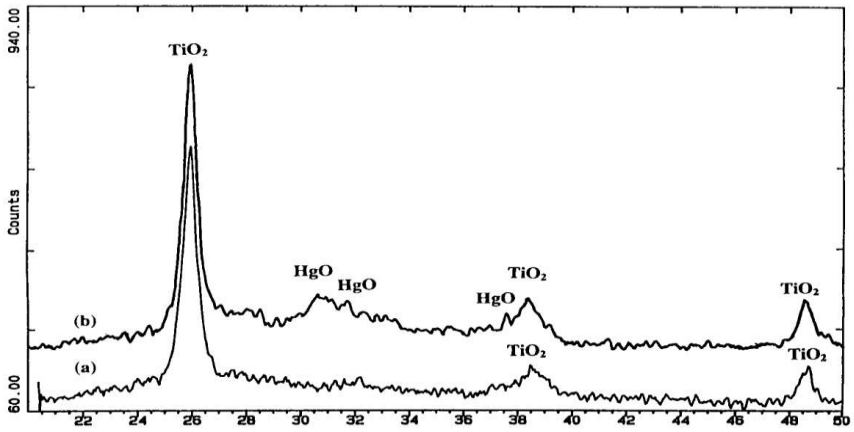

Figure 15. The X-ray diffraction patterns of the collected particles (Wu et al. 1998).

Using SEM and EDS, Snider et al. 2010 detected lightly white mercury deposits on the TiO_2 particles as reaction products under UVA-irradiated TiO_2 as illustrated in Figure 16 (a). Ti and Hg on the TiO_2 particles were also detected by EDS as shown in Figure 16 (b). Pitoniak et al. 2003 and Yuan et al. 2012b also obtained similar results with EDS using SiO_2-TiO_2 composite and TiO_2-WO_3 nanofibers with UV irradiation, respectively.

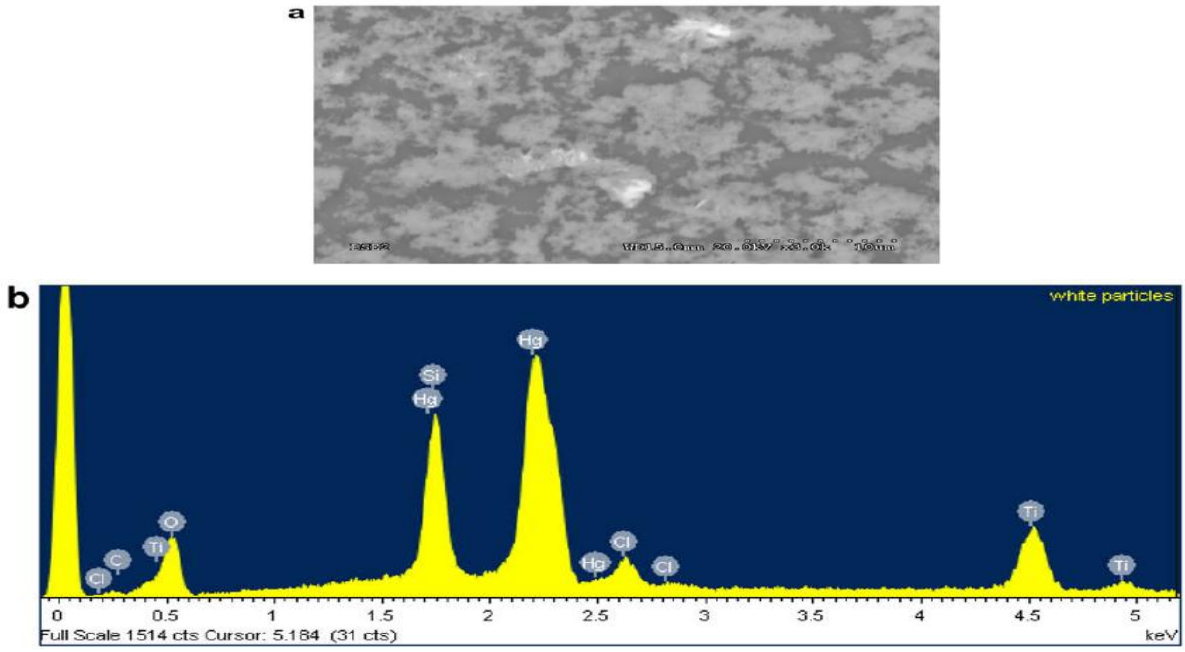

Figure 16. (a) SEM image (3000×magnification) of TiO_2 displaying white paches and (b) EDS of marked area shows the presence of Ti and Hg (Snider et al. 2010).

Wang et al. 2012 also determined the reaction products of Hg^0 removal using titania nanotubes (TNTs) under UV irradiation and XPS measurement, and the results are shown in Figure 17. The XPS spectra in Hg4f region was detected. The peaks located at 100.6 and 104.6 eV ($4f_{7/2}$ and $4f_{5/2}$), were identified as HgO on the TiO_2 photocatalyst surface.

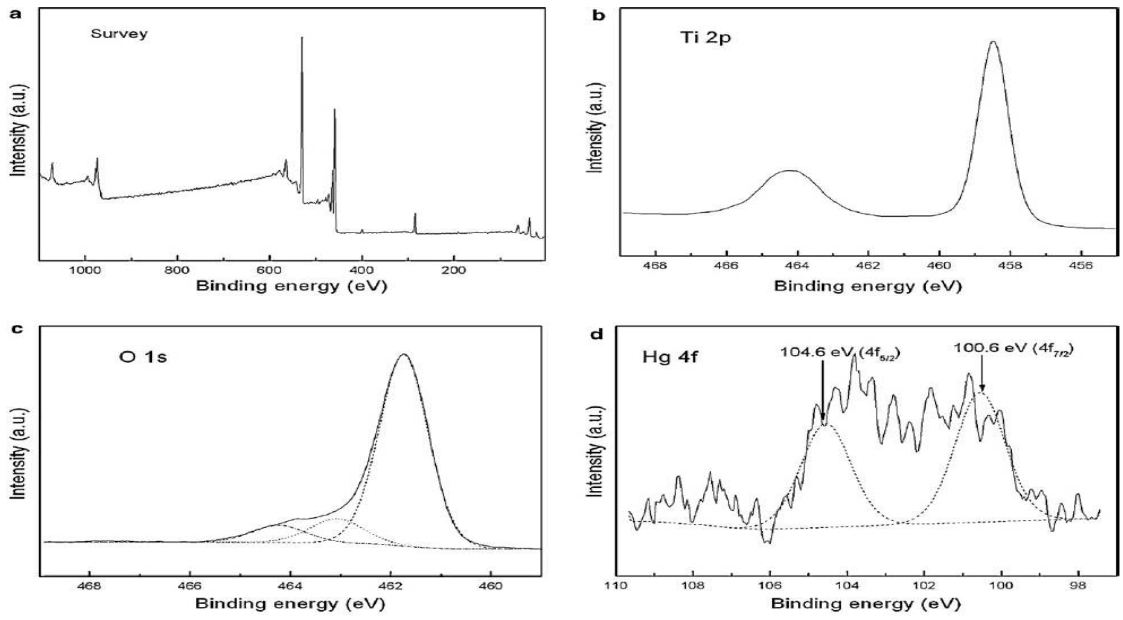

Figure 17. XPS spectra of the used TNTs (a. survey spectra; b. Ti2p band; c. O1s band; d. Hg4f band) (Wang et al.

2012).

While reported studies have focused on the analysis of reaction products on catalyst/adsorbed surfaces, analysis and verification of gaseous reaction products of Hg^0 removal are rarely reported. Furthermore, the mass balance calculations for total Hg, which are also important for elucidating Hg^0 removal mechanism, recovery of mercury resources as well as avoiding new secondary contamination, are still missing in the open literature, and require serious attention in future studies.

3.7.2 Removal mechanism of Hg^0 using TiO_2 photocatalytic AOTs

Wu and his collaborators (Kwon et al. 2008; Pitoniak et al. 2003; Li et al. 2006, 2007 and 2008), using in situ-generated TiO_2 and SiO_2-TiO_2 nanocomposite with UV irradiation identified three essential processes as the main mechanisms for Hg^0 removal. These include: (1) Hg^0 in flue gas is physically absorbed on the photocatalyst though weak bonding; (2) the adsorbed Hg^0 is then oxidized to HgO by free radicals generated on the photocatalyst under UV irradiation, which further enhances the binding of Hg^0 with photocatalyst; (3) reemission of captured Hg^0 on the photocatalyst surface by desorption and photocatalytic reduction due to the interaction of water vapor and free photons. This major contribution to the understanding of the reaction mechanism is illustrated in Figure 18. Also, the chemical reaction mechanism and pathways, including a series of elementary reactions proposed by several investigators are summarized in detail in Table 5 (Tsai et al. 2012 and 2013; Yuan et al. 2012b, 2012b and 2012c; Li et al. 2006, 2007 and 2008).

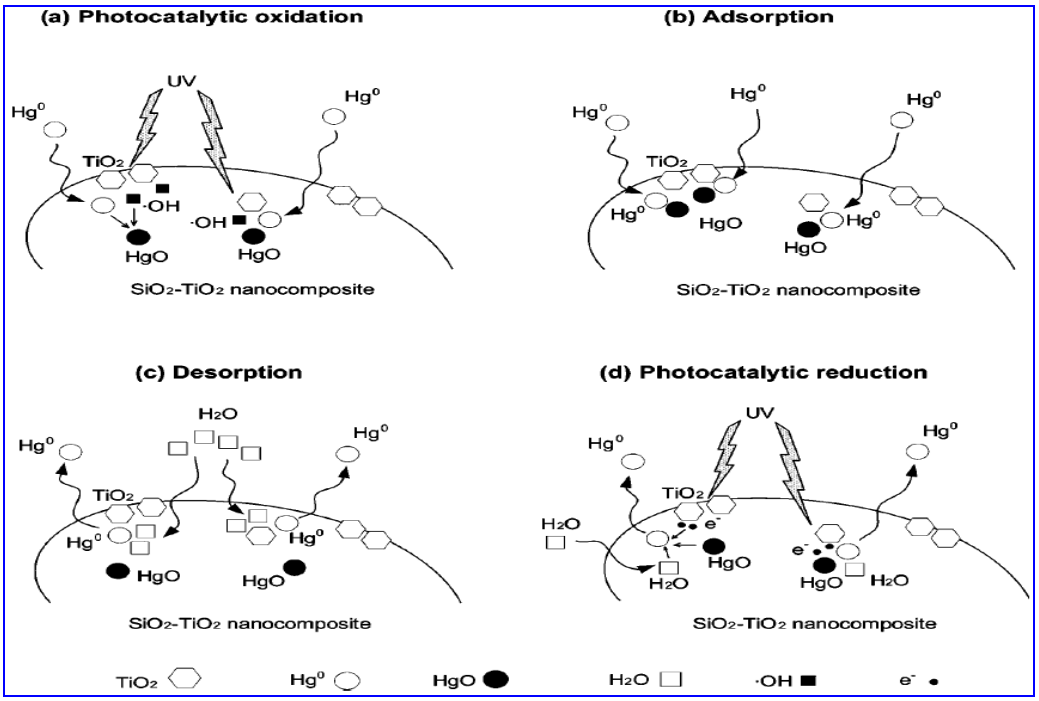

1232

1233 **Figure 18.** Mechanisms of Hg^0 capture and reemission on the surface of SiO_2-TiO_2 nanocomposite (Pitoniak et al.

1234 2003).

1235 **Table 5.** TiO_2 photocatalytic mechanism and scheme for removal of Hg^0 in flue gas.

Overall removal process	Specific adsorption and chemical reaction
Adsorption process	$TiO_2(s) + O_2(g) \rightarrow O_{2,ads}(s)$ (adsorbed O_2)
	$TiO_2(s) + H_2O(g) \rightarrow H_2O_{ads}(s)$ (adsorbed H_2O)
	$TiO_2(s) + Hg^0(g) \rightarrow Hg^0{}_{ads}(s)$ (adsorbed Hg^0)
	$TiO_2(s) + OH^-(g) \rightarrow OH^-{}_{ads}(s)$ (adsorbed OH^-)
Excitation process	$TiO_2(s) + hv \rightarrow e^- + h^+$
Recombination process	$e^- + h^+ \rightarrow heat$
Trapping process	$e^- + O_{2,ads}(s) \rightarrow O_2^- \cdot (s)$
	$h^+ + H_2O_{ads}(s) \rightarrow \cdot OH(s) + H^+(s)$
	$h^+ + OH^-{}_{ads}(s) \rightarrow \cdot OH\ (s)$

Chain reaction transfer	$O_2^- \cdot (s) + H^+(s) \rightarrow HO_2 \cdot (s)$
	$HO_2 \cdot (s) + HO_2 \cdot (s) \rightarrow H_2O_2(s) + O_2(s)$
	$H_2O_2(s) + e^- \rightarrow \cdot OH(s) + OH^-(s)$
Hydroxy attack process	$Hg^0_{ads}(s) + \cdot OH(s) \rightarrow HgOH(s)$
	$HgOH(s) + \cdot OH(s) \rightarrow HgO(s) + H_2(s)$
	$HgOH(s) \rightarrow HgO(s) + H^+(s)$
	$O_2^- \cdot (s) + Hg^0(s) \rightarrow HgO(s)$
Hg^0 reemission	$HgO(s) + H_2O(s) + 2e^- \rightarrow Hg^0(g) + 2OH^-(s)$

While mechanistic studies of Hg^0 removal using TiO_2 photocatalytic oxidation has attained some progress, much of what we know are derived from research results of other fields, and the key reaction pathways or main rate-determining steps have not been identified based on reliable experimental evidences. Also, the capture and identification of some key reactive intermediates or radicals in the photocatalytic Hg^0 removal process are still rarely reported.

3.7.3 Kinetics of Hg^0 removal using TiO_2 photocatalytic AOTs

Kinetic constants and kinetic models are the important basis for the optimization of adsorbent/catalyst, and the design of reactor. The kinetics of Hg^0 removal using TiO_2 photocatalytic oxidation was studied by several researchers (Yuanet al. 2012d; Snider et al. 2010; Lee et al. 2004; Rodrı´guez et al. 2004; Li et al. 2007; Snider et al. 2012), and preliminary results reported. Lee et al. 2004 investigated the kinetics of Hg^0 removal using in situ generated TiO_2 in differential bed and entrained flow systems. The results showed that the overall reaction orders with respect to the gaseous Hg^0 concentration and the UV intensity were found to be 1.4±0.1 and 0.35±0.05 for the differential bed reactor, whereas the two values were 1.1±0.1 and 0.39 for the aerosol flow reactor. At the

low-temperature range (<80℃), Hg^0 removal was found to be a reaction-controlled process, while it was adsorption-controlled process at the higher temperatures (>110℃). Rodríguez et al. 2004 developed a mechanistic model to predict Hg oxidation rate on TiO_2 surfaces with UV irradiation. The results showed that the model agreed well with experimental data for Hg capture rate and could effectively predict the effects of process parameters on Hg oxidation rate. Li et al. 2007 studied the kinetics using SiO_2-TiO_2 nanocomposite with UV irradiation in a fix-bed reactor. A Langmuir-Hinshelwood (L-H) model was used to analyze the kinetic data with a good agreement, indicating the validity of using the L-H model to describe the kinetic process of Hg^0 photocatalytic oxidation removal. Based on the L-H theory, Yuan et al. 2012d also established an L-H kinetic model of Hg^0 removal using WO_3-TiO_2 nanofibers with UV irradiation, which also showed a good agreement with the experimental data. Snider et al. 2010 determined the L-H adsorption constant and apparent surface deposition rate kinetic parameters of Hg^0 removal by UVA-irradiated TiO_2 to be $K_{Hg} = (5.1 \pm 2.4) \times 10^{-14}$ cm^3 and $k = (7.4 \pm 2.5) \times 10^{14}$ min^{-1} cm^{-2}. Also, Snider et al. 2012 further determined the second-order rate constant of the gas-phase reaction of NO_2 with Hg^0 using UVA-irradiated TiO_2 to be $(3.5 \pm 0.5) \times 10^{-35}$ cm^3.

3.8 Reactor and process flow of Hg^0 removal using TiO_2 photocatalytic AOTs

3.8.1 Reactor of Hg^0 removal using TiO_2 photocatalytic AOTs

Photocatalytic reactor type, photocatalyst and light source are three essential elements for a photocatalytic reaction system. An efficient photocatalytic reactor is extremely important for improving pollutant removal efficiency, increasing energy efficiency as well as reducing investment and operating costs. In recent years, a variety of photocatalytic reactors have been developed in flue gas purification field (Lee et al. 2010; Daghrir et al. 2013; Kumar et al. 2011; Worathanakul et al. 2008; Linsebigler et al. 1995; Kwon et al. 2008; Suriyawong et al. 2009), but the most commonly used include mainly the four types described in Figure 19 (a)-(d). The two reactors in Figure 19 (a) and (b) consist of a container and UV lamps, separately. The number of UV lamp may be changed

1272 from one to multiple according to the needs of the experiment. The reactor shell is often composed of glass
1273 (usually quartz glass) with high light transmission because UV-light has very low penetration ability in the vast
1274 majority of the mediums (Breault et al. 2006). To maximize the photocatalyst's exposure to the light source, the
1275 reactor in Figure 9(a) was sometimes also designed as a rotary structure (Lee et al. 2004; Lee et al. 2005). These
1276 reactors are the most widely used in laboratory research due to their simple structure and easy operation. However,
1277 it is difficult for them to realize large-scale applications due to the low utilization rate of light energy and the
1278 structural limitations of scale-up. The two photocatalytic reactors with built-in structure (Figure 19 (c) and (d)) are
1279 considered to have better developmental prospects because both of them are able to fully utilize UV light and
1280 easily realize amplification. The photocatalytic fixed bed reactor shown in Figure 19 (c), has received a wide
1281 range of applications in laboratory research due to its simple structure and easy operation. However, such reactors
1282 have several shortcomings such as low adsorption or mass transfer rate, small light irradiation surface for catalysts,
1283 easy agglomeration of catalysts, as well as poor heat transfer performance (Lee et al. 2010; Daghrir et al. 2013;
1284 Kumar et al. 2011; Fujishima et al. 1972; Kaluza et al. 1971; Wu et al. 1998; Lee et al. 2001; Worathanakul et al.
1285 2008). Related results (Chen et al. 2014; Yuan et al. 2012b; Yuan et al. 2012d; Lee et al. 2004) have shown that
1286 the adsorption and mass transfer process, especially at high temperatures, is usually the rate-controlling step of
1287 photocatalytic removal of Hg^0 in flue gas. Moreover, in the actual photocatalytic process, UV lamps often will
1288 release a lot of heat, thereby increasing the bed temperature in photocatalytic reactor. Prior studies (Kwon et al.
1289 2008; Pitoniak et al. 2007; Chen et al. 2014; Yuan et al. 2012d; Yuan et al. 2012e) have confirmed that high
1290 temperature decreases the photocatalytic oxidation of Hg^0 in flue gas, and greatly reduces the operating
1291 performance of the UV lamp (Breault et al. 2006). Thus enhancement of heat and mass transfer process is one of
1292 the most important ways to improve the photocatalytic efficiency of Hg^0 removal.

1293 Fluidized bed usually have much better heat and mass rate as compared to fixed bed, and has received

1294 widespread attention in many industries (Breault et al. 2006; Corella et al. 2006; Li et al. 2004; Berruti et al. 1995;
1295 Basu et al. 1999). In the field of air pollution purification, photocatalytic fluidized bed has also received
1296 considerable attention because of its excellent performances in enhancing heat and mass, improving gas-solid
1297 contact, preventing agglomeration of catalysts, as well as providing better light radiation (McCullagh et al. 2011;
1298 Geng et al. 2010; Kumazawa et al. 2003; Nelson et al. 2007; Lim et al. 2005; Satoru et al. 2005). Therefore,
1299 Figure 19 (d), may be regarded a good choice for enhancing photocatalytic removal of Hg^0 in flue gas though
1300 studies using fluidized beds are yet to be reported. Related results (Chang et al. 2002; Tendero et al. 2006) showed
1301 that corona discharge process in electrostatic precipitator (ESP) could produce UV irradiation. Based on this
1302 feature of ESP, Biswas et al. 1998 and Wu et al. 1998 proposed a process of Hg^0 capture using TiO_2 injection in
1303 electrostatic precipitator (ESP), showing a better prospect due to its greater adsorption capacity for Hg^0, lower
1304 processing costs, and potential multi-pollutants removal capability as compared to activated carbon injection
1305 technology. The related photocatalytic reactor and process flow are shown in Figure 19 (e) and Figure 20 (d),

1306 Unlike the application of UV light, if the sunlight is used as the light source of photocatalytic reaction, as
1307 shown in Figure 19 (b) and Figure 20 (c), a flat plate reactor is probably the most common structure for
1308 visible-light photocatalytic reaction. Depending on the amount of the flue gas to be treated, the flat plate reactor
1309 using sunlight may be one or more arranged in parallel. At present, for photocatalytic removal of Hg^0 using visible
1310 light, the most commonly used light source is mainly an indoor simulation lamp light such as halogen lamp and
1311 xenon. Studies using sunlight is rare because of the uncertainty of climate conditions, but such a technology
1312 requires serious consideration because of its excellent prospects.

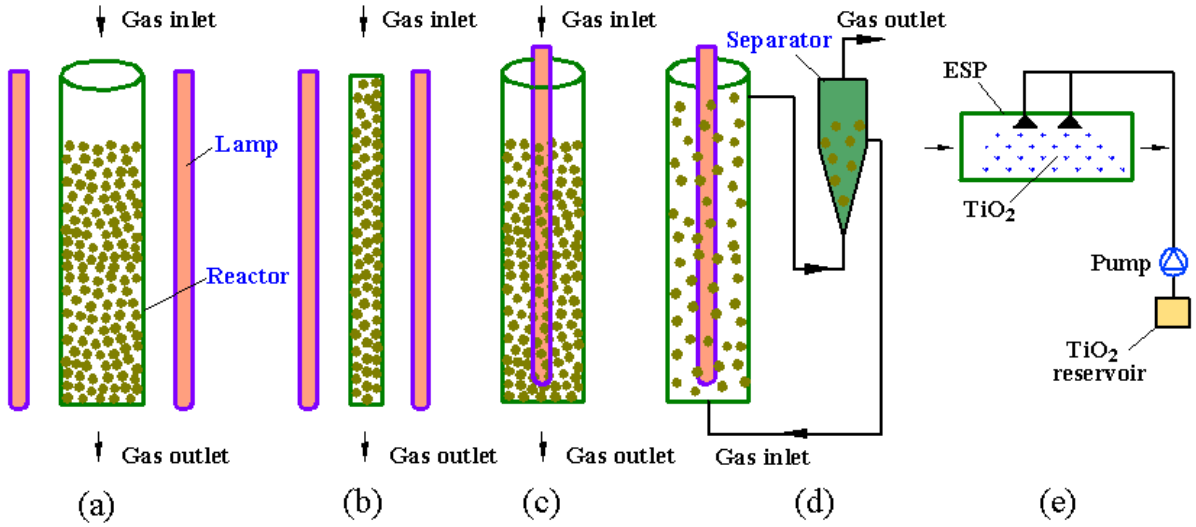

Figure 19. Common and potential photocatalytic reactors for removing Hg^0 from flue gas: (a) cylindrical fixed bed using external UV lamp; (b) plate-type fixed bed using external UV lamp or visible light; (c) cylindrical fixed bed using built-in UV lamp; (d) circulating fluidized bed using built-in UV lamp; (e) TiO_2 injection in electrostatic precipitator (ESP).

3.8.2 Process flow of Hg^0 removal using TiO_2 photocatalytic AOTs

Related studies (Satoru et al. 2005; Zhao et al. 2008; Maggos et al. 2007; Todorova et al. 2014; Li et al. 2008; Zuo et al. 2006; Kima et al. 2002; Portela et al. 2010; Portela et al. 2012) have shown that TiO_2 photocatalytic AOTs also have good removal performance for SO_2 and NO_x in coal-fired flue gas and VOCs and H_2S in exhaust. Simultaneous removal of multi-pollutants in flue gas has been recognized as a cost-effective control strategy for coal-fired flue gas purification (Wang et al. 2007; Hutson et al. 2008; Su et al. 2013; Adewuyi et al. 2013; Ding et al. 2014; Obradović et al. 2011). Therefore, in order to control application costs, TiO_2 photocatalytic AOTs should also be fully considered for the simultaneous removal of SO_2, NO_x and Hg^0 in coal-fired flue gas. The schematic diagram of this strategy is shown in Figure 20 (a)-(c). Figure 20 (a) and Figure 20 (b) respectively show the potential scale-up of photocatalytic fixed bed and photocatalytic circulating fluidized bed reactors, as well as the corresponding process flows using UV light as light source. Figure 20 (c) describes the potential photocatalytic

horizontal flat plate reactor and the corresponding process flow using sunlight as light source.

Based on the existing results in product measurements (Kwon et al. 2008; Pitoniak et al. 2003; Yuan et al. 2012b; Snider et al. 2010; Zhao et al. 2008; Maggos et al. 2007; Todorova et al. 2014), the main gaseous products such as $NO_2(g)/HNO_3(g)/SO_3(g)/H_2SO_4(g)/HgO(g)$ and the main solid products such as $HNO_3(s)/H_2SO_4(s)/HgO(s)$ will be first produced from the oxidations of NO_x, SO_2 and Hg^0 from flue gas in photocatalytic reactor. According to the process flow, the gaseous products will be washed in the back WFGD device, and the solid products will be deposited on the surface of photocatalyst, and finally can be recovered by desorption and regeneration of photocatalyst. Related studies (Kwon et al. 2008; Pitoniak et al. 2003; Yuan et al. 2012b; Dou et al. 2008) have verified that with the continuous accumulation or deposition of solid products on the surface of the catalyst, the activity of catalyst will continue to decline, and may be deactivated.

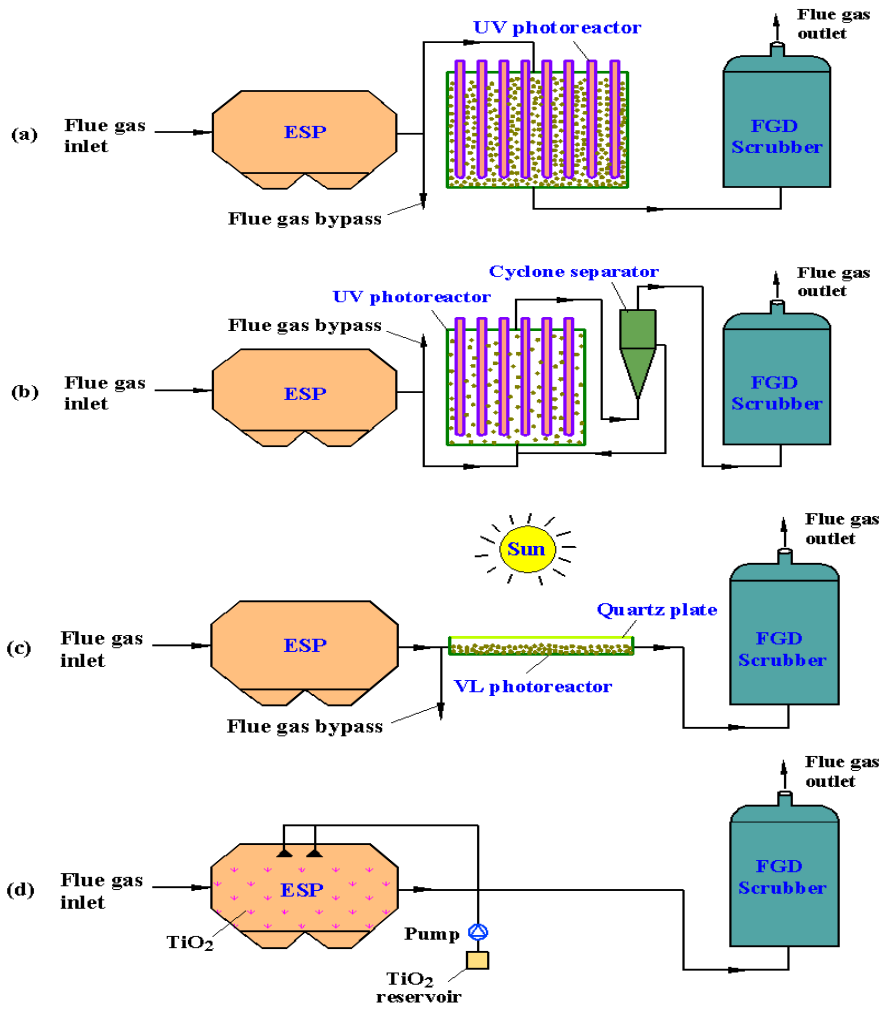

Figure 20. Potential scale-up and process flow of Hg^0 photocatalytic removal: (a) fixed bed using UV light; (b) circulating fluidized bed using UV light; (c) horizontal flat plate using sunlight; (d) electrostatic precipitator (ESP) injection.

Therefore, the catalyst often requires periodic regeneration and activation. In order to achieve continuous removal of contaminants, it is necessary to install two parallel reactors. When one is used for the regeneration of catalyst and the recovery of products, the other will be used for removing pollutants. Figure 20 (d) describes the potential photocatalytic reactor using TiO_2 injection in electrostatic precipitator (ESP) and the corresponding process flow. In this process, these reaction products are adsorbed by fly ash and titanium particles to form pollutant-containing aerosols and particles, which will be captured by the ESP.

4. Photochemical AOTs for removing Hg^0 in flue gas

4.1 Overview of photochemical AOTs for removing Hg^0 in flue gas

As previously described, the activity and stability of photocatalyst are still very low, and the utilization rate of light energy is also very low due to the inevitable refraction/reflection of light encountering particles (Liu et al. 2011a). Unlike TiO_2 photocatalytic AOTs, photochemical AOTs can directly generate active substances, mainly including $\cdot OH$, $\cdot O$, $HO_2\cdot$, $SO_4^{-}\cdot$, O_3, etc. by releasing high energy photons to destroy the molecular bond of O_2, O_3, H_2O, H_2O_2 and persulfate without the existence of photocatalysts (Liu et al. 2011a). As shown in Figure 2, the common photochemical AOTs mainly include UV, UV/H_2O_2, homogeneous/heterogeneous Photo-Fenton, homogeneous/heterogeneous Photo-Fenton-Like, UV/O_3, UV/persulfate, UV/H_2O_2/persulfate, UV/O_3/H_2O_2, etc. (Ayoub et al. 2010; Feng et al. 2013; Sharma et al. 2012; Oller et al. 2011; Antonopoulou et al. 2014; Vallejo et al. 2015; Asghar et al. 2014; Ye et al. 2014). In the past few decades, these photochemical AOTs have been widely studied and applied in the field of water treatment and soil remediation, and have shown a good prospect (Ayoub et al. 2010; Feng et al. 2013; Sharma et al. 2012; Oller et al. 2011; Antonopoulou et al. 2014; Vallejo et al. 2015;

1363 Asghar et al. 2014; Ye et al. 2014). In recent years, some researchers try to use several photochemical AOTs to
1364 remove gaseous pollutants such as SO_2, NO_x, VOCs, Hg^0, etc., and also show a good prospect (Dickinson, et al.
1365 1926; Granite et al. 1999; Granite et al. 2001; Jia et al. 2001; Liu et al. 2013a; Liu et al. 2014a; Liu et al. 2014c;
1366 Liu et al. 2013b; Zhan et al. 2013; Liu et al. 2010a; Liu et al. 2010b; Liu et al. 2010c; Ye et al. 2014). These
1367 gaseous pollutants can be oxidized or degraded by generated active substances such as ·OH, ·O, HO_2·, SO_4^-·, O_3,
1368 etc. in various gas phase reactors (homogeneous reaction) (Dickinson, et al. 1926; Granite et al. 1999; Granite et
1369 al. 2001; Jia et al. 2001; Ye et al. 2014) or gas-liquid reactors (heterogeneous) (Liu et al. 2013a; Liu et al. 2014a;
1370 Liu et al. 2014c; Zhan et al. 2013; Liu et al. 2012a; Liu et al. 2010a; Liu et al. 2010b; Liu et al. 2010c). These
1371 photochemical AOTs for removing gaseous Hg^0 can be divided into two categories of dry and wet methods.

1372 **4.2 Dry photochemical AOTs for Hg^0 removal**

1373 In 1926, using oxygen/mercury mixtures, Dickinson and Sherrill demonstrated the photochemical formation
1374 of mercuric oxide (HgO) (Dickinson et al. 1926), and the experiments were reproduced by Granite and Pennline
1375 (Granite et al. 1999, 2000, 2001, 2002, 2003). The overall reaction between mercury and O_2 in the presence of
1376 253.7 nm UV can be described by the equation (42) (Dickinson et al. 1926; Granite et al. 1999, 2000, 2001, 2002,
1377 2003).

1378 $$Hg^0(g) + 2O_2(g) + 253.7\,\text{nm light} \rightarrow HgO(g) + O_3(g) \quad (42)$$

1379 In this reaction, Hg^0 serves as a sensitizer for the formation of O_3, and O_3 can oxidize Hg^0 to form mercuric oxide
1380 (HgO), which has been confirmed by Granite et al. and Dickinson et al. (Dickinson et al. 1926; Granite et al. 1999,
1381 2000, 2001, 2002, 2003). Based on this basic principle, Granite and coworkers, for the first time tried to use this
1382 novel technology to successfully remove mercury from coal-fired flue gas, and also obtained a US patent (Granite
1383 et al. 1999, 2000, 2001, 2002, 2003). Jia et al. 2010 and Liu et al. 2013a and 2013b have also done some related
1384 studies to improve this technology from the perspective of chemistry and reactor/process design, which are

described in the following sections.

4.2.1 Effects of flue gas components on Hg^0 removal using dry photochemical AOTs

Granite and Pennline (Granite et al. 1999, 2000, 2001, 2002, 2003) studied the effects of O_2 and NO on photochemical oxidation of Hg^0 using 253.7 nm UV radiation, and their results showed that as an essential component for the formation of O_3, O_2 played a promotional role. However, the presence of NO decreased Hg^0 removal, which was attributed to the loss of O_3 due to the fast reaction between NO and O_3. Jia et al. 2010 further investigated the effects of other flue gas components, including O_2, NO, SO_2, H_2O, CH_4, CO, CO_2 and alcohol vapor, and found that the addition of SO_2, NO, H_2O or alcohol vapor adversely affected the photochemical oxidation of Hg^0, whereas adding O_2, CH_4, CO or CO_2 alone enhanced the process. Similar results were also obtained by Liu et al. 2013a and 2013b in studying the effects of O_2, NO, SO_2 and H_2O on the oxidation of Hg^0 using 253.7 nm UV radiation.

4.2.2 Effects of operating parameters on Hg^0 removal using dry photochemical AOTs

Granite and Pennline (Granite et al. 1999, 2000, 2001, 2002, 2003), studied the effects of UV radiation intensity and temperature and found that the UV intensity had a dramatic impact on Hg^0 removal, with decrease in intensity resulting in a significant decrease in Hg^0 capture, while increasing temperature had the opposite effect, consistent with the results of Jia and Anthony (Jia et al. 2010) and Liu et al. 2013a and 2013b. Liu et al. 2013a and 2013b tested the effects of residence time and the results showed that increasing residence time initially increased Hg^0 oxidation efficiency before leveling off (Liu et al. 2013a and 2013b). With the increase of Hg^0 inlet concentration within the range of 10-80 $\mu g/m^3$, photochemical oxidation efficiency of Hg^0 only had a slight decrease, showing that this technology had a good adaptability for the changes of Hg^0 concentrations in coal-fired flue gas.

4.2.3 Products and mechanism of Hg^0 removal using dry photochemical AOTs

1407 Some effective measurements such Ontario-Hydro method, XPS and SEM-EDS were used to analyze HgO,
1408 the reaction product of Hg^0 photochemical oxidation, and found it to consist of gaseous and solid forms (Granite
1409 et al. 1999, 2000, 2001, 2002, 2003; Jia et al. 2010; Liu et al. 2013a and 2013b). The solid HgO deposited on the
1410 surface of lamp tube or reactor, white gaseous HgO remains in the flue gas stream to be captured in the back
1411 washing or adsorbing reactor (Granite et al. 2002, 2003; Liu et al. 2013a and 2013b). Based on these results,
1412 Granite and Pennline 1999, 2000, 2001, 2002, 2003) proposed for the first time, the following reaction
1413 mechanisms:

1414 **(A)** Hg^0 is first excited by UV photons from 254-nm mercury lamp according to the following equation (43);

1415 $$Hg^0(g) + hv\ (253.7\,nm\ light) \rightarrow Hg^0{}^*(g) \quad (43)$$

1416 **(B)** Quenching of the excited state Hg^0* with O_2 returns the excited state (Hg^0*) to its ground state (Hg^0*) and
1417 produces excited state oxygen (O_2*) according to the following equation (44);

1418 $$Hg^0{}^*(g) + O_2(g) \rightarrow Hg^0(g) + O_2{}^*(g) \quad (44)$$

1419 **(C)** The active substances used for oxidation of Hg^0 are formed through quenching of O_2* and O_2 and the reaction
1420 between $\cdot O$ and O_2 (Eq. 4) to form O_3 and $\cdot O$ (eq.45).

1421 $$O_2{}^*(g) + O_2(g) \rightarrow O_3(g) + \cdot O(g) \quad (45)$$

1422 **(D)** Both of O_3 and $\cdot O$ can react with Hg^0 to form HgO as in equations (5) and (6). The overall reaction can be
1423 described by equation (42) by superimposing reactions (4)-(6) and (43)-(45).

1424 **(E)** The other compounds in flue gas may also oxidize Hg^0 under the excitation of 254 nm UV light. For example,
1425 Hg^0 can react with H_2O in flue gas to form HgO according to reaction (46):

1426 $$Hg^0(g) + H_2O(g) + hv(g) \rightarrow HgO(g) + H_2(g) \quad (46)$$

1427 **(F)** Hg^0 will be oxidized by HCl under the radiation of 254 nm UV light as shown in reaction (47):

1428 $$2Hg^0(g) + 2HCl(g) + hv \rightarrow Hg_2Cl_2(g) + H_2(g) \quad (47)$$

(G) The photochemical oxidation of Hg^0 by NO_2 will result in the formation of HgO as shown in reaction (48):

$$Hg^0(g) + NO_2(g) + hv \rightarrow HgO(g) + NO(g) \quad (48)$$

(H) The slow sensitized oxidation of Hg^0 by CO_2 has also been reported with the 254 nm UV radiation, and is described in reaction (49):

$$Hg(g) + CO_2(g) + hv \rightarrow HgO(g) + CO(g) \quad (49)$$

(H) Hg^0 will react with SO_3 under the excitation of 254 nm UV light according to the following reaction (50):

$$Hg(g) + SO_3(g) + hv \rightarrow HgO(g) + SO_2(g) \quad (50)$$

(I) The results of Jia et al. 2010 also indicated that, compared with adding O_2 alone (53.4%), the joint addition of CH_4 and O_2 resulted in a much higher removal efficiency (91.1%). Therefore, they speculated that when the excited state (Hg^0*) collide with CH_4 molecules, H atoms may be produced and, in turn, can further induce reactions as follows (51)-(53) (Jia et al. 2010).

$$Hg^0*(g) + CH_4(g) \rightarrow Hg^0(g) + CH_3\cdot(g) + \cdot H(g) \quad (51)$$

$$O_2(g) + \cdot H(g) \rightarrow \cdot OH(g) + \cdot O(g) \quad (52)$$

$$Hg^0(g) + \cdot O(g) \rightarrow HgO(g) \quad (53)$$

In addition, the elementary reactions between Hg^0 and $\cdot OH$ in gas phase also have been reported (Sommar et al. 2001; Jack et al. 2005) as previously described in reactions (8-11).

4.3 Wet photochemical AOTs for Hg^0 removal

Although the dry photochemical AOTs have demonstrated good prospects for Hg^0 removal, it also has some shortcomings in actual applications. As previously noted, a part of generated HgO will deposit on the surface of UV lamp tube to form white stains (Granite et al. 2002; Jia et al. 2010). This significantly reduces UV transmittance because of the very low penetration of 254nm UV light (254nm UV light cannot even pass through an ordinary glass) (Liu et al. 2011a). Also, due to the significant complexity of coal-fired flue gas system, slagging

and fouling may inevitably occur on the surface of UV lamp tube, which is similar to the slagging and fouling of several heat transfer surfaces in coal-fired boilers, and finally will result in a decline in Hg^0 removal. As a result of these shortcomings of dry photochemical AOTs, several novel wet photochemical AOTs for removing Hg^0 in flue gas, including UV/H_2O_2, homogeneous UV/Fenton, homogeneous UV/Fenton-like and heterogeneous UV/Fenton-like, have been proposed recently by Liu et al. 2010a, 2010b, 2014c, 2014d, 2014e, 2015a, Zhan et al. 2013 and Zhang et al. 2011b. Also, several novel gas-liquid photochemical reactors, including photochemical bubble reactor and photochemical spray reactor, and their removal processes have been reported by Liu et al. Liu et al. 2010a, 2010b, 2014c, 2014d, 2014e, 2015a and Zhan et al. 2013. These wet photochemical AOTs have shown some great promise for Hg^0 removal.

4.3.1 Effects of operating parameters on Hg^0 removal using wet photochemical AOTs

(1) UV radiation intensity

Liu et al. 2014a, 2014c, 2014d, 2015a investigated the effects of UV radiation intensity on Hg^0 removal using UV/H_2O_2 process in a photochemical bubble reactor and a photochemical spray reactor, respectively, and their results showed that Hg^0 removal was greatly promoted with increasing UV radiation intensity. Similar results were also obtained by Liu et al. 2015a and Zhang et al. 2013 in studying Hg^0 removal using homogeneous and heterogeneous Photo-Fenton-like reactions in a photochemical bubble reactor. Related studies (2014a, 2014c, 2014d, 2015a) showed that under UV radiation, 1mol H_2O_2 can produce 2mol $\cdot OH$ to oxidize Hg^0 in flue gas via equations (54) and (55).

$$H_2O_2(l) + h\nu \rightarrow 2\cdot OH(l) \tag{54}$$

$$Hg^0(l) + 2\cdot OH(l) \rightarrow Hg(OH)_2(l) \xrightarrow{heat} HgO(l) + H_2O(l) \tag{55}$$

Under UV radiation, O_2 can also produce $\cdot O$ and O_3 by the reactions (56) and (57) as follows.

$$O_2(l) + h\nu \rightarrow \cdot O(l) + \cdot O(l) \tag{56}$$

$$\cdot O(l) + O_2(l) \rightarrow O_3(l) \quad (57)$$

Both O_3 and $\cdot O$ have strong oxidants and can oxidize Hg^0 by the reactions (58) and (59) as follows.

$$Hg^0(l) + O_3(l) \rightarrow HgO(l) + O_2(l) \quad (58)$$

$$Hg^0(l) + \cdot O(l) \rightarrow HgO(l) \quad (59)$$

Under UV radiation, O_3 can also react with H_2O to produce H_2O_2 by the reaction (60) to provide additional source of $\cdot OH$ through reactions (54) and (55) (Li et al. 2013).

$$O_3(l) + H_2O(l) + hv \rightarrow H_2O_2(l) + O_2(l) \quad (60)$$

The results of Jia et al. 2010 and Granite et al. 2000, 2001, 2002 showed that under UV radiation, Hg^0 also could directly react with H_2O to produce HgO by the following photochemical reaction (61).

$$Hg^0(l) + H_2O(l) + hv \rightarrow HgO(l) + H_2(l) \quad (61)$$

An increase in UV radiation intensity can produce more effective UV photons, $\cdot OH$, $\cdot O$ and O_3, thereby enhancing Hg^0 removal. However, the results of Liu et al. 2014a, 2014c, 2014d, 2015a and Zhang et al. 2011b also found that Hg^0 removal efficiency did not maintain a linear relationship with increasing UV radiation intensity, with the effect leveling off at excess intensity. Therefore, to reduce energy consumption of reaction system, an appropriate UV radiation intensity should be maintained in future industrial applications.

(2) UV wavelength

Based on the basic principles of photochemical reactions 2014a, 2014c, 2014d, oxidants such as $\cdot OH$, $\cdot O$ and O_3 mainly derived from the photolysis of O_2 and H_2O_2 molecules by UV photons by molecular bond breakage, and the energy of the UV light photons depends on the UV light wavelength as shown in the Planck's equation (62) (Liu et al. 2011a):

$$\varepsilon = hv = h\frac{c}{\lambda} \quad (62)$$

where ε - energy of photon, J; ν - ultraviolet frequency, 1/s; h -Planck constant, 6.626×10^{-34} J·s; c -speed of

1495 light, 2.998×10^8 m/s; λ - ultraviolet wavelength, 100-380nm. It can be inferred from this equation that as the UV
1496 wavelength becomes shorter, the energy of UV photon will become bigger. Liu et al. 2014a, 2014c, 2014d, 2015
1497 studied the effects of UV wavelength on Hg^0 removal using three most common UV wavelengths (185 nm, 254
1498 nm, 365 nm) and compared with visible light (350-770 nm) source. The results indicated that 254nm UV-light
1499 obtained the highest Hg^0 removal efficiency, and the visible light has almost no effect on Hg^0 oxidation. Also,
1500 similar results were also obtained by Liu et al. 2015a and Zhang et al. 2011 in studying Hg^0 removal using
1501 homogeneous and heterogeneous Photo-Fenton-like reactions in a photochemical bubble reactor. While shorter
1502 wavelength photons have the requisite energy to destroy the molecular bonds in H_2O_2 and O_2 to produce
1503 more ·OH, ·O and O_3, they also have shorter propagation distance of UV light in solution because of the heat
1504 dissipation of UV-light in the propagation medium. By carefully considering both propagation distance and UV
1505 photon energy, 254 nm was found to achieve the best Hg^0 removal performance (Liu et al. 2014a, 2014c, 2014d,
1506 2015a; Zhang et al. 2011).

1507 **(3) Effects of H_2O_2 concentration**

1508 Liu et al. 2014a, 2014c, 2014d, 2015a investigated the effects of H_2O_2 concentration on Hg^0 removal by
1509 UV/H_2O_2 process in a photochemical bubble reactor and a photochemical spray reactor, respectively, and found
1510 that the addition of a small amount of H_2O_2 enhanced Hg^0 removal but higher levels had the opposite effect. Liu et
1511 al. 2015a, Zhan et al. 2013 and Zhang et al. 2013 also obtained similar results in studying Hg^0 removal using
1512 homogeneous UV/Fenton reaction, and homogeneous/heterogeneous Photo-Fenton-like reactions, respectively. As
1513 shown in reactions (54) and (55), UV photolysis of H_2O_2 produces additional ·OH to oxidize Hg^0 in flue gas, in
1514 addition to oxidation by the added H_2O_2 as in reaction (63).

1515 $$Hg^0(l) + H_2O_2(l) \rightarrow HgO(l) + H_2O(l) \quad (63)$$

1516 However, excessive addition H_2O_2 also acts a scavenger of ·OH, which has the stronger oxidation potential (Liu et

al. 2014a, 2014b, 2014c, 2015a; Zhang et al. 2013), as in reaction (64), a situation which is not conducive to Hg^0 removal.

$$\cdot OH(l) + H_2O_2(l) \rightarrow H_2O(l) + HO_2 \cdot (l) \quad k = 2.7 \times 10^7 M^{-1}s^{-1} \tag{64}$$

(4) Effects of Fe^{2+}/Fe^{3+}/Cu^{2+} concentration

Related studies (Hsueh et al. 2005; Tony et al. 2009; Kwan et al. 2003; Cravotto et al. 2007; Ntampegliotis et al. 2006; Fan et al. 2009) showed that transition metal ions such as Fe^{2+}, Fe^{3+}, Cu^{2+}, Mn^{2+}, Co^{2+}, etc. could effectively improve the yield of ·OH in UV/Fenton and Photo-Fenton-Like (PFL) systems, therefore enhancing oxidation of pollutants. Zhan et al. 2013 examined the effects of Fe^{2+} concentration on Hg^0 removal using homogeneous UV/Fenton reaction, and the results showed that Hg^0 removal was greatly enhanced by adding low concentration of Fe^{2+}, but was greatly reduced by adding high concentration of Fe^{2+}. Liu et al. 2015 obtained similar results using Fe^{3+}-induced homogeneous PFL reaction. However, Liu et al. 2015a also obtained different results using Cu^{2+}-induced homogeneous PFL reaction, indicating that Hg^0 removal was monotonically enhanced by adding Cu^{2+}. In general, increasing Fe^{2+}, Fe^{3+} and Cu^{2+} concentrations increase the yield of ·OH in UV/Fenton and PTL systems via reactions (65)-(73), thereby promoting removal of Hg^0 (Liu et al. 2015a; Zhan et al. 2013; Hsueh et al. 2005; Tony et al. 2009; Kwan et al. 2003; Cravotto et al. 2007; Ntampegliotis et al. 2006; Fan et al. 2009).

$$Fe^{2+}(l) + H_2O_2(l) \rightarrow Fe^{3+}(l) + \cdot OH(l) + OH^-(l) \tag{65}$$

$$Fe^{3+}(l) + H_2O_2(l) \rightarrow [Fe(HO_2)]^{2+}(l) + H^+(l) \tag{66}$$

$$[Fe(HO_2)]^{2+}(l) \xrightarrow{UV} Fe^{2+}(l) + HO_2 \cdot (l) \tag{67}$$

$$Cu^{2+}(l) + H_2O_2(l) \rightarrow Cu^+(l) + HO_2 \cdot (l) + H^+(l) \tag{68}$$

$$Cu^+(l) + H_2O_2(l) \rightarrow Cu^{2+}(l) + \cdot OH(l) + OH^-(l) \tag{69}$$

$$[Cu(HO_2)]^+(l) \xrightarrow{UV} Cu^+(l) + HO_2 \cdot (l) \tag{70}$$

1539 $$Fe^{3+}(l) + H_2O_2(l) \rightarrow Fe^{2+}(l) + HO_2 \cdot (l) + H^+(l) \quad (71)$$

1540 $$Fe^{2+}(l) + H_2O_2(l) \rightarrow Fe^{3+}(l) + \cdot OH(l) + OH^-(l) \quad (72)$$

1541 $$[Fe(HO_2)]^{2+}(l) \xrightarrow{UV} Fe^{2+}(l) + HO_2 \cdot (l) \quad (73)$$

1542 However, adding excessive Fe^{2+} will result in scavenging of ·OH by Fe^{2+} and radical recombination through the
1543 side reactions (74)-(77) with very large reaction rates (Liu et al. 2015a; Zhan et al. 2013; Hsueh et al. 2005; Tony
1544 et al. 2009; Kwan et al. 2003; Cravotto et al. 2007; Ntampegliotis et al. 2006; Fan et al. 2009), thereby inhibiting
1545 Hg^0 removal.

1546 $$Fe^{2+}(l) + \cdot OH(l) \rightarrow Fe^{3+}(l) + OH^-(l) \qquad k = 3.0 \times 10^8 M^{-1}s^{-1} \quad (74)$$

1547 $$\cdot OH(l) + \cdot OH(l) \rightarrow H_2O_2(l) \qquad k = 5.5 \times 10^9 M^{-1}s^{-1} \quad (75)$$

1548 $$\cdot OH(l) + HO_2 \cdot (l) \rightarrow H_2O(l) + O_2(l) \qquad k = 1.0 \times 10^{10} M^{-1}s^{-1} \quad (76)$$

1549 $$HO_2 \cdot (l) + HO_2 \cdot (l) \rightarrow H_2O_2(l) + O_2(l) \qquad k = 3.4 \times 10^7 M^{-1}s^{-1} \quad (77)$$

1550 **(4) Effects of temperature**

1551 Heterogeneous gas-liquid reacting systems are affected by temperature via the coupled effects of a chemical
1552 reaction rate, solubility of gas in solution and mass transfer rate. Liu et al. 2014a, 2014c, 2014d, 2015a and Zhang
1553 et al. 2013 studied the effects of temperature on Hg^0 removal using UV/H_2O_2 process,
1554 homogeneous/heterogeneous PTL reactions, and found oxidation of Hg^0 to be slightly reduced with increasing
1555 reaction temperature. On the other hand, Zhan et al. 2013 found Hg^0 removal using homogeneous UV/Fenton
1556 reaction to be promoted by low temperature, but was significantly inhibited by high temperature. Liu et al. 2014a,
1557 2014c, 2014d, 2015a, Zhan et al. 2013 and Zhang et al. 2013 suggested that increasing temperature increased
1558 chemical reaction rate of Hg^0 removal, and accelerated the decomposition of H_2O_2 but also reduced the solubility
1559 of Hg^0 in water with the net effect of reducing Hg^0 removal.

1560 **(5) Effects of solution pH**

Liu et al. 2014a, 2014c, 2014d, 2015a and Zhang et al. 2013 investigated the effects of solution pH on Hg^0 removal by UV/H_2O_2 process and homogeneous/heterogeneous PFL reactions, respectively, found that Hg^0 removal to significantly decrease with increasing solution pH in all systems. It is well known that H_2O_2 in alkaline solution produce HO_2^-, which can consume ·OH and H_2O_2 as shown in reactions (78) and (79) (Zhan et al. 2013; Liu et al. 2013c; Liu et al. 2012a; Liu et al. 2011b).

$$H_2O_2(l) \leftrightarrow HO_2^- (l) + H^+(l) \quad (78)$$

$$\cdot OH(l) + HO_2^- (l) \rightarrow H_2O(l) + O_2^- \cdot (l) \quad (79)$$

Increasing solution pH promotes higher OH^- concentration which neutralizes H^+, and shifts reaction (78) to the left to further raise the yield of HO_2^- and reduce the effectiveness of Hg removal. Some studies have also confirmed that H_2O_2 and Fenton-Like reagents often provide stronger oxidizing environment under acidic conditions (Liu et al. 2014a, 2014b, 2014c, 2015a).

(6) Effects of gas flow/liquid-gas ratio

The gas flow/liquid-gas ratio is an important parameter for the design and operation of reactor. Related studies (Liu et al. 2011a) indicated that a small gas flow or large liquid-gas ratio generally helped improve removal efficiency of pollutants. However, a small gas flow or large liquid-gas ratio generally also requires a larger reactor volume, thereby increasing the investment and operating costs of systems. Liu et al. 2014a, 2014c, 2014d, 2015a and Zhang et al. 2013 investigated the effects of gas flow/liquid-gas ratio on Hg^0 removal using homogeneous/heterogeneous PTL reactions and UV/H_2O_2 process in a photochemical bubble reactor and a photochemical spray reactor, and showed that Hg^0 oxidation efficiency significantly decreased with increasing gas flow or reducing liquid-gas ratio.

(7) Effects of Hg^0 inlet concentration

Liu et al. 2014a, 2014c, 2014d, 2015a and Zhang et al. 2013 studied the effects of Hg^0 inlet concentration on

1583 Hg^0 oxidation in UV/H_2O_2 process and homogeneous/ heterogeneous PFL reactions reported that the changes of
1584 Hg^0 inlet concentration had only a slight effect on Hg^0 oxidation, suggesting that wet photochemical AOTs have
1585 an excellent adaptability to changes in Hg^0 concentration in the flue gas.

1586 **4.3.2 Effects of flue gas components on Hg^0 removal using wet photochemical AOTs**

1587 Liu et al. 2014a, 2014c, 2014d, 2015a and Zhang et al. 2013 investigated the effects of O_2, SO_2, CO_2 and NO
1588 on Hg^0 removal by UV/H_2O_2 process and homogeneous/heterogeneous PFL reactions, and found the addition of
1589 SO_2 or NO to reduce Hg^0 oxidation, while O_2 slightly enhanced the reaction but CO_2 has no noticeable effect.
1590 Zhan et al. 2013 also investigated the effects of O_2, SO_2 and NO on Hg^0 removal using UV/Fenton process, and
1591 they found that an appropriate O_2 concentration promoted Hg^0 oxidation, but O_2 concentration higher than 9%
1592 inhibited the reaction. SO_2 had an inhibitory effect on Hg^0 oxidation, but the inhibition was slower with further
1593 increase in SO_2 concentration, while NO had no obvious effect on Hg^0 oxidation.

1594 In the presence of O_2 in the flue gas, the yield of O_3 and $\cdot O$ would increase by the above reactions (56)-(60)
1595 (Liu et al. 2014a, 2014c, 2014d, 2015a), thereby promoting Hg^0 removal. However, addition of excess O_2 would
1596 also result in the excessive consumption of active free radicals, negatively impacting Hg^0 removal (Liu et al.
1597 2014a, 2014c, 2014d, 2015a). On the other hand, NO could compete with Hg for available oxidants such
1598 as $\cdot OH$, $\cdot O$, O_3 and H_2O_2 via reactions (80)-(86), reducing the oxidation rate of Hg^0 (Liu et al. 2014a, 2014c,
1599 2014d, 2015a).

1600 $$NO(l) + \cdot OH(l) \rightarrow HNO_2(l) \quad (80)$$

1601 $$NO(l) + \cdot O(l) \rightarrow NO_2(l) \quad (81)$$

1602 $$NO(l) + O_3(l) \rightarrow NO_2(l) + O_2(l) \quad (82)$$

1603 $$HNO_2(l) + H_2O_2(l) \rightarrow HNO_3(l) + H_2O(l) \quad (83)$$

1604 $$NO_2(l) + \cdot OH(l) \rightarrow HNO_3(l) \quad (84)$$

$$2NO_2(l) + H_2O_2(l) \rightarrow 2HNO_3(l) \quad (85)$$

$$2NO(l) + 3H_2O_2(l) \rightarrow 2HNO_3(l) + 2H_2O(l) \quad (86)$$

Similarly, SO_2 would compete with the oxidants via reactions (87)-(94) to reduce Hg^0 removal (Liu et al. 2014a, 2014c, 2014d, 2015a).

$$SO_2(l) + H_2O(l) \leftrightarrow HSO_3^-(l) + H^+(l) \quad (87)$$

$$HSO_3^-(l) \leftrightarrow SO_3^{2-}(l) + H^+(l) \quad (88)$$

$$HSO_3^-(l) + \cdot OH(l) \rightarrow \cdot SO_3^-(l) + H_2O(l) \quad (89)$$

$$SO_3^{2-}(l) + \cdot OH(l) \rightarrow \cdot SO_3^-(l) + OH^-(l) \quad (90)$$

$$HSO_3^-(l) + H_2O_2(l) \rightarrow SO_4^{2-}(l) + H^+(l) + H_2O(l) \quad (91)$$

$$SO_3^{2-}(l) + H_2O_2(l) \rightarrow SO_4^{2-}(l) + H_2O(l) \quad (92)$$

$$HSO_3^-(l) + \cdot O(l) \rightarrow SO_4^- \cdot (l) + \cdot H(l) \quad (93)$$

$$SO_3^{2-}(l) + O_3(l) \rightarrow SO_4^{2-}(l) + O_2(l) \quad (94)$$

However sulfuric and nitric acids produced from reactions (80)-(94) will reduce solution pH, which is not beneficial to Hg^0 removal. The results will depend on the different reaction systems and experimental conditions, reflecting the difference in results between Liu et al. 2014a, 2014c, 2014d, 2015a, Zhang et al. 2013 and Zhan et al. 2013.

4.3.3 Products and active intermediates of Hg^0 removal using wet photochemical AOTs

Liu et al. 2014a, 2014c, 2014d, 2015a, using a fluorescence spectrometry method, determined the reaction products of Hg^0 removal from flue gas in UV/H_2O_2 process and homogeneous PFL reactions and observed that Hg^{2+} was the main reaction product in solution resulting from almost complete oxidation of Hg^0. The result was also verified by mass balance calculation of total Hg in different reaction systems and are summarized in Table 6.

Table 6. Comparison of products and mass balance of total Hg in different reaction systems.

Reaction systems and Reactors	UV/H_2O_2 (Liu et al. 2014a) Spray reactor		UV/H_2O_2 (Liu et al. 2014c) Bubbling reactor		UV/H_2O_2 (Liu et al. 2014d) Spray reactor		Fe^{3+}-induced (Liu et al. 2015a) Photo-Fenton-like Bubbling reactor		Cu^{2+}-induced (Liu et al. 2015a) Photo-Fenton-like Bubbling reactor	
Type of mercury	Hg^0	Total Hg	Hg^0	Total Hg	Hg^0	Total Hg	Hg^0	Total Hg	Hg^0	Total Hg
Mea-value (μg/L)	0	3.41	0	5.46	0	3.48	0	1.73	0	1.77
Cal-value (μg/L)	—	3.73	—	6.19	—	3.83	—	2.07	—	1.96
Relative error (%)	—	8.58%	—	11.79%	—	9.1%	—	16.4%	—	9.0%

In order to better understand reaction mechanism of Hg^0 removal, Liu et al. 2014a and 2014c monitored the key active intermediate, ·OH in the UV/H_2O_2 process, which is difficult to detect in solution due to its high reactivity and short life span, using "indirect capture" method. The basic principle of this method is the addition of a capturing agent to react with ·OH to product more stable intermediates, thereby indirectly detecting the presence of ·OH (Liu et al. 2014a and 2014c). The capturing agent, salicylic acid (SA), was used to capture ·OH by a hydroxylation reaction, which produced relatively more stable hydroxylated products, 2,3-DHBA and 2,5-DHBA. The 2,3-DHBA and 2,5-DHBA, with a relatively longer life than ·OH, were determined by liquid-mass spectrometry (LC-MS) with UV and MS detectors (Liu et al. 2014a and 2014c). The relevant reaction is given in equation (95), and the resulting LC-MS chromatograph is illustrated in Figure 21:

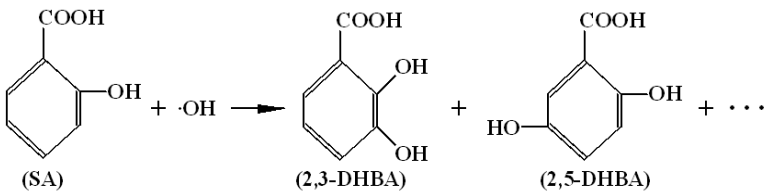

(95)

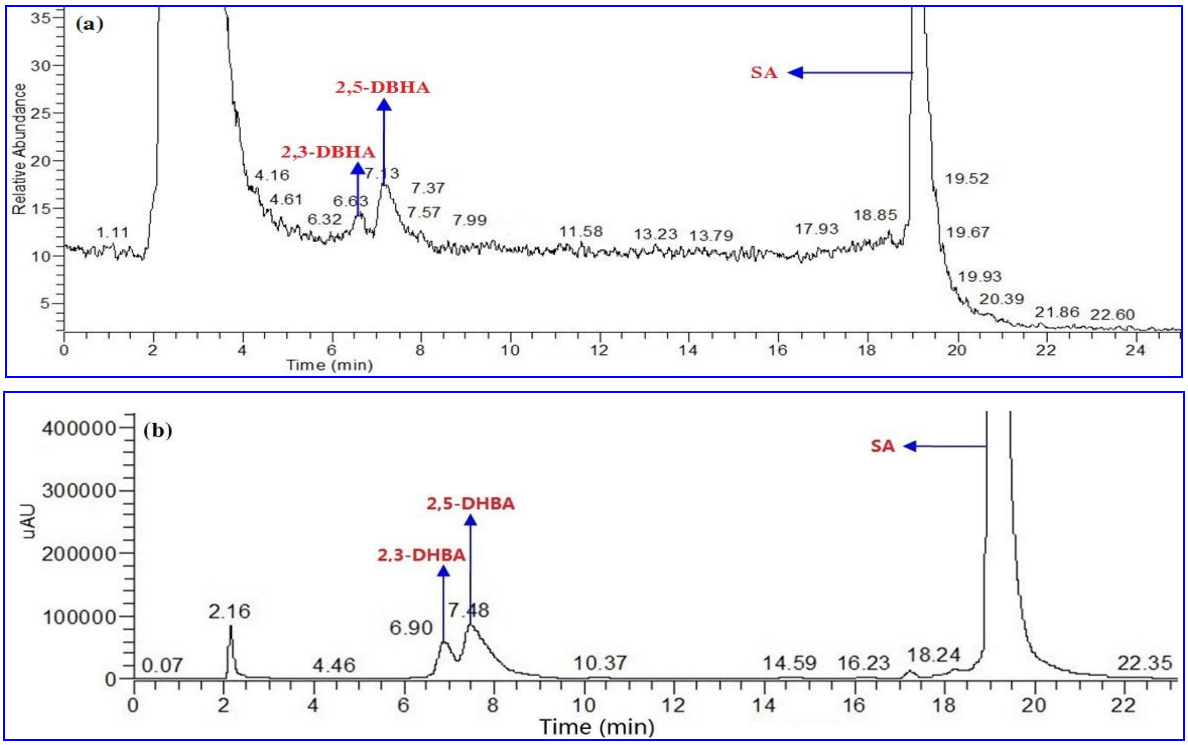

Figure 21. Determination of hydroxylated products 2,3-DHBA and 2,5-DHBA by the MS detector (a) and the UV detector (b) in liquid-mass spectrometry (LC-MS) (Liu et al. 2014a and 2014c).

Liu et al. 2015a used another effective method, electron spin resonance (ESR) spectrometer combining with 5,5-dimethy l-1- pyrrolidine N-oxide (DMPO) as a spin trap agent, to detect ·OH and also achieved good results. As shown in Figure 22, under catalysis of Fe^{3+} and Cu^{2+}, both of the typical four-line ESR spectrums were detected in solution. The hyperfine splitting constants a_N = 15.2 G and a_H = 14.7 G were in good agreement with the literature data a_N = 15.0 G and a_H = 14.8 G (Liu et al. 2014b), showing that ·OH was also produced in homogeneous Photo-Fenton-Like reactions. These results provided powerful supports for studying the reaction mechanism and pathways of Hg^0 removal by wet photochemical AOTs.

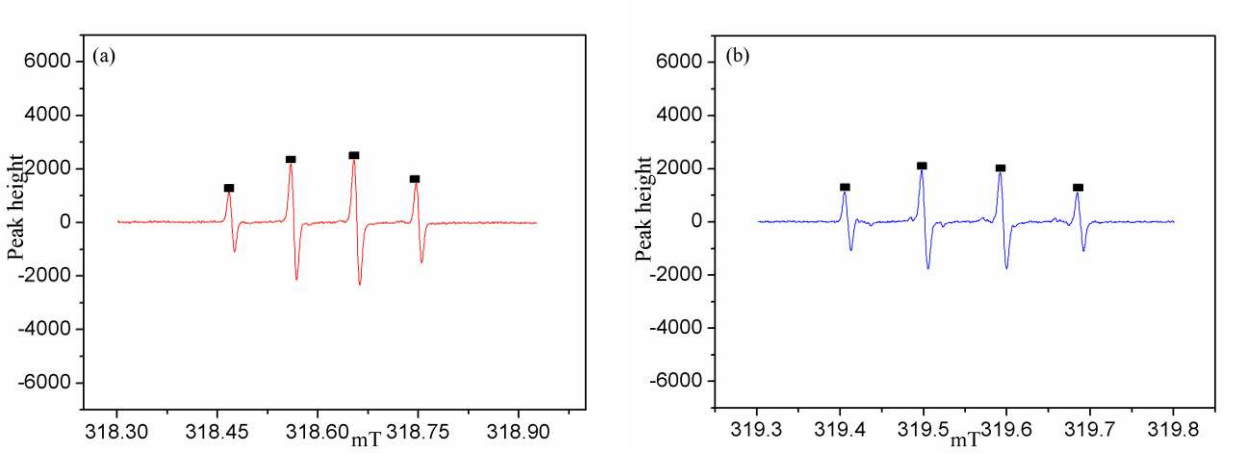

1650

1651 **Figure 22.** ESR spectrums of ·OH radical adducts in two homogeneous Photo-Fenton-Like reactions: (a) catalysis

1652 of Fe^{3+}; (b) catalysis of Cu^{2+} (Liu et al. 2015a).

1653 **4.3.4 Mechanism of Hg^0 removal using wet photochemical AOTs**

1654 Liu et al. (2014a, 2014c, 2014d) studied the reaction mechanism and pathways of Hg^0 removal in the

1655 UV/H_2O_2 process systematically based on the determination of the reactive intermediates and reaction products.

1656 The reaction mechanism and pathways are hypothesized to consist of the following five steps: **(a)** active

1657 substances such as ·OH, ·O and O_3 are produced through UV photolysis of O_2 and H_2O_2; **(b)** removals of Hg^0 by

1658 oxidations of ·OH, ·O and O_3; **(c)** removal of Hg^0 by photoexcitation reaction of Hg^0 with H_2O; **(d)** removal of

1659 Hg^0 by oxidation of H_2O_2; **(e)** termination of radical chain reactions (Liu et al. 2014a, 2014c, 2014d, 2015a).

1660 Among these pathways depicted in Figure 23, photochemical, ·OH and ·O/O_3 oxidations are suggested to play a

1661 major role in Hg^0 removal, while Hg^0 removal by H_2O_2 oxidation only plays a secondary role.

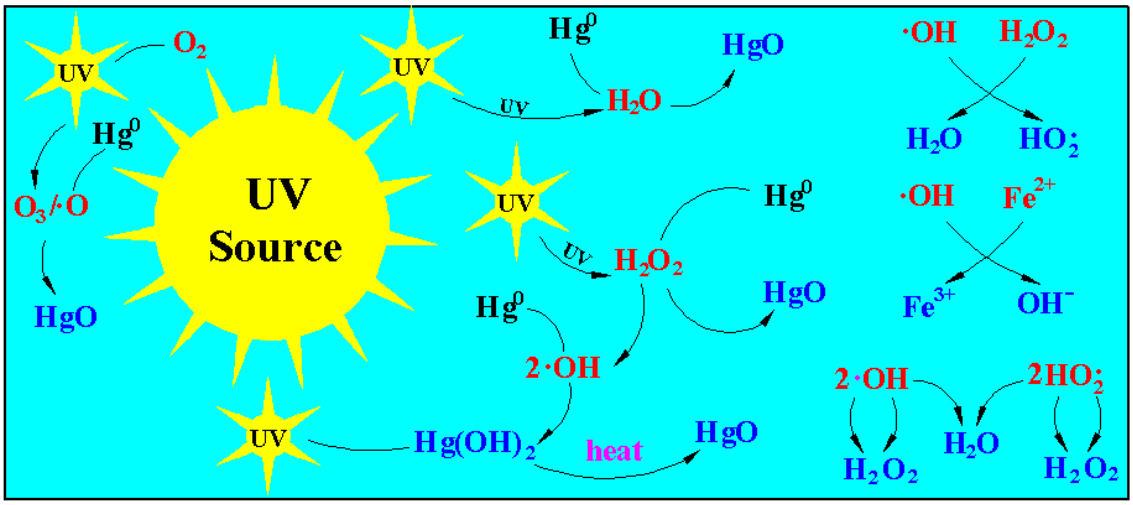

Figure 23. Schematic diagram of reaction mechanism and pathways of Hg^0 removal by UV/H_2O_2 process.

4.4 Reactor and process flow of Hg^0 removal using wet photochemical AOTs

4.4.1 Reactor of Hg^0 removal using wet photochemical AOTs

Photochemical reactors for gaseous Hg^0 removal are divided into two categories based on whether it is a dry or wet process. Granite et al. 2001, 2002, 2003, and Jia et al. 2010 made a contribution for the development of dry photochemical reactors for Hg^0 removal. A dry photochemical reactor with external UV lamp for removing Hg^0 in flue gas was developed by Granite et al. 2001, 2002, 2003, which is described in Figure 24(a). Jia et al. 2010 further designed a dry photochemical reactor with built-in UV lamp, which is described in Figure 24(b). Both dry photochemical reactors have demonstrated a good mercury removal performance.

Zhan et al. 2013 designed a wet photochemical reactor with external UV lamp, which is described in Figure 24(c). However, the wet external structure is not as conducive to large-scale application due to its low light utilization and structural defects. Liu et al. (2014a, 2014c, 2014d, 2015a) developed two more practical wet photochemical reactors, including a photochemical bubbling reactor and a photochemical spray reactor, to remove NO, SO_2 and Hg^0 in flue gas using UV/H_2O_2 and two Photo-Fenton-like AOTs, and achieved good results. The results of Liu et al. 2012b, 2012c, 2013b showed that the photochemical bubbling reactor was more suitable for processing a slow or medium speed reaction system, while the photochemical spray reactor was more suitable for

processing a fast reaction system due to its large gas-liquid contact area. The two wet photochemical reactors are described in Figure 24(d) and (e).

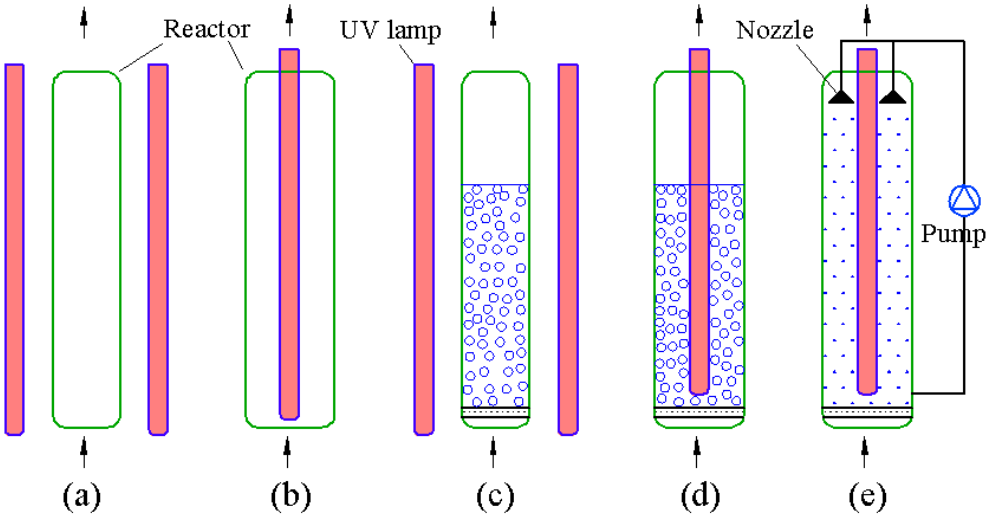

Figure 24. Dry and wet photochemical reactors for removing Hg^0 in flue gas: (a) Dry photochemical reactor with external UV lamp; (b) Dry photochemical reactor with built-in UV lamp; (c) Wet photochemical bubbling reactor with external UV lamp; (d) Wet photochemical bubbling reactor with built-in UV lamp; (e) Wet photochemical spray reactor with built-in UV lamp.

4.4.2 Process flow of Hg^0 removal using wet photochemical AOTs

Granite et al. 2001, 2003 and 2003 and Jia et al. 2010 presented typical apparatus and process flow for a dry removal process; and Granite et al. and Anthony et al., Liu et al. 2013a and 2013b presented results for further development of this technology. These results show that 254 nm UV light source can be directly coupled to the existing flue of boiler or incinerator, and installed at different positions in the flue gas system, including upstream of the dust collector and gas-gas heat exchanger (GGH), and after GGH and before the inlet of the WFGD system. The front is defined as a high temperature arrangement, and the back is a low-temperature arrangement. The two kinds of arrangements are described in Figure 25 (a) and (b) as follows, respectively.

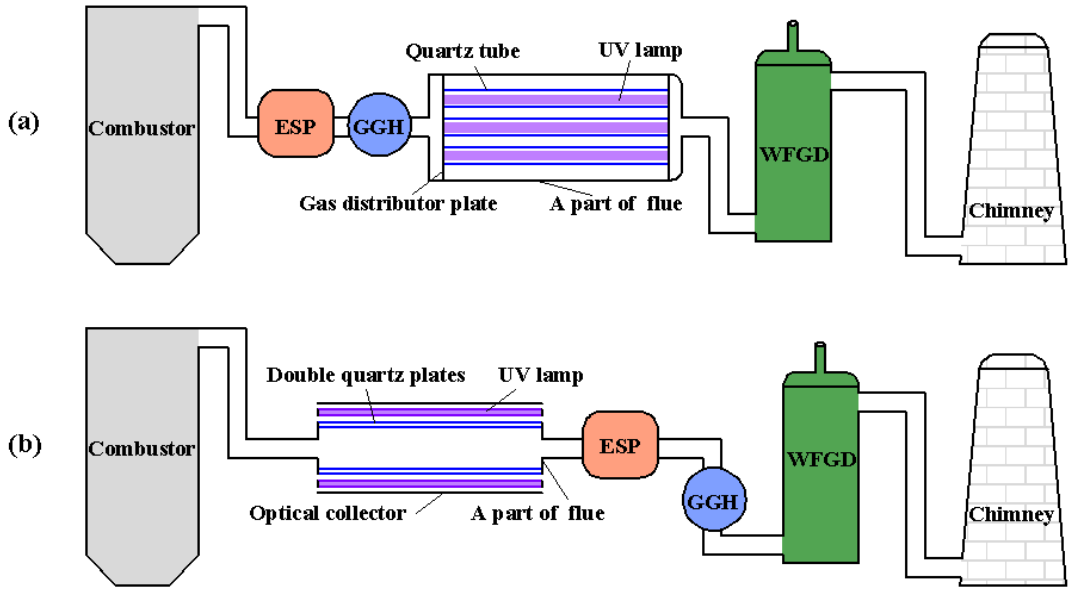

Figure 25. Process flow of Hg^0 removal using dry photochemical oxidation: (a) Low temperature arrangement of dry photochemical reactor; (b) High temperature arrangement of dry photochemical reactor.

Liu et al. 2013a and 2013b suggested that UV-light source should be installed after the GGH and before the inlet of WFGD device because 254nm UV lamp was only suitable for operating at low temperatures. The optimum operating temperature is 5-50℃, and high temperature will greatly reduce the operational efficiency of 254 nm UV lamp) (Liu et al. 2011a), which is described in Figure 25(a) (low temperature arrangement of reactor). However, to take advantage of Hg^{2+} removal via adsorption by fly ash in the precipitator, the UV-light source could also be installed before the precipitator/GGH. In this case, flue gas temperature is usually higher than 130℃ (Liu et al. 2011a), using a built-in arrangement in Figure 25(a) is inappropriate due to the adverse effects of high temperature on UV lamp operation. Compared to the built-in arrangement in the Figure 25(a), an external arrangement in Figure 25(b) not only can make full use of removal capacity of Hg^{2+} by fly ash in the precipitator, but also avoids the adverse influence of high temperature on UV lamp operation. To prevent the loss of heat in flue gas, a double quartz plate with vacuum sandwich may be used to separate the high temperature flue gas and UV lamps (Liu et al. 2013a and 2013b). An optical collector is also necessary to make full use of UV light. Besides, based on the treatment amount of flue gas, this kind of external photochemical reactor may be amplified

1710 by using parallel connection of several same reactors (Liu et al. 2013a and 2013b).

1711 The Hg^0 in flue gas from combustor will be oxidized into gaseous and solid HgO. A large number of studies
1712 (Liu et al. 2014a, 2014c, 2014d, 2015a) has shown that, compared with Hg^0, HgO is easier to remove in a dust
1713 collector or a WFGD device through adsoprtion on fly ash or solution washing. This method has a simple process
1714 and low cost, and can be easily used to revamp the existing thermal power units to achieve mercury removal
1715 in combination with electrostatic/bag type dust collector or WFGD device. At present, the application of this
1716 technology still faces some problems. For example, the product HgO, particulate matters or some other substances
1717 in actual flue gas may deposite on the surface of UV lamp or quartz glass, and significantly reduce UV
1718 transmittance because of the very low penetration capacity of 254nm UV light (254nm UV light can not even pass
1719 through an ordinary glass). In addition, the recovery and utilization of mercury resources deposited on the surface
1720 of UV lamp or quartz glass have not been effectively addressed.

1721 Liu and coworkers 2010c and 2010d have extensively studied the wet removal process and developed two
1722 novel techniques, which are described in Figure 26(a) and (b). It can be seen that the two kinds of processes have
1723 similar process flows and devices, but the key photochemical reactors are different. In Figure 26(a), a
1724 photochemical bubbling reactor is used to remove pollutants. In Figure 26(b), the photochemical bubbling reactor
1725 is replaced by a photochemical spray reactor. Liu et al., demonstrated that both of two photochemical reactors are
1726 very effective in removing Hg^0 and SO_2 in flue gas, but the latter has a higher efficiency for NO removal than the
1727 former because of its far greater surface area and better light transmission efficiency (Liu et al. 2010c, 2010d,
1728 2014a, 2014c, 2014d, 2015a). Given the current and urgent need for the simultaneous removal of NO_x, SO_2 and
1729 Hg^0 from flue gas, the photochemical spray reactor has better prospects for development and applications.

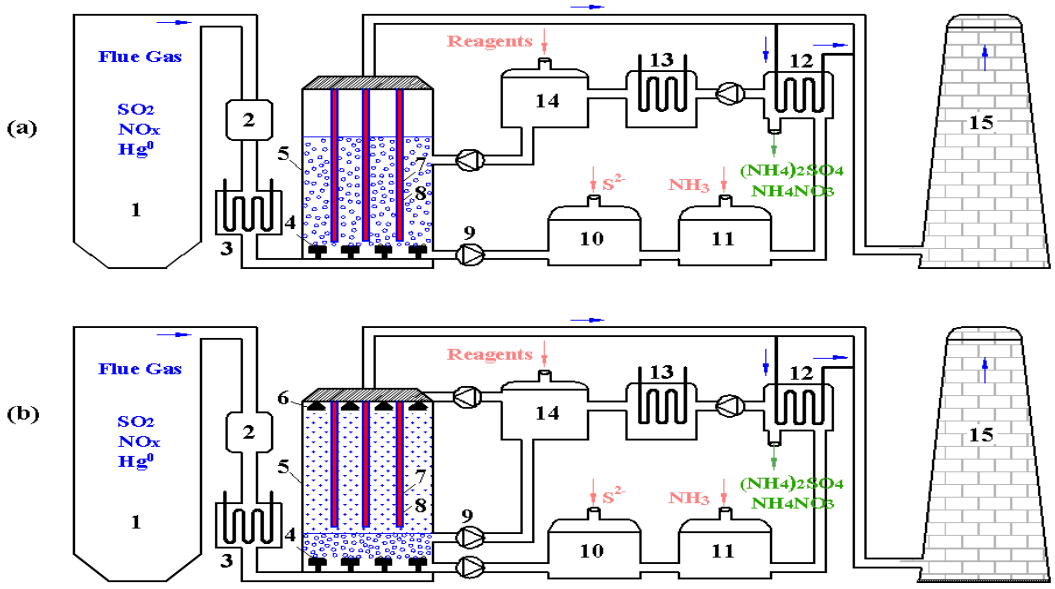

1. Boiler, Furnace or Incinerator; 2. Deduster; 3. Heat Exchanger; 4. Gas Distribution Nozzles; 5. Photochemical Spray Reactor; 6. Atomizing Nozzles; 7. UV Lamps; 8. Quartz Tubes; 9. Circulation Pumps; 10. Hg Separation Tower; 11. NH_3 Neutralizing Tower; 12. Evaporating and Crystallizing Tower; 13. Water Vapor Vondensing Tower; 14. Reagent Addition Tower; 15. Chimney.

Figure 26. Process flow of Hg^0 removal using wet photochemical oxidation: (a) wet photochemical bubbling reactor; (b) wet photochemical spray reactor (Liu et al. 2010c, 2010d and Zhang et al. 2013).

The process flow for the simultaneous removal of NO_x, SO_2 and Hg^0 from flue gas in a photochemical spray reactor is shown in Figure 26 and described as follows: The flue gas system containing $SO_2/NO_x/Hg$ generated by **Boiler, Furnace or Incinerator 1** enters **Deduster 2** and **Heat Exchanger 3** to remove dust and reduce flue gas temperature, and proceeds to the **Photochemical Spray Reactor 5** through **Gas Distribution Nozzles 4** to make a gas-liquid reaction with the oxidizing medium from **Atomizing Nozzles 6 and Reagent Addition Tower 14**. As reported by Liu et al. Liu et al. 2010a, 2010c, 2010d, 2014a, 2014c, 2014d, 2015a, the SO_2, NO_x and Hg can be oxidized to H_2SO_4, HNO_3 and Hg^{2+}, respectively, by a series of oxidation reactions. The Hg^{2+} in mixed solutions can be separated in **Hg Separation Tower 10** by the addition of S^{2+} to react with Hg^{2+} producing HgS precipitates, which can be recycled by simple precipitation separation. The remaining H_2SO_4 and HNO_3 mixed solution can be used to manufacture fertilizers, $(NH_4)_2SO_4$ and NH_4NO_3, by adding NH_3 in **NH_3 Neutralizing Tower 11** with

1746 evaporation and crystallization in **Evaporating and Crystallizing Tower 12** using flue gas waste heat. The
1747 produced water vapor can be condensed into water in **Water Vapor Vondensing Tower 13**, and is recycled back
1748 to the **Reagent Addition Tower 14.** The cleaned flue gas is discharged into the atmosphere by **Chimney 15**.

1749 Liu et al. 2010c and 2010d suggested that the process has several advantages: (1) It can achieve the
1750 simultaneous removal of multi-gaseous pollutants, including SO_2, NO_x and Hg^0; (2) The reaction products can be
1751 recycled by producing agricultural fertilizers such as $(NH4)_2SO_4$ and NH_4NO_3; (3) The dirt on the surface of
1752 quartz tube of UV lamp is easily washed by high-speed liquid spray, avoiding the attenuation of UV-light in wet
1753 photochemical AOTs due to the deposition of dirt; (4) Removal process has no secondary pollution, and even
1754 water can also be recycled; and (5) most of the devices such as light source, spray tower and product
1755 post-processing system are very mature products, which have been widely applied in water treatment and flue gas
1756 purification industries, and can be almost applied directly on this technology. There are about more than 800000
1757 widely used small and medium size coal-fired boilers, industrial furnaces and refuse incinerators in China alone
1758 (Liu et al. 2011a). It is economical to install individual desulfurization, denitrification or mercury removal
1759 equipment for flue gas cleanup. Therefore, this process has a good prospect for multicomponent pollution control
1760 for small- and medium-scale burners and a pilot scale construction is currently underway under the supervision of
1761 the author (Liu and collaborators).

1762 5. Activated oxidant AOTs

1763 While plasma oxidation, photocatalytic oxidation and photochemical oxidation processes have excellent
1764 technological prospects, to date, they have not achieved large-scale applications due to several unresoved issues.
1765 Among these issues, the instability of system operation and the high energy consumption of electrical installations
1766 such as plasma and light source are two of the main obstacles preventing large-scale applications (Liu et al.
1767 2011a). Meanwhile, alternative AOTs involving ion-activated and heat-activated H_2O_2 and persulfate are gaining

popularity due to some good laboratory results in removing Hg^0 from flue gas using various reactor types (Xu et al.2008; Liu et al. 2014b; Lu et al. 2007; Zhao et al. 2014b; Zhao et al. 2014c; Martinezm et al. 2007; Ye et al. 2006; Tan et al. 2007; Liu et al. 2015b).

5.1 An overview of Hg^0 removal using activated H_2O_2 AOTs

5.5.1 Homogeneous Fenton-(like) processes

Fenton reaction (H_2O_2/Fe^{2+}) was discovered in 1894 by H. J. H. Fenton, who reported that H_2O_2 could be activated by Fe^{2+} to oxidize tartaric acid (Fenton et al. 1984). Following this discovery, Fenton-Like reactions with similar characteristics, mainly including H_2O_2/Fe^{3+}, H_2O_2/Cu^{2+}, H_2O_2/Mn^{2+}, H_2O_2/Co^{2+}, etc., have been reported and received world-wide applications in the field of wastewater treatment and soil remediation, as well as flue gas purification, due to their very strong oxidative capabilities and environmentally benign features (Bokare et al. 2014; Babuponnusamiet al. 2014; Garrido-Ramírez et al. 2010; Pouran et al. 2014a; Bagal et al. 2014; Pouran et al. 2014b).

Recently, Lu et al. 2007 investigated for the first time Hg^0 oxidation using Fe^{3+}-based and Cu^{2+}-based Fenton-Like reactions in both bench-scale and pilot-scale wet scrubbers, and found that Fe^{3+}-based Fenton-Like gave better results compared to Cu^{2+}-based ones, obtaining on the average, 75% Hg^0 oxidation. Based on the bench-scale results, a pilot-scale testing for mercury removal based on Fe^{3+}-based Fenton reaction was further carried out by Tan et al. 2007, and a 30-40% of Hg^0 oxidation was achieved in optimized testing conditions. Although Lu et al. 2007 conducted initial research for this technology, but most of the process parameters were not optimized, and Hg^0 removal mechanisms were not studied in depth. Liu et al. 2015b further improved on the studies using Fe^{3+}-based and Cu^{2+}-based Fenton-Like reactions in a spray reactor, and reported that 100% of Hg^0 oxidation was achieved in optimized conditions. Furthermore, both Fe^{3+}-based and Cu^{2+}-based Fenton-Like reactions showed good performance for the simultaneous removal of multi-pollutants. The highest simultaneous

removal efficiencies of Hg^0, SO_2 and NO were up to 100%, 100%, 85.3% and 100%, 100%, 75.3% using catalysis of Fe^{3+} and Cu^{2+} catalysts, respectively. In addition, Liu et al. 2015c further studied the Hg^0 removal using Fenton reagent in a bubble reactor, and also obtianed a good result.

Zhao et al. 2014d designed a semi-dry two-stage-treatment process of the pre-oxidation combined with the absorption to remove Hg^0 in flue gas. The basic experimental procedure and devices are described in Figure 27. It can be seen from the Figure 27 that the vaporized Fenton-based liquid-phase complex absorbent (LCA) initially oxidized Hg^0 in a preoxidation device, and then the produced Hg^{2+} was absorbed in a $Ca(OH)_2$ in adsorbent bed or $CaCO_3$ slurry in a WFGD device. Zhao et al. 2014a noted that the semi-dry two-stage-treatment process can effectively decrease the consumption of water and expensive oxidant, greatly reducing flue gas purification costs.

In addition to ion activation, thermal activation of H_2O_2 also show a good prospect for flue gas purification because this technique can apply the high temperature waste heat from boiler to decompose H_2O_2 to generate ·OH (Martinez et al. 2007). Martinez et al. 2007 investigated the feasibility of using H_2O_2 injection for oxidation of Hg^0 in flue gas and established a detailed kinetic mechanism modeling, and the results demonstrated that the application of H_2O_2, as source of ·OH radicals, accelerated the oxidation of Hg^0 into Hg^{2+}.

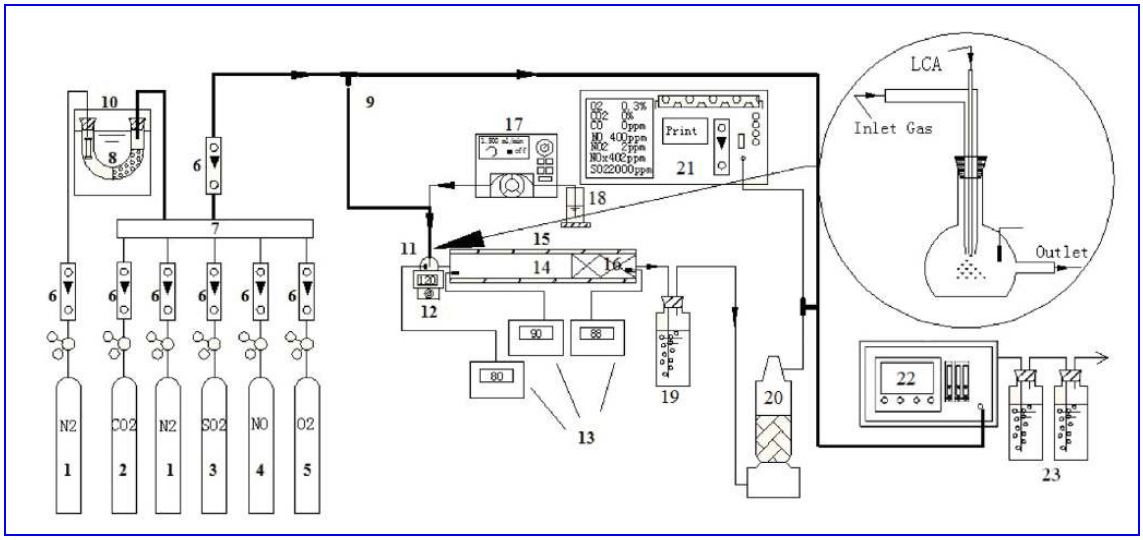

Figure 27. Schematic diagram of the experimental apparatus (Zhao et al. 2014c). (1-5) N_2, CO_2, SO_2, NO, O_2 gas cylinders; (6) Flow meters; (7) Buffer bottle; (8) Mercury osmotic tube; (9) Tee joint; (10) Thermostat water bath;

(11) Vaporization device; (12) Thermal control electric heater; (13) Digital regulators; (14) Reactor; (15) Tube type resistance furnace; (16) Ca-based absorbent; (17) Peristaltic pump; (18) LCA solution; (19) KCl solution; (20) Dry tower; (21) Flue gas analyzer; (22) Cold atom fluorescence mercury detector; (23) H_2SO_4-$KMnO_4$ solution.

5.5.2 Heterogeneous Fenton-(like) processes

The homogeneous Fenton and Fenton-like processed have high oxidation ability for Hg^0 in flue gas, they have several significant disadvantages that constitute the major limitations. First, additional post-treatment processes have to be used to separate the transition metal ions at the end of removal process, which will increase the costs. Second, the homogeneous Fenton solution requires quite low pH value to maintain high reactivity, which is not easy to be controlled. In recent years, the heterogeneous Fenton-like processes have been used widely to degrade organic pollutants from wastewater treatment because of its several advantages in broad pH window and without request for separation of ions (Wang et al. 2016). Zhou et al. 2015a, 2015b, 2015c recently developed several heterogeneous catalysts, such as $Cu_{0.3}Fe_{2.7-x}Ti_xO_4$, $Fe_{3-x}Cu_xO_4$, $Fe_{2.45}Ti_{0.55}O_4$ composites. Based on these catalysts the authors constituteed several novel heterogeneous Fenton-like oxidation systems to remove Hg^0 from coal-fired flue gas, and the results showed that these heterogeneous Fenton-like oxidation systems have good mercury removal performance.

5.1.1 The main influencing factors of Hg^0 removal using activated H_2O_2 AOTs

In studying Hg^0 oxidation using Fe^{3+}-based and Cu^{2+}-based Fenton-Like reactions, Lu et al. 2007 found that solution pH had a significant effect on oxidation of Hg^0 and a suitable pH window was found to be 1.0 to 3.0. Better Hg removal results were achieved by combining sulfur removal and Hg removal, and Hg removal capability using the Fenton-Like reactions was not dependent on the configuration of the wet scrubber. Liu et al. 2015b further studied the effects of several factors on Hg^0 removal using Fe^{3+}- and Cu^{2+}-based Fenton-Like reactions in spray reactor and Fe^{2+}-based Fenton in bubble reactor, and the results indicated that H_2O_2, Fe^{2+}, Fe^{3+}

1829 and Cu^{2+} concentration and liquid-gas ratio significantly promoted Hg^0 removal. Solution pH, NO and SO_2
1830 concentration significantly reduced Hg^0 removal, but inlet Hg^0 concentration and reaction temperature only had a
1831 small impact on Hg^0 removal.

1832 Zhao et al. 2014c also studied the influence of process parameters on Hg^0 in flue gas using the
1833 above-mentioned semi-dry two-stage-treatment process, and showed that Hg^0 removal efficiency to increase with
1834 increasing oxidant addition rate and reaction temperature, and then decreased with exceeding a certain value. Hg^0
1835 oxidation was inhibited with increasing solution pH and Hg^0 inlet concentration. Zhou et al. 2015a, 2015b, 2015c
1836 studied the effects of several factors on Hg^0 removal using several novel heterogeneous Fenton-like oxidation
1837 systems, and the results showed that several factors, such as reaction temperature, solution pH, catalyst dosage,
1838 H_2O_2 dosage, NO content, etc., had significant effect on Hg^0 removal. However, changing the content of SO_2 in
1839 flue gas often only had little impact on the Hg^0 removal.

1840 **5.1.2 Product, intermediate, mechanism of Hg^0 removal using activated H_2O_2 AOTs**

1841 Martinez et al. 2007 studied the kinetic reaction mechanism of Hg^0 oxidation using H_2O_2 injection through a
1842 plug flow reactor model from CHEMKIN 4.0, and carried out a sensitivity analysis to determine the dependence
1843 of model solution on the model input parameters. The sensitivity analysis of the reaction mechanism indicated that
1844 the pathway for the oxidation of Hg^0 followed the interactions between Cl_2 and the added supply of H_2O_2. The
1845 majority of Cl_2 in flue gas was converted into atomic Cl· and HOCl through the reaction with ·OH radicals. The
1846 added ·OH radicals converted Cl_2 into Cl·, which triggered the formation of $HgCl_2$ through HgCl as an
1847 intermediate substance. Hence, the authors concluded that the supply of ·OH radicals through H_2O_2 dissociation
1848 enhanced the oxidation of Hg^0 by the aforementioned pathway. Zhao et al. 2014c determined the products and
1849 reaction mechanism of Hg^0 removal using the two-stage-treatment process, and verified them to be $Hg_2(OH)_2$,
1850 HgCl and $HgCl_2$ by using XRD and atomic fluorescence spectrometry (AFS) . The reaction mechanism of Hg^0

1851 removal was found to include several steps: (1) generation of active species such as ·OH, Cl·, $ClOH\cdot^-$, etc. by the
1852 initiation of Fenton reaction; (2) pre-oxidation of Hg^0 in flue gas by these active species; and (3) generation of
1853 reaction products, $Hg_2(OH)_2$, HgCl and $HgCl_2$, by the back absorption.

1854 Liu et al. 2015b also measured the products and intermediates of Hg^0 removal in Fe^{2+}-based and Cu^{2+}-based
1855 Fenton-Like reactions using liquid fluorescence spectrometer and ESR spectrometer, and determined that Hg^{2+}
1856 was the final product of Hg^0 removal and ·OH produced in solution. Liu et al. 2015b also suggested the following
1857 mechanistic steps by analyzing reaction products and monitoring ·OH: **(A)** ·OH is produced in solution through a
1858 series of catalytic and free radical chain reactions according to the equations (65),(66),(68) and (69); **(B)** Hg^0 is
1859 removed by ·OH and H_2O_2 oxidations according to equations (55) and (63). In the two removal pathways, Hg^0
1860 removal by oxidation of ·OH plays a major role, and Hg^0 removal by oxidation of H_2O_2 only plays a secondary
1861 role in removal of Hg^0; **(C)** radical chain reactions will terminate by reactions (64) and (74)-(77) discussed earlier.
1862 Zhou et al. 2015a, 2015b, 2015c also studied the removal mechanism of Hg^0 removal using several novel
1863 heterogeneous Fenton-like oxidation systems based on the preliminary experimental analysis and discussions.

1864 **5.1.3 Kinetics of Hg^0 removal using activated H_2O_2 AOTs**

1865 At present, the reports related to kinetics of Hg^0 removal using activated H_2O_2 oxidation are rare. Zhao et al.
1866 2014d evaluated the macrokinetics of Hg^0 oxidation using a two-stage-treatment process, and they found that the
1867 reaction was a pseudo first-order with respect to Hg^0, and the apparent activation energy was 14.3 kJ/mol.

1868 **5.2 An overview of Hg^0 removal using activated persulfate AOTs**

1869 Persulfate or peroxydisulfate anion ($S_2O_8^{2-}$) is a strong oxidant with a redox potential of 2.01V, and is
1870 considered as a promising choice for clean-up applications because of the ease of storage and transport,
1871 pH-independence, stability and low cost (Khan et al. 2010). Persulfate is a strong oxidizing agent, but it is
1872 kinetically slow under ordinary conditions (Adewuyi et al. 2013; Adewuyi et al. 2010; Fang et al. 2012). Related

studies showed that $S_2O_8^{2-}$ can be activated to generate ·OH and sulfate radicals ($SO_4\cdot^-$) with higher redox potential of 2.6-3.1V either by the homolysis of the oxidant bond using heat (Tan et al. 2013; Ji et al. 2015), ultrasound (Hao et al. 2014; Wang et al. 2014;), microwave (Chou et al. 2015; Qi et al. 2014) or light (Wang et al. 2014; Lin et al. 2011), or by a redox reaction caused by catalysis of various substances (Oncu et al. 2015; Yan et al. 2015; Yang et al. 2011; Liang et al. 2013; Lee et al. 2013; Li et al. 2014c; Li et al. 2014d; Usman et al. 2012) as summarized in Figure 28. Compared to ·OH, $SO_4\cdot^-$ is more selective and demonstrate higher standard reduction potential at neutral pH (Adewuyi et al. 2010; Hao et al. 2014; Oncu et al. 2015; Yang et al. 2011). In recent years, activated persulfate technologies have rapidly evolved with successful applications in the field of wastewater treatment, remediation of contaminated soils and groundwater as well as flue gas purification.

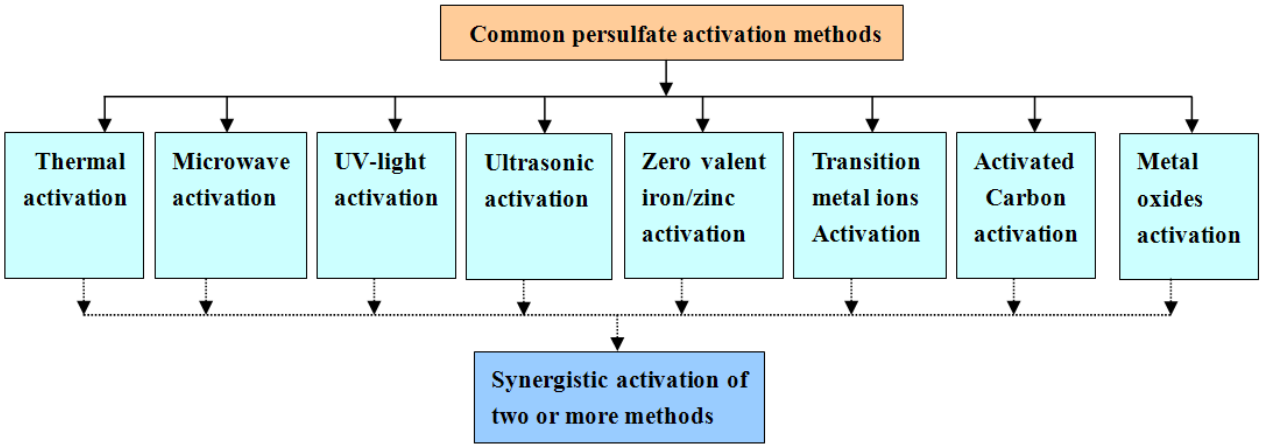

Figure 28. Common activated persulfate methods

Ye et al. 2006 and Xu et al. 2008 used Ag^+-activated and Cu^{2+}-activated $K_2S_2O_8$ to oxidize Hg^0 from flue gas in a simple bubbler, and their results showed that 97.0% and 81.9% of Hg^0 conversion were achieved by Ag^+- and Cu^{2+}-activated $K_2S_2O_8$, respectively. Liu et al. 2014b developed a novel technique on removal of Hg^0 from flue gas by heat-activated $(NH_4)_2S_2O_8$ in a bubbling reactor, which uses the flue gas waste heat from boilers (usually above 130℃) to provide free heat for activation of persulfate. They reported the highest removal efficiency for Hg^0 up to 99.6 %, with reaction product recyclable, and deemed this process to have a good prospect. Zhao et al.

2014b proposed an integrative process of preoxidation of Hg^0 to Hg^{2+} by a vaporized liquid-phase multi-component oxidant made up of H_2O_2 and $Na_2S_2O_8$ coupled with $Ca(OH)_2$ absorption for removing Hg^0 in flue gas. This technique has a process and apparatus similar to Figure 27, but the radical chain reactions were induced by heat-activated persulfate. Zhao et al. 2014b also showed that this method is effective for the simultaneous removal of SO_2, NO and Hg^0 in flue gas, with efficiencies of 100, 83.2 and 91.5 % for SO_2, NO and Hg^0, respectively, under optimal conditions.

5.2.1 The main influencing factors of Hg^0 removal using activated persulfate AOTs

Ye et al. 2006 and Xu et al. 2008 examined the effects of several factors on Hg^0 removal using Ag^+- and Cu^{2+}-activated $K_2S_2O_8$ in a bubbler, and found that Hg^0 conversion efficiency increased with increasing $K_2S_2O_8$, Ag^+ or Cu^{2+} concentration. Low temperature and neutral solution were more conducive to Hg^0 conversion. Liu et al. 2014b also tested the effects of several factors on Hg^0 removal by heat-activated $(NH_4)_2S_2O_8$ in a bubbling reactor, and found that $(NH_4)_2S_2O_8$ concentration and the activation temperature significantly promoted, while solution pH greatly inhibited Hg^0 removal, but the concentrations of Hg^0, NO and SO_2 had insignificant effect.

Zhao et al. 2014b investigated the effects of several factors on Hg^0 removal using an integrative process of preoxidation and absorption previously described and showed that Hg^0 removal efficiency significantly increased with increasing molar ratio of $Na_2S_2O_8$ to H_2O_2, reaction temperature or addition rate of mixed oxidant; and then almost kept constant, greatly decreased and slightly reduced when molar ratio, reaction temperature or addition rate exceeded a certain value, respectively. Hg^0 removal was almost unaffected by pH of mixed oxidant when the pH was between 1.5 and 5.5, but was significantly reduced as pH increased from 5.5 to 7.5. The effect of NO was either promotional or inhibitory depending on its concentration, while the influences of other gases such as O_2, CO_2 and SO_2 could be neglected.

5.2.2 Product, intermediate and mechanism of Hg^0 removal using activated persulfate AOTs

Ye et al. 2006 and Xu et al. 2008 conducted comparative studies to determine the difference in reaction products and mechanism of Hg^0 removal between Ag^+- and Cu^{2+}-activated $K_2S_2O_8$ using cold vapor generation atomic absorption spectrometry (CVAAS) and the addition of tert-butanol inhibitors. The results showed that Hg^0 oxidation was achieved simultaneously via "direct oxidation" by $K_2S_2O_8$ and "indirect reaction" by free radicals, and the final product was Hg^{2+} in liquid phase. Zhao et al. 2014b investigated the product and mechanism of Hg^0 removal using an integrative process of preoxidation and absorption basing on the analysis of XPS for the deposited mercury species, and they found that both HgO and $HgSO_4$ were the main products of Hg^0 removal. The radical chain reactions of Hg^0 removal were induced by heat-activated persulfate, and H_2O_2 played an important role in the free radical chain reactions, improving the yield of free radicals. The reaction mechanism and pathways of Hg^0 removal using this integrative process of pre-oxidation and absorption is also described in Figure 29.

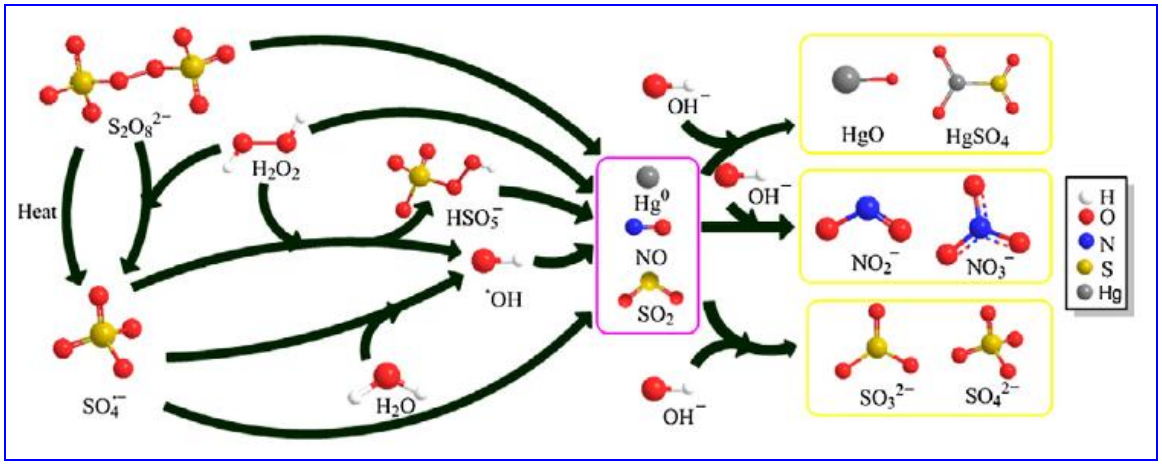

Figure 29. Mechanism of Hg^0 removal using integrative process of preoxidation and absorption (Zhao et al. 2014a).

Liu et al. 2014b studied the reaction mechanism and pathways of Hg^0 removal by heat-activated $(NH_4)_2S_2O_8$, and measured the reaction products and intermediates using liquid fluorescence spectrometer, ion chromatography (IC) and ESR spectrometer. The results indicated that $SO_4^{\cdot-}$ and ·OH in solution were successfully captured using ESR spectrometer, which are shown in Figure 30. Hg^{2+} was the main product of Hg^0 removal, and Hg^0 was mainly

1930 removed by oxidations of $S_2O_8^{2-}$, $SO_4^{-}\cdot$ and $\cdot OH$. The reaction mechanism and pathways of Hg^0 removal using

1931 heat-activated $(NH_4)_2S_2O_8$ proposed are as in reactions (96)-(99).

1932 **(A)** Generation of $SO_4^{-}\cdot$ and $\cdot OH$ by reactions (96) and (97).

1933 $$S_2O_8^{2-}(l) \xrightarrow{heat} 2SO_4^{-}\cdot(l) \quad (96)$$

1934 $$SO_4^{-}\cdot(l) + H_2O(l) \rightarrow \cdot OH(l) + HSO_4^{-}(l) \qquad k = 6.6\times10^2\ s^{-1} \quad (97)$$

1935 **(B)** Oxidative removal of Hg^0 by $SO_4^{-}\cdot$ and $\cdot OH$ via reactions (55) and (98).

1936 $$2SO_4^{-}\cdot(l) + Hg^0(l) \rightarrow Hg^{2+}(l) + 2SO_4^{2-}(l) \quad (98)$$

1937 **(C)** Oxidative removal of Hg^0 by $S_2O_8^{2-}$ via reaction (99).

1938 $$S_2O_8^{2-}(l) + Hg^0(l) \rightarrow Hg^{2+}(l) + 2SO_4^{2-}(l) \quad (99)$$

1939 **(D)** Termination of radical reactions via reactions (64), (74)-(77) and (100)-(102).

1940 $$\cdot OH(l) + S_2O_8^{2-}(l) \rightarrow OH^{-}(l) + S_2O_8^{-}\cdot(l) \qquad k = 1.2\times10^7\ M^{-1}s^{-1} \quad (100)$$

1941 $$SO_4^{-}\cdot(l) + S_2O_8^{2-}(l) \rightarrow SO_4^{2-}(l) + S_2O_8^{-}\cdot(l) \qquad k = 6.1\times10^5\ M^{-1}s^{-1} \quad (101)$$

1942 $$SO_4^{-}\cdot(l) + SO_4^{-}\cdot(l) \rightarrow S_2O_8^{2-}(l) \qquad k = 4.0\times10^8\ M^{-1}s^{-1} \quad (102)$$

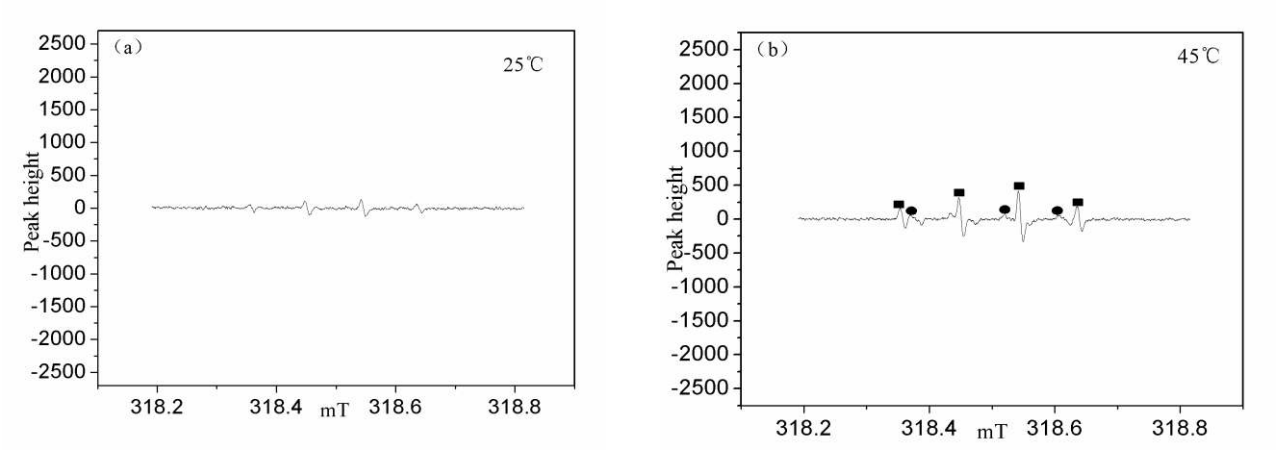

1943

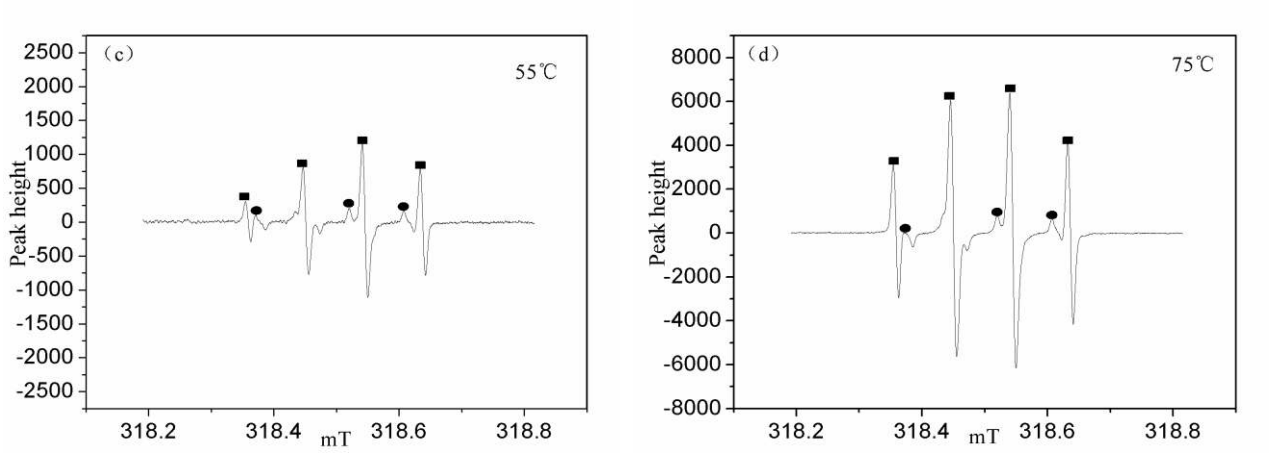

Figure 30. ESR spectra of $SO_4^{-}\cdot$ and ·OH radical adducts at 25℃ (a), 45℃ (b), 55℃ (c) and 75℃ (e). (Circles represent the DMPO-SO_4 and triangles represent the DMPO-OH.) (Liu et al. 2014b).

5.2.3 Kinetics of Hg^0 removal using activated persulfate AOTs

The kinetic parameters and kinetic model are the essential basis for the design and amplification of reactor as well as the numerical simulation of Hg^0 removal process. Ye et al. 2006 studied the kinetics of Hg^0 removal using Ag^+-activated $K_2S_2O_8$ was studied, and determined the kinetic rate constants and activation energy. They found the chemical reaction to be the rate-controlling step for Hg^0 removal. Zhao et al. 2014b studied the macrokinetics of Hg^0 oxidation using an integrative process of preoxidation and absorption, and they found that the reaction was a pseudo first-order with respect to Hg^0, and the apparent activation energy was 14.3 kJ/mol. Liu et al. 2014b investigated the mass-transfer reaction kinetics of Hg^0 removal using heat-activated $(NH_4)_2S_2O_8$ in a bubbling reactor. Their results indicated that when $(NH_4)_2S_2O_8$ concentration was more than 0.1 mol/L and solution pH was lower than 9.71, Hg^0 removal was a pseudo-first-order rapid reaction for Hg^0, and the Hg^0 absorption process could be represented by the following kinetic model (103):

$$N_{Hg^0} = p_{Hg^0,G}\left(\frac{1}{k_{Hg^0,G}} + \frac{1}{H_{Hg^0,L}\left(k_{ov1}\cdot D_{Hg^0,L}\right)^{1/2}}\right)^{-1} \quad (103)$$

where N_{Hg^0} is Hg^0 absorption rate, $mol/m^2\cdot s$; $k_{Hg^0,G}$ is gas phase mass transfer coefficient, $mol/s\cdot m^2\cdot Pa$; $p_{Hg^0,G}$ is Hg^0 partial pressure in gas phase body, Pa; $H_{Hg^0,L}$ is solubility coefficient of Hg^0 in liquid phase,

$mol/(L \cdot Pa)$; k_{ovl,Hg^0} is pseudo-first-order reaction with respect to Hg^0, s^{-1}; $D_{Hg^0,L}$ is the diffusion coefficient of Hg^0 in liquid phase, m^2/s.

Based on the results of reaction mechanism previously described in section 5.2.2 and mass-transfer reaction kinetics, Liu et al. 2014b further proposed a macroscopic kinetic mechanism model of Hg^0 removal involving mass transfer and chemical reaction, which include mainly the following several parts: (1) Hg^0 (g) in gas-phase body firstly reaches the gas-liquid interface by diffusion through gas film, and keep a gas-liquid equilibrium in gas-liquid interface; (2) Hg^0 (l), which has been dissolved in liquid phase enters the liquid film by diffusion through gas-liquid interface, and reacts with $S_2O_8^{2-}/SO_4^{-}\cdot/\cdot OH$ from liquid phase body in a reaction surface; (3) In the reaction surface, a series of chemical reactions (55) and (96)-(99) for Hg^0 removal will occur, other side reactions including (64), (74)-(77) and (100)-(102) occur; and (4) The gaseous products will return to the gas phase body by diffusion through two-film. However, the liquid product such as Hg^{2+} will enter liquid phase body by diffusion through liquid film. The macroscopic kinetic mechanism model of Hg^0 removal from flue gas by thermally activated $(NH_4)_2S_2O_8$ in a bubbling reactor also can be presumably described as in Figure 31.

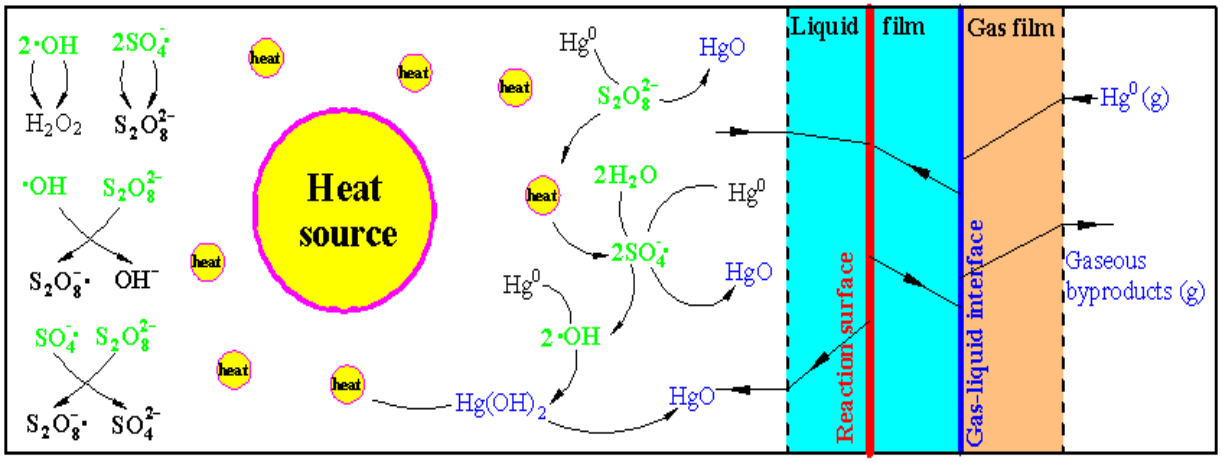

Figure 31. Macroscopic kinetic mechanism model of Hg^0 removal from flue gas by thermally activated $(NH_4)_2S_2O_8$ in a bubbling reactor (Liu et al. 2014b).

5.3 An overview of Hg^0 removal using activated O_3 AOTs

As a well-known oxidant, ozone (O_3) has been widely used for water treatment and flue gas purification (Umar et al. 2013; Ding et al. 2014; Sun et al. 2011; Sun et al. 2013; Wang et al. 2005; Wang et al. 2007; Wen et al. 2009; Wen et al. 2008). To improve utilization rate of O_3 and oxidation ability of process, O_3 is often activated to generate ·OH, ·O, HO_2·, etc. with stronger oxidizing power for removing pollutants using a variety of methods very similar with those used for activating persulfate as illustrated in Figure 28 (Umar et al. 2013; Ding et al. 2014; Sun et al. 2011; Sun et al. 2013; Wang et al. 2005; Wang et al. 2007; Wen et al. 2009; Wen et al. 2008; Einaga et al. 2015; Oh et al. 2014; Lucas et al. 2014; Moussavi et al. 2009; Medellin-Castillo et al. 2013; Kim et al. 2011; Song et al. 2007). In the field of flue gas mercury control, Wang (2005 and 2007) and Wen (2008 and 2009) used an ozone injection process to oxidize Hg^0, NO and SO_2 from flue gas, and proposed a reaction mechanism of Hg^0 removal with 70 elementary reactions. The results showed that Hg^0 oxidation was enhanced by adding more O_3, and a more than 80% Hg^0 oxidation was achieved. The optimal temperature range for Hg^0 oxidation was 473K–523K. Hg^0 removal was achieved by the oxidations of O_3, ·OH, H_2O_2, NO_2 and NO_3 according to the previous reactions (5) and (8) and the following reactions (104)-(106), with the elementary reaction (106) playing a key role in Hg^0 oxidation.

$$H_2O_2(g) + Hg^0(g) \rightarrow HgO(g) + H_2O(g) \quad (104)$$

$$NO_2(g) + Hg^0(g) \rightarrow HgO(g) + NO(g) \quad (105)$$

$$NO_3(g) + Hg^0(g) \rightarrow HgO(g) + NO_2(g) \quad (106)$$

5.4 Reactor and process flow of Hg^0 removal using activated oxidizer AOTs

Currently, the common reactors for Hg^0 removal using activated oxidizer AOTs mainly include bubble column reactor, spray tower reactor, flue injection & adsorption reactor and combined flue injection and flue gas desulfurization tower, and are described in Figure 32. Among these reactors shown in Figure 32 (a), the spray tower has attained widespread industrial application in the field of flue gas purification due to its simple structure,

2000 low flow resistance and large gas-liquid contact area (Zhang et al. 1985). The bubble column tower, Figure 32 (b),
2001 is also popular in laboratory settings due to its simple structure and easy operation, but so far, of limited industrial
2002 applications. In these reactors, the chemical reaction rate caused by free radicals is usually very fast, and hence,
2003 the mass transfer process is often the rate-controlling step (Liu et al. 2012b, 2012c, 2013d; Khan et al. 2010;
2004 Adewuyi et al. 2014) Liu et al. 2014b recently investigated the mass-transfer reaction kinetics of Hg^0 removal
2005 using heat-activated $(NH_4)_2S_2O_8$ in a bubbling reactor, and found the reaction to be rapid and pseudo-first order
2006 with respect to Hg^0, with the mass transfer process as the rate-controlling step. It was also demonstrated that a
2007 reactor with a larger specific interfacial area was the most effective method for enhancing Hg^0 removal (Liu et al.
2008 2014b). The gas-liquid specific surface area of the spray tower (200 m^{-1}) is about ten times that of the bubble
2009 column tower (20 m^{-1}), therefore, it was suggested that the spray tower might be more suitable for Hg^0 removal
2010 using heat-activated $(NH_4)_2S_2O_8$ (Zhu et al. 2005). As described in Figure 33(a), the corresponding process flows
2011 are very similar to typical WFGD process. While industrial applications of flue injection of activated carbon for
2012 waste incineration flue gas purification are well-known, its application as oxidizer for flue gas purification is rare
2013 (Scala et al. 2001; Careya et al. 2011; Zhuang et al. 2011). Compared to the processes of bubbling tower and spray
2014 tower, this kind of flue injection reactor as shown in Figure 32(c) appears to be more suitable for the revamping of
2015 existing boilers. For example, the Hg^0 and NO with low solubility in water may be first oxidized to Hg^{2+} and
2016 $NO_2/HNO_2/HNO_3$, and then can be further washed in existing WFGD device. The specific process flow is
2017 described in Figure 33 (b).

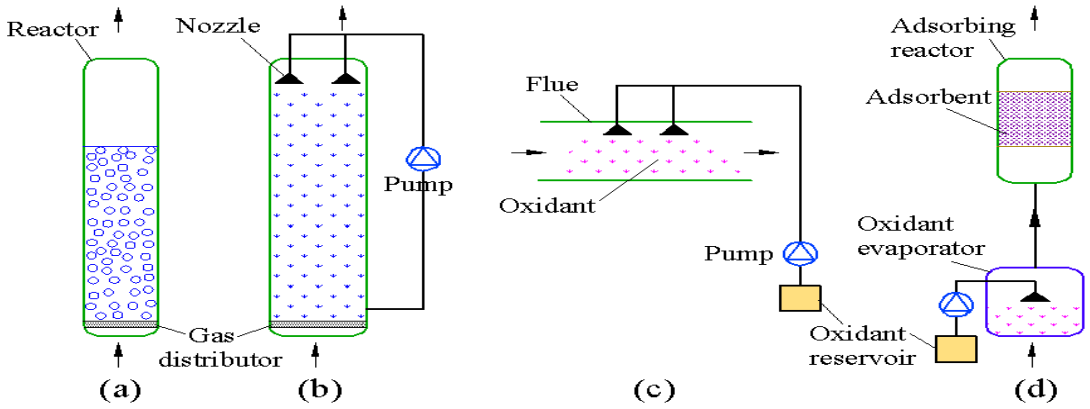

2018

2019 **Figure 32**. Reactor of Hg^0 removal using activated oxidizer AOTs: (a) bubble column tower; (b) spray tower

2020 reactor; (c) flue injection of oxidizer; (d) Pre-oxidation & adsorption.

2021

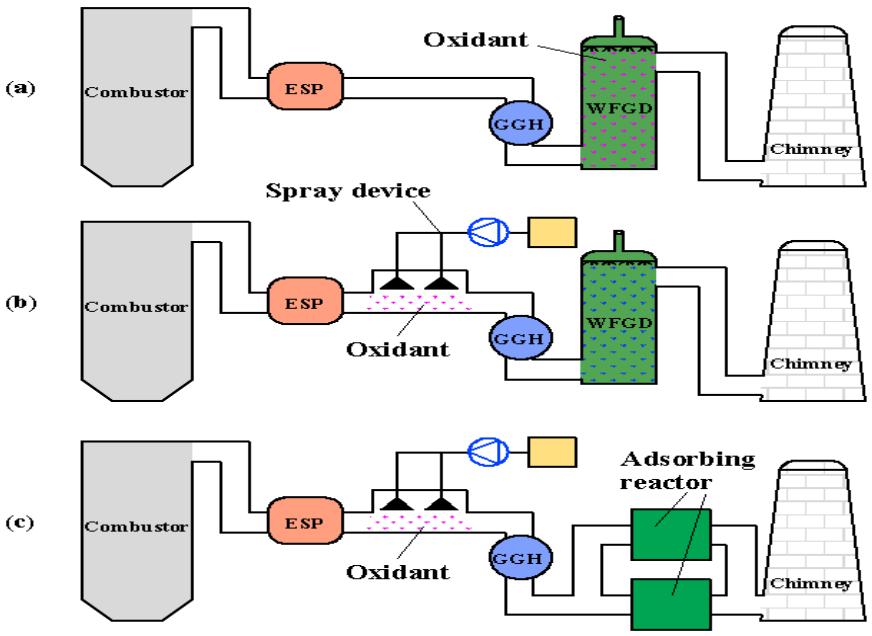

2022

2023 **Figure 33**. Process flow of Hg^0 removal using activated oxidizer AOTs: (a) spray tower reactor process; (b) flue

2024 injection process of oxidizer; (e) pre-oxidation & adsorption process.

2025 At present, although adsorption removal of mercury has demonstrated good prospects, almost all of the

2026 adsorbents have very low adsorption performance for Hg^0 and NO (Liu et al. 2008; Liu et al. 2010d). However, a

2027 large number of modified methods have been recently developed to enhance performance of adsorbents for Hg^0

2028 and NO in flue gas, which appear to have demonstrated significant progress (Liu et al. 2008; Ahmaruzzaman et al.

2010; Wilcox et al. 2012; Liu et al. 2010d). Unfortunately, these lab-scale studies are still difficult to be adapted for industrial applications due to unstable performance and high modification costs. Zhao et al. 2014b and 2014c have proposed the preoxidation & absorption reactor shown in Figure 32 (d), and the corresponding two-stage integrative process shown in Figure 33(c), and similar to Figure 33 (b), which effectively avoid the aforementioned dual problems. In these processes, both Hg^0 and NO in flue gas are oxidized to Hg^{2+} and $NO_2/HNO_2/HNO_3$, which are then easily adsorbed in the back adsorption reactor. It should be noted tha,t to achieve continuous operation of the removal process, it might be necessary to install two parallel adsorption reactors; one for the regeneration of adsorbent and the recovery of products, and the other for the adsorption of pollutants. For this kind of oxidizer flue injection method, it is very necessary to take some effective anti-corrosion measures to protect heat transfer surfaces as well as other rear-mounted devices in flue gas duct due to the inevitable destruction of equipment resulting from erosion and the process oxidants.

6. Summary, concluding remark and future research directions

Recently, AOTs have received significant world-wide attention for multicomponent gas purification and control of air toxics. It is obvious from these discussions that AOTs have great potential for further development and application in the field of Hg^0 control and multicomponent flue gas purification. However, there are still a number of technical issues to be resolved before the realization of the ultimate goal of industrial applications. Major challenges for broader application of AOPs for Hg^0 removal include further development of fundamental understanding of the reaction pathways and dynamics and engineering advancement in materials and equipment to counter the corrosive and erosive effects of reaction products to make these processes more energy-sustainable. These issues are briefly discussed here and some potential research directions also proposed.

(1) Due to very strong oxidizing environment induced by free radicals, AOTs have demonstrated good prospects for the development of clean processes, especially in the field of water treatment, soil remediation as

well as flue gas purification, including the simultaneous and multi-pollutant removal of mainly Hg^0, SO_2, NO_x, H_2S and VOCs in flue gas. This review has discussed a number of new AOTs for effective purification of Hg^0-containing flue gas and outlined new research opportunities and directions. However, due to the very low concentration of mercury in flue gas and huge amount of flue gas, using an independent device to control mercury emission is considered to be an uneconomical method. It is almost impossible, especially for a large number of small/medium-scale burners in civil and industrial sectors, to simultaneously install desulfurization, denitrification and demercurization equipment due to the huge cost. Simultaneous removal of multi-pollutants in flue gas has been recognized as a cost-effective control strategy, which has shown excellent prospects. As previously discussed, AOTs often have excellent removal capability of multi-pollutants due to the non-selectivity and strong oxidation potential of the hydroxyl radical (·OH). Therefore, further studies are necessary in the future to demonstrate the potential of AOPs for the simultaneous removal of SO_2, NO_x and Hg^0 in a single reactor of separation vessel. Such technologies could make a single wet flue gas desulfurization (WFGD) scrubber more cost-effective and could obviate the need to install additional costly equipment as SCR and carbon adsorption for multicomponent gas purification.

(2) Actual flue gas components are extremely complex, and current studies have mostly considered Hg^0 removal only and evaluated the effects of limited components of the flue gas, mainly other gas constituents, and not solid components. For example, fly ash particles or alkali metal salts in actual flue gas may corrode and block the electrodes and discharge spaces of plasma reactor as well as photocatalysts. Deposition of particles and oxidation products on the surface of photocatalysts, plasma electrode and UV lamp quartz tube also result in the decline of photocatalyst activity and system operating efficiency, and even system failure. In future studies, effects of more practical flue gas components should be addressed, and some suitable anti-corrosion and anti-blocking measures developed.

2073 **(3)** Reaction products of Hg^0 removal using AOTs are very important information for recovery of mercury
2074 resources, avoiding new mercury secondary pollution and revealing reaction mechanism. For example, Hg^0
2075 removal using plasma AOTs involves complex reaction pathways and product mixtures. In addition, for AOTs,
2076 capture and identification of reactive intermediates are very useful for understanding the reaction mechanism of
2077 Hg^0 removal. To date, studies on the determination of products are limited and often involve a single solid, liquid
2078 or gaseous phase. However, the removal products of Hg^0 may simultaneously exist in two or three phases.
2079 Moreover, mercury mass balance calculations are very useful for verifying the transfer paths of Hg^0 in the flue gas
2080 system. The plasma, photocatalytic, wet photochemical and oxidant activated AOTs studies currently reported in
2081 the open literature have not adequately addressed the issues of mass balance and the recycling of Hg^0 removal
2082 products. As a result, a more detailed investigation on mechanistic reaction pathways and recycling of Hg^0
2083 removal products is required in future studies.

2084 **(4)** For TiO_2 photocatalytic AOTs, future studies should be focused on developing photocatalysts with
2085 high-performance and high-reliability, especially visible-light-activated (VLA) materials, sensitized processes,
2086 and semiconductor composites using new and efficient doping or coupling techniques to strengthen the activity
2087 and stability of TiO_2 photocatalysts for Hg^0 oxidation. To address the issue of the oxidation products of Hg^0
2088 continuously depositing on photocatalyst and resulting in its deactivation, efficient methods of regeneration and
2089 activation of TiO_2 are needed for further development of this technology. In addition, reemission of HgO on
2090 surface of TiO_2, a phenomenon caused by the competition of water vapor active catalyst sites requires serious
2091 attention. In coal-fired plants where water vapor content of the flue gas is very high, developing effective
2092 measures to inhibit the reemission of HgO is crucial.

2093 **(5)** Design and amplification of reactor is another important task for the application of these technologies. An
2094 efficient reactor will improve pollutant removal efficiency, increase energy efficiency, as well as reduce costs of

system. Kinetic parameters and kinetic model are the essential basis for the design and amplification of reactor as well as the numerical simulation of Hg^0 removal process. For gas-liquid (wet AOPs) and gas-solid (TiO_2 photocatalytic AOPs) systems where the removal process are affected by simultaneous mass transfer (or adsorption) and chemical reaction, detailed investigations to determine the extent of mass transfer intensification as a function of process and operating parameters are needed. Mathematical models should be developed and solved numerically to obtain species and product concentrations and distribution, correlate experimental data, estimate mass transfer and kinetic rate parameters, and predict process performance and appropriate practical limits. However, for plasma, photocatalytic and photochemical reactors for Hg^0 removal, studies on reactor design and amplification are very limited, and require more attention.

This paper provides a state-of-art and unified fundamental chemistry, reaction kinetics and mechanisms and processes of AOPs for the removal of Hg^0 in flue gas in the absence and presence of other flue gas components. It evaluates the performance and economic feasibility of AOPs for multicomponent gas purification and establishes strategies for moving from laboratory studies to large-scale development and industrial use. It is hoped that this review has stimulated thinking beyond the main four AOTs presented and should spur further studies to better demonstrate the potential applications and cost benefits, and future engineering-based research into the continued use of AOPs as environmentally benign technologies for the removal Hg^0 and other pollutants from flue gases.

Acknowledgments

This study was supported by National Natural Science Foundation of China (No.51576094; No.51206067), China Postdoctoral Science Foundation Special Project and General Project (No.2015T80516; No.2013M531281), and Training Project of Jiangsu University Youth Backbone Teacher. The authors also wish to acknowledge the contribution of the United States National Science Foundation (NSF) for funding received by YGA via Grant CBET-0651811.

Reference

An, J.T., Shang. K.F., Lu, N., Jiang, Y.Z., Wang, T.C., Li, J., Wu, Y., 2014a. Performance evaluation of non-thermal plasma injection for elemental mercury oxidation in a simulated flue gas. J. Hazard. Mater. 268, 237–245.

Ahmaruzzaman, M., 2010. A review on the utilization of fly ash. Prog. Energ. Combust. 36, 327–363.

Ayoub, K., Hullebusch, E.D.V., Cassir, M., Bermond, A., 2010. Application of advanced oxidation processes for TNT removal, A review. J. Hazard. Mater. 2010, 10–28.

Antonopoulou, I.M., Evgenidou, E., Lambropoulou, D., Konstantinou, I., 2014. A review on advanced oxidation processes for the removal of taste and odor compounds from aqueous media. Water. Res. 53, 215–234.

Asghar, A., Raman, A.A.A., Daud, W.M.A.W., 2014. Advanced oxidation processes for in-situ production of hydrogen peroxide/hydroxyl radical for textile wastewater treatment, a review. J. Clean. Prod. 2, 1–13.

Adewuyi, Y.G., Sakyi, N.Y., 2013. Simultaneous Absorption and Oxidation of Nitric Oxide and Sulfur Dioxide by Aqueous Solutions of Sodium Persulfate Activated by Temperature. Ind. Eng. Chem. Res. 52, 11702−11711.

An, J.T., Shang, K.F., Lu, N., Jiang, Y.Z., Wang, T.C., Li, J., Wu, Y., 2014b. Oxidation of Elemental Mercury by Active Species Generated From a Surface Dielectric Barrier Discharge Plasma Reactor. Plasma Chem. Plasma Process. 34, 217–228.

Asahi, R., Morikawa, T., Ohwaki, T., Aoki, K., Taga, Y., 2001. Visible light photocatalysis in nitrogen-doped titanium oxides. Science 293, 269−271.

Asilturk, M., Sayilkan, F., Arpac, E., 2009. Effect of Fe^{3+} ion doping to TiO_2 on the photocatalytic degradation of Malachite Green dye under UV and vis-irradiation. J. Photochem. Photobiol. A 203, 64−71.

Adewuyi, Y.G., Sakyi, N.Y., 2010. Removal of Nitric Oxide by Aqueous Sodium Persulfate Simultaneously Activated by Temperature and Fe^{2+} in a Lab-scale Bubble Reactor. 49, 8749–8760.

Adewuyi, Y.G., Khan, M.A., Sakyi, N.Y., 2014. Kinetics and Modeling of the Removal of Nitric Oxide by Aqueous Sodium Persulfate Simultaneously Activated by Temperature and Fe^{2+}. Ind. Eng. Chem. Res. 53, 828−839.

2139 Barnea, Z., Sachs, T., Chidambaram, M., Sasson, Y., 2013. A novel oxidative method for the absorption of Hg^0 from flue gas of coal
2140 fired power plants using task specific ionic liquid scrubber. J. Hazard. Mater. 244–245, 495–500.
2141 Bokare, A.D., Choi, W.Y., Review of iron-free Fenton-like systems for activating H_2O_2 in advanced oxidation processes. J. Hazard.
2142 Mater. 275, 121–135.
2143 Bagal, M.V., Gogate, P.R., 2914. Wastewater treatment using hybrid treatment schemes based on cavitation and Fenton chemistry, A
2144 review. Ultrason. Sonochem. 21,1–14.
2145 Babuponnusami, A., Muthukumar, K., 2014. A review on Fenton and improvements to the Fenton process for wastewater treatment.
2146 J. Environ. Chem. Eng. 2,557–572.
2147 Bogaerts, A., Erik, N., Gijbels, R., 2002. Gas discharge plasmas and their applications. Spectrochim. Acta B 57, 609–658.
2148 Basfar, A.A., Fageeh, O.I., Kunnummal, N., Al-Ghamdi, S., Chmielewski, A.G., Lickid, J., Pawelec, A., 2008. Electron beam flue
2149 gas treatment (EBFGT) technology for simultaneous removal of SO_2 and NO_x from combustion of liquid fuels. Fuel 8–9,
2150 1446–1452.
2151 Byun, Y., Koh, D.J., Shin, D.N., 2011a. Removal mechanism of elemental mercury by using non-thermal plasma. Chemosphere 83,
2152 69–75.
2153 Byun, Y.C., Ko, K.B., Cho, M.Y., Namkung, W., Shin, D.N., 2008. Oxidation of elemental mercury using atmospheric pressure
2154 non-thermal plasma. Chemosphere 72, 652–658.
2155 Byun, Y., Koh, D.J., Shin, D.N., Cho, M., Namkung, W., 2011b. Polarity effect of pulsed corona discharge for the oxidation of
2156 gaseous elemental mercury. Chemosphere 84, 1285–1289.
2157 Bo, Z., Fen, L.W., Gang, Y., Min, Y.H., 2009. Kinetic simulation of $NO/N_2/O_2/Hg_0$ streamer under dielectric barrier discharge. J.
2158 Eng. Thermophys 2, 343–346.
2159 Biswas, P., Wu, C.Y., 1998. Control of Toxic Metal Emissions from Combustors Using Sorbents, A Review. J. Air & Waste Manage.
2160 Assoc. 48,113–127.

Burda, C., Lou, Y., Chen, X,, Samia, A.C.S., Stout, J., Gole, J.L., 2003. Enhanced nitrogen doping in TiO_2 nanoparticles. Nano. Lett. 3,1049−1051.

Binitha, N.N., Yaakob, Z., Reshmi, M.R., Sugunan, S., Ambili, V.K., Zetty, A.A., 2009. Preparation and characterization of nano-silver doped mesoporous titania photocatalysts for dye degradation. Catal. Today 147,S76−S80.

Bessekhouad, Y., Robert, D., Weber, J.V., 2004. Bi_2S_3/TiO_2 and CdS/TiO_2 heterojunctions as an available configuration for photocatalytic degradation of organic pollutant. J. Photochem. Photobiol. A 163,569−580.

Breault, R.W., 2006. Combustion of coal in circulating fluidized-bed boilers, a review. Powder Technol. 1–2,9–17.

Berruti, F., Pugsley, T.S., Godfroy, L., Chaouki, J., Patience, G.S., 1995. Hydrodynamics of circulating fluidized bed risers, A review. Can. J. Chem. Eng. 5,579–602.

Basu, P., 1999. Combustion of coal in circulating fluidized-bed boilers, a review. Chem. Eng. Sci. 22,5547–5557.

Bagal, M.V., Gogate, P.R., 2014. Wastewater treatment using hybrid treatment schemes based on cavitation and Fenton chemistry, A review. Ultrason. Sonochem. 21,1–14.

Cheng, G.W., Bai, B.F., Zhang, Q., Cai, M., 2014. Hg^0 removal from flue gas by ionic liquid/H_2O_2. J. Hazard. Mater. 280,767–773.

Chi, Y., Yan, N.Q., Qu, Z., Qiao, S.H., Jia, J.P., 2009. The performance of iodine on the removal of elemental mercury from the simulated coal-fired flue gas. J. Hazard. Mater. 166,776–781.

Chiu, C.H., His, H.C., Lin, C.C., 2014. Control of mercury emissions from coal-combustion flue gases using $CuCl_2$-modified zeolite and evaluating the cobenefit effects on SO_2 and NO removal. Fuel Process. Technol. 126,138–144.

Chen, W.M., Ma, Y.P., Yan, N.Q., Qu, Z., Yang, S.J., 2014. The co-benefit of elemental mercury oxidation and slip ammonia abatement with SCR-Plus catalysts. Fuel 133,263–269.

Cheng, G.W., Zhang, Q., Bai, B.F., 2014. Removal of Hg^0 from flue gas using Fe-based ionic liquid. Chem. Eng. J. 252,159–165.

Chang, J.S., 2001. Recent development of plasma pollution control technology, a critical review. Sci. Technol. Adv. Mater. 2,571–576.

Chen, H.L., Lee, H.M., Chen, S.H., Chang, M.B., Yu, S.J., Li, S.N., 2009. Removal of Volatile Organic Compounds by Single-Stage

and Two-Stage Plasma Catalysis Systems, A Review of the Performance Enhancement Mechanisms, Current Status, and Suitable Applications. Environ. Sci. Technol. 43,2216–2227.

Chang, J.S., Lawless, P.A., 2002. Corona discharge process. Plasma Sci. IEEE Transaction 6,1152–1166.

Chmielewski, A.G., 2007. Industrial applications of electron beam flue gas treatment-From laboratory to the practice. Radiation Phys. Chem. 8–9,1480–1484.

Chmielewski, A.G., Iller, E., Zimek, Z., Licki, J., 1992. Pilot plant for electron beam flue gas treatment. Int. J. Radiation Applications and Instrumentation. Part C. Radiation Physics and Chemistry. 4, 321–325

Chmielewski, A.G., Sun, Y.X., Licki, J., Bułka, S., Kubica, K., Zimek, Z., 2003. NO_x and PAHs removal from industrial flue gas by using electron beam technology with alcohol addition. Radiation Phys. Chem. 3–4,555–560.

Chang, M.B., Kushner, M.J., Rood, M.J., 1992. Removal of SO_2 and the simultaneous removal of SO_2 and NO from simulated flue gas streams using dielectric barrier discharge plasmas. Plasma Chem. Plasma Process 4,565–580.

Chang, J.S., Urashima, K., Tong, Y.X., Liu, W.P., Wei, H.Y., Yang, F.M., Liu, X.J., 2003. Simultaneous removal of NO_x and SO_2 from coal boiler flue gases by DC corona discharge ammonia radical shower systems, pilot plant tests. J. Electrosta 3–4,313–323.

Chen, Z.Y., Mannava, D.P., Mathur, V.K., 2006. Mercury Oxidization in Dielectric Barrier Discharge Plasma System. Ind. Eng. Chem. Res. 45,6050–6055.

Chen, H.L., Lee, H.M., Chen, S.H., Chang, M.B., 2008. Review of Packed-Bed Plasma Reactor for Ozone Generation and Air Pollution Control. Ind. Eng. Chem. Res. 7,2122–2130.

Chen, D., Jiang, Z., Geng, J., Wang, Q., Yang, D., 2007. Carbon and nitrogen Co-doped TiO_2 with enhanced visible light photocatalytic activity. Ind. Eng. Chem. Res. 46,2741−2746.

Chen, D., Jiang, Z., Geng, J., Wang, Q., Yang, D., 2007. Carbon and nitrogen Co-doped TiO_2 with enhanced visible light photocatalytic activity. Ind. Eng. Chem. Res. 46,2741−2746.

Chen, S.S., His, H.C., Nian, S.H., Chiu, C.H., 2014. Synthesis of N-doped TiO_2 photocatalyst forlow-concentration elemental

2207 mercury removal under various gas conditions. App. Catal. B, Environ. 160–161,558–565.

2208 Coehoorn, R., Haas, C., De, G.R.A., 1987. Electronic structure of $MoSe_2$, MoS_2, and WSe_2. II. The nature of the optical band gaps.

2209 Phys. Rev. B35,6203−6206.

2210 Cho, J.H., Lee, T.G., Eom, Y.J., 2012. Gas-phase elemental mercury removal in a simulated combustion flue gas using TiO_2 with

2211 fluorescent light. J. Air Waste Manage. 10,1208–1213.

2212 Corella, J., Toledo, J.M., Molina, G., 2007. A Review on Dual Fluidized-Bed Biomass Gasifiers. Ind. Eng. Chem. Res. 46,

2213 6831–6839.

2214 Cravotto, G., Carlo, S.D., Ondruschka, B., Tumiattic, V., Roggero, C.M., 2007. Decontamination of soil containing POPs by the

2215 combined action of solid Fenton-like reagents and microwaves. Chemosphere 8,1326–1329.

2216 Chou, Y.C., Lo, S.L., Kuo, J., Yeh, C.J., 2015. Microwave-enhanced persulfate oxidation to treat mature landfill leachate. J. Hazard.

2217 Mater. 284,83–91.

2218 Careya, T.R., Hargrove, O.W., 2011.Richardson CF, Chang R, Meserole FB. Factors Affecting Mercury Control in Utility Flue Gas

2219 Using Activated Carbon. J. Air Waste Manageme. 12,1166–1174.

2220 De, M., Azargohar, R., Dalai, A.K., Shewchuk, S.R.,2013. Mercury removal by bio-char based modified activated carbons. Fuel

2221 103,570–578.

2222 Dranga, B.A., Koeser, L.L.H., 2012. Oxidation Catalysts for Elemental Mercury in Flue Gases–A Review. Catalysts 2,139–170.

2223 Ding, J., Zhong, Q., Zhang, S.L., Song, F.J., Bu, Y.F., 2014. Simultaneous removal of NO_x and SO_2 from coal-fired flue gas by

2224 catalytic oxidation-removal process with H_2O_2. Chem. Eng. J. 243,176–182.

2225 Dhali, S.K., Sardja, I., 1991. Dielectric-barrier discharge for processing of SO_2/NO_x. J. Appl. Phys. 69,6319–6325.

2226 Daghrir, R., Drogui, P., Robert, D., 2013. Modified TiO_2 For Environmental Photocatalytic Applications, A Review. Ind. Eng. Chem.

2227 Res. 52,3581−3599.

2228 Diwald, O., Thompson, T.L., Goralski, E.G., Walck, S.D., Yates, J.T., 2004. Photochemical activity of nitrogen-doped rutile TiO_2

(110) in visible light. J. Phys. Chem. B 108,52−57.

Dozzi, M.V., Saccomanni, A., Selli, E., 2012. Cr(VI) photocatalytic reduction, Effects of simultaneous organics oxidation and of gold nanoparticles photodeposition on TiO_2. J. Hazard. Mater. 211−212,188−195.

Depero, L.E., Marino, A., Allieri, B., Bontempi, E., Sangaletti, L., Casale, C., Notaro, M., 2000. Morphology and microstructural properties of TiO_2 nanopowders doped with trivalent Al and Ga cations. J. Mater. Res.15,2080−2086.

Dai, X.W., Wang, T.T., Fang, J.H., Wu, J., 2012. Experimental study of titanium-based photocatalysts and catalytic oxidation of mercury in the flue gas. 2012 Thermal Power Plant Pollution Removal and Energy Saving Technology Seminar. WuXi.

Dou, B.L., Hui, C., Ge, H.H., Chen, B.B., Ting, W., 2008. Preparation of TiO_2 Nanoparticles by Sol-gel Method and Its Application in Mercury Pollutant Removal. J. Power Eng. 5,779–782.

Dickinson, R.G., Sherrill, M.S., 1926. Formation of Ozone by Optically Excited Mercury Vapor. Proc. Natl. Acad. Sci. 12, 175 –178.

Ding, J., Zhong, Q., Zhang, S.L., 2014. Simultaneous desulfurization and denitrification of flue gas by catalytic ozonation over Ce–Ti catalyst. Fuel Process Technol. 128, 449–455.

Evans, D., Rosocha, L.A., Anderson, G.K., John, J., 1993. Plasma remediation of trichloroethylene in silent discharge plasmas. J. Appl. Phys. 74, 5378–5385.

El-Bahy, Z.M., Ismail, A.A., 2009. Mohamed RM. Enhancement of titania by doping rare earth for photodegradation of organic dye (Direct blue). J. Hazard. Mater. 166,138−143.

Einaga, H., Yamamoto, S., Maeda, N., Teraoka, Y., 2015. Structural analysis of manganese oxides supported on SiO_2 for benzene oxidation with ozone. Catal. Today 242, 287–293.

Fuente-Cuesta, A., Diaz-Somoano, M., Lopez-Anton, M.A., Cieplik, M., Fierro, J.L.G., Martínez-Tarazona, M.R., 2012. Biomass gasification chars for mercury capture from a simulated flue gas of coal combustion. J. Environl. Manage. 98,23–28.

Fang, J.J., 2013. The mechanism study on the photocatalytic removal effect of coal fly ash on Hg and NO in the coal-fired derived flue gas. ShangHai, Shanghai University of Electric Power.

Fang, P., Cen, C.P., Tang, Z.J., 2012. Experimental Study on the Oxidative Absorption of Hg^0 by $KMnO_4$ Solution. Chem. Eng. J. 102,198–199.

Fang, P., Cen, C.P., Wang, X.M., Tang, Z.J., Tang, Z.X., Chen, D.S., 2014. Simultaneous removal of SO_2, NO and Hg^0 by wet scrubbing using urea+$KMnO_4$ solution. Chem. Eng. J. 249,72–78.

Feng, L., Hullebusch, E.D.V., Rodrigo, M.A., Esposito, G., Oturan, M.A., 2013. Removal of residual anti-inflammatory and analgesic pharmaceuticals from aqueous systems by electrochemical advanced oxidation processes. A review. Chem. Eng. J 228, 944–964.

Frank, N.W., 1995. Introduction and historical review of electron beam processing for environmental pollution control. Radiation Phys. Chem. 6,989–1002.

Frank, N.W., 1992. Status and perspectives for the electron beam technology for flue gases treatment. International Journal of Radiation Applications and Instrumentation. Part C. Radiation Phys. Chem. 4,267–272.

Fujishima, A., Honda, K., 1972. Electrochemical photolysis of water at a semiconductor electrode. Nature 238,37–38.

Fresno, F., Tudela, D., Javier, M.A., Rivera, F., Coronado, J.M., Soria, J., 2006. Triphenyltin hydroxide as a precursor for the synthesis of nanosized tin-doped TiO_2 photocatalysts. Appl. Organomet Chem. 20,220−225.

Fan, C., Xue, P., Sun, Y., 2006. Preparation of nano-TiO_2 doped with cerium and its photocatalytic activity. J. Rare. Earth 24,309−313.

Fan, H.J., Huang, S.T., Chung, W.H., 2009. Degradation pathways of crystal violet by Fenton and Fenton-like systems, Condition optimization and intermediate separation and identification. J. Hazard Mater. 1–3,1032–1044.

Fenton, H.J.H., 1894. Oxidation of tartaric acid in the presence of iron. Chem. Soc. J. Lond. 65,899–910.

Fang, J.Y., Shang, C., 2012. Bromate Formation from Bromide Oxidation by the UV/Persulfate Process. Environ. Sci. Technol. 46,8976−8983.

Gao, Y.S., Zhang, Z., Wu, J.W., Duan, L.H., Umar, A., Sun, L., Guo, Z.H., Wang, Q., 2013. A Critical Review on the Heterogeneous

2273 Catalytic Oxidation of Elemental Mercury in Flue Gases. Environ. Sci. Technol. 47,10813−10823.

2274 Granite, E.J., Pennline, H.W., 2002. Photochemical Removal of Mercury from Flue Gas. Ind. Eng. Chem. Res. 41,5470–5476.

2275 Gultekin, I., Ince, N.H., 2007. Synthetic endocrine disruptors in the environment and water remediation by advanced oxidation

2276 processes. J. Environ. Manage. 85,816–832.

2277 Gasparik, R., Ihara, S., Yamabe, C., Satoh, S., 2000. Effect of CO_2 and Water Vapors on NO_x Removal Efficiency under Conditions

2278 of DC Corona Discharge in Cylindrical Discharge Reactor. Jpn. J. Appl. Phys. 39,306–312.

2279 Goodsite, M.E., Plane, J.M.C., Skov, H., 2004. A theoretical study of the oxidation of Hg^0 to $HgBr_2$ in the troposphere. Environ. Sci.

2280 Technol. 38,1772–1776.

2281 Granite, E.J., King, W.P., Stanko, D.C., Pennline, H.W., 2008. Implications of mercury interactions with band-gap semiconductor

2282 oxides. Main Group Chem.7,227–237.

2283 Grabowska, E., Remita, H., Zaleska, A., 2010. Photocatalytic activity of TiO_2 loaded with metal clusters. Physicochem. Probl. Miner

2284 Process. 45,29−38.

2285 Geng, Q.J., Guo, Q.J., Yue, X.H., 2010. Adsorption and Photocatalytic Degradation Kinetics of Gaseous Cyclohexane in an Annular

2286 Fluidized Bed Photocatalytic Reactor. Ind. Eng. Chem. Res. 49, 4644–4652.

2287 Granite, E.J., Pennline, H.W., Hoffman, J.S., 1999. Effects of Photochemical Formation of Mercuric Oxide. Ind. Eng. Chem. Res. 38,

2288 5034–5037.

2289 Granite, E.J., Pennline, H.W., Stanko, D.C., 2000. Photochemical Removal of Mercury from Flue Gas. In Proceedings of the 17th

2290 Annual International Pittsburgh Coal Conference. University of Pittsburgh, Pittsburgh, PA.

2291 Granite, E.J., Pennline, H.W., 2001. Photochemical Removal of Mercury from Flue Gas. Proceedings of the 11th International

2292 Conference on Coal Science. National Energy Technology Laboratory, Pittsburgh, PA.

2293 Granite, E.J., Pennline, H.W., 2003. Method for Removal of Mercury from Various Gas Streams, US Patent, 6576092B2.

2294 Granite, E.J., Pennline, H.W., 2002. Photochemical Removal of Mercury from Flue Gas. In Proceedings of 223rd ACS National

Meeting; American Chemical Society, Washington, DC.

Garrido-Ramírez, E.G., Theng, B.K.G., Mora, M.L., 2010. Clays and oxide minerals as catalysts and nanocatalysts in Fenton-like reactions-A review. App. Clay Sci. 47,182–192.

Hou, W.H., Zhou, J.S., Qi, P., Gao, X., Luo, Z.Y., 2014. Effect of H_2S/HCl on the removal of elemental mercury in syngas over CeO_2–TiO_2. Chem. Eng. J. 241,131–137.

Hutson, N.D., Krzyzynska, R., Srivastava, R.K., 2008. Simultaneous Removal of SO_2, NO_x, and Hg from Coal Flue Gas Using a $NaClO_2$- Enhanced Wet Scrubber. Ind. Eng. Chem. Res. 47,5825–5831.

Hower, J.C., Senior, C.L., Suuberg, E.M., Hurt, R.H., Wilcox, J.L., Olson, E.S., 2010. Mercury capture by native fly ash carbons in coal-fired power plants. Prog. Energ. Combust. 36,510–529.

Hussain, M., Russo, N., Saracco, G., 2011. Photocatalytic abatement of VOCs by novel optimized TiO_2 nanoparticles. Chem. Eng, J. 1,138–149.

Huang, L., Xia, L.Y., Ge, X.X., Jing, H.Y., Dong, W.B., Hou, H.Q., 2012. Removal of H_2S from gas stream using combined plasma photolysis technique at atmospheric pressure. Chemosphere 2,229–234.

Helfritch, D.J., Harmon, G., Feldman, P.L., 1996. Mercury vapor control by means of corona discharge. Presentation at the 89th Annual Meeting of Air & Waste Management Association. Paper 96-ES96. 41, Nashville, TN, June, 23–28.

Helfritch, D.J., Harmon, G., Feldman, P.L., 1998. The oxidation of mercury vapor in combustion flue gas by corona discharge, in, Proc. Pan-American Workshop Commercialization of Advanced Oxidation Technologies, London, ON, Canada.

He, J., Reddy, G.K., Thiel, S.W., Smirniotis, P.G., Pinto, N.G., 2011. Ceria-modified manganese oxide/titania materials for removal of elemental and oxidized mercury from flue gas. J. Phys. Chem. C 115,24300–24309.

Hashimoto, K., Irie, H., Fujishima, A., 2005. TiO_2 Photocatalysis, A Historical Overview and Future Prospects. Jap. J. App. Phy. 12,8269–8285.

His, H.C., Tsai, C.Y., 2012a. Synthesis of TiO_{2-x} visible-light photocatalyst using N_2/Ar/He thermal plasma for low-concentration

elemental mercury removal. Chem. Eng. J. 191,378– 385.

His, H.C., Tsai, C.Y., 2012b. Preparation of oxygen-vacant TiO_{2-x} and activated carbon fiber composite using a single-step thermal plasma method for low-concentration elemental mercury removal. Chem. Eng. J 200–202,18–24.

Hong, X., Wang, Z., Cai, W., Lu, F., Zhang, J., Yang, Y., Ma, N., Liu, Y., 2005. Visible light activated nanoparticle photocatalyst of iodinedoped titanium dioxide. Chem. Mater. 17,1548−1552.

Hsieh, C.T., Fan, W.S., Chen, W.Y., Lin, J.Y., 2009. Adsorption and visible light derived photocatalytic kinetics of organic dye on Codoped titania nanotubes prepared by hydrothermal synthesis. Sep Purif Technol 67,312−318.

Hernàndez-Alonso, M.D., Fresno, F., Suàrez, S., Coronado, J.M., 2009. Development of alternative photocatalyst to TiO_2, Challenges and opportunities. Energy Environ. Sci. 2,1231−1257.

Ho, W., Yu, J.C., Lin, J., Yu, J., Li, P., 2004. Preparation and photocatalytic behavior of MoS_2 and WS_2 nanocluster sensitized TiO_2. Langmuir 20,5865−5869.

Hsueh, C.L., Huang, Y.H., Wang, C.C., Chen, C.Y., 2005. Degradation of azo dyes using low iron concentration of Fenton and Fenton-like system. Chemosphere 10,1409–1414.

Hao, F.F., Guo, W.L., Wang, A.Q., Leng, Y.Q., Li, H.L., 2014. Intensification of sonochemical degradation of ammonium perfluorooctanoate by persulfate oxidant. Ultrason. Sonochem. 21,554–558.

Huang, W.J., Qu, Z., Chen, W.M., Xu, H.M., Yan, N.Q., 2016. An enhancement method for the elemental mercury removal from coal-fired flue gas based on novel discharge activation reactor. Fuel 171, 59–64.

Ilieva, M., Nakova, A., Tsakova, V. TiO_2/WO_3 hybrid structures produced through a sacrificial polymer layer technique for pollutant photo- and photo-electrooxidation under ultraviolet and visible light illumination. J. Appl. Electrochem. 42, 121−129.

Josepha, C.G., Puma, G.L., Bono, A, 2009. Krishnaiah D. Sonophotocatalysis in advanced oxidation process, A short review. Ultrason. Sonochem. 16,583–589.

Jeong, J., Jurng, J., 2007. Removal of gaseous elemental mercury by dielectric barrier discharge. Chemosphere 68,2007–2010.

Jani, M.A., Takaki, K., Fujiwara, T., 1999. Streamer Polarity Dependence of NO_x Removal by Dielectric Barrier Discharge with a Multipoint-to-Plane Geometry. J. Phys. D, Appl. Phys. 32,2560–2566.

Jeon, S.H., Eom, Y.J., Lee, T.G., 2008. Photocatalytic oxidation of gas-phase elemental mercury by nanotitanosilicate fibers. Chemosphere 71,969–974.

Ji, T., Yang, F., Lv, Y., Zhou, J., Sun, J., 2009. Synthesis and visible light photocatalytic activity of Bi-doped TiO_2 nanobelts. Mater. Lett. 63,2044−2046.

Jia, L., Dureau, R., Ko, V., Anthony, E.J., 2010. Oxidation of Mercury under Ultraviolet (UV) Irradiation. Energ. Fuel 24,4351–4356.

Calvert, J.G., Lindberg, S.E., 2005. Mechanisms of mercury removal by O_3 and ·OH in the atmosphere. Atmospheric Environment 39, 3355–3367.

Ji, Y.F., Dong, C.X., Kong, D.Y., Lu, J.H., Zhou, Q.S., 2015. Heat-activated persulfate oxidation of atrazine, Implications for remediation of groundwater contaminated by herbicides. Chem. Eng. J. 263,45–54.

Klasson, K.T., Boihem, L.L., Uchimiya, J.M., Lima, I.M., 2014. Influence of biochar pyrolysis temperature and post-treatment on the uptake of mercury from flue gas. Fuel ProcessTechnol. 123,27–33.

Klavarioti, M., Mantzavinos, D., Kassinos, D., 2009. Removal of residual pharmaceuticals from aqueous systems by advanced oxidation processes. Environ. Int. 35,402–417.

Kim, H.H., 2004. Nonthermal Plasma Processing for Air-Pollution Control, A Historical Review, Current Issues, and Future Prospects. Plasma Process Polym. 2,91–110.

Kogelschatz, U., 2004. Atmospheric-pressure plasma technology. Plasma Phys. Control Fusion 46,B63–B75.

Kawamura, K., Hirasawa, A., Aoki, S., Kimura, H., Fujii, T., Mizutani, S., Higo, T., 1979. Pilot plant experiment of NO_x and SO_2 removal from exhaust gases by electron beam irradiation. Radiation Phy. Chem. 1–2,5–12.

Kawamura, K., Katayama, T., Kawamura, K., 1981. The pilot plant experiment of electron beam irradiation process for removal of

NO_x and SO_x from sinter plant exhaust gas in the iron and steel industry. Radiation Phy. Chem.1–2,389–398.

Kawamura, K., Aoki, S.J., Kimura, H., Adachi, K., Kawamura, K., Katayama, T., Kengaku, K., Sawada, Y., 1980. Pilot plant experiment on the treatment of exhaust gas from a sintering machine by electron beam irradiation. Environ. Sci. Technol. 14,288–293.

Kogelschatz, U., 2003. Dielectric-Barrier Discharges, Their History, Discharge Physics, and Industrial Applications. Plasma Chem. Plasma Process 1,1–46.

Koutsospyros, A.D., Yin. S.M., Christodoulatos, C., Becker, K., 2005. Plasmochemical degradation of volatile organic compounds (VOC) in a capillary discharge plasma Reactor. Plasma Sci. IEEE Transaction 2,42–49.

Ko, K.B., Byun, Y., Cho, M., Namkung W, Dong, N.S., 2008a. Influence of HCl on oxidation of gaseous elemental mercury by dielectric barrier discharge process. Chemosphere 71,1674–1682.

Ko, K.B., Byun, Y., Cho, M., Namkung, W., Hamilton, I.P., Shin, D.N., Koh, D.J., Kim, K.T., 2008b. Pulsed corona discharge for oxidation of gaseous elemental mercury. Appl. Phy. Let. 92,251503-3–251503-3.

Ko, K.B., Byun, Y., Cho, M., Namkung, W., 2008c. Influence of gas components on the oxidation of elemental mercury by positive pulsed corona discharge. Main Group Chem. 3,69–75.

Kumar, S.G., Devi, L.G., 2011. Review on Modified TiO_2 Photocatalysis under UV/Visible Light, Selected Results and Related Mechanisms on Interfacial Charge Carrier Transfer Dynamics. J. Phys. Chem. A 115,13211–13241.

Kaluza, U., Boehm, H. P., 1971. Titanium dioxide catalyzed photooxidation of mercury. J. Catal. 22,347–358.

Kwon, S., Fan, M., Cooper, A.T., Yang, H., 2008. Photocatalytic applications of micro-and nano-TiO_2 in environmental engineering. Crit. Rev. Env. Sci. Tec. 3,197–226.

Kment, S., Kmentova, H., Kluson, P., Krysa, J., Hubicka, Z., Cirkva, V., Gregora, I., Solcova, O., 2010. Notes on the photoinduced characteristics of transition metal-doped and undoped titanium dioxide thin films. J. Colloid Interface Sci. 348,198−205.

Kannaiyan, D., Kim, E., Won, N., Kim, K.W., Jang, Y.H., Cha, M.A., Ryu, D.Y., Kim, S., Kim, D.H., 2010. On the synergistic

coupling properties of composite CdS/TiO_2 nanoparticle arrays confined in nanopatterned hybrid thin films. J. Mater. Chem. 20,677−682.

Kumazawa, H., Inoue, M., Kasuya, T., 2003. Photocatalytic Degradation of Volatile and Nonvolatile Organic Compounds on Titanium Dioxide Particles Using Fluidized Beds. Ind. Eng. Chem. Res. 42,3237–3244.

Kima, S. B., Hwang, H.T., Hong, S.C., 2002. Photocatalytic degradation of volatile organic compounds at the gas–solid interface of a TiO_2 photocatalyst. Chemosphere 4,437–444.

Kwan, W.P., Voelker, B.M., 2003. Rates of Hydroxyl Radical Generation and Organic Compound Oxidation in Mineral-Catalyzed Fenton-like Systems. Environ. Sci. Technol. 37,1150–1158.

Khan, N.E., Adewuyi, Y.G., 2010. Absorption and Oxidation of Nitric Oxide (NO) by Aqueous Solutions of Sodium Persulfate in a Bubble Column Reactor. Ind. Eng. Chem. Res.;49,8749–8760.

Kim, S.J., Kim, S.C., Seo, S.G., Lee, D.J., Lee, H., Park, S.H., Jung, S.C., 2011. Photocatalyzed destruction of organic dyes using microwave/UV/O_3/H_2O_2/TiO_2 oxidation system. Catal. Today 164,384–390.

Li, H.L., Wu, C.Y., Li, Y., Li, L.Q., Zhao, Y.C., Zhang, J.Y., 2013. Impact of SO_2 on elemental mercury oxidation over CeO_2–TiO_2 catalyst. Chem. Eng. J. 219,319–326.

Li, X., Liu, Z.Y., Kim, J.S., Lee, J.Y., 2014a. Theoretical study of mercury species adsorption mechanism on MnO_2(110) surface. Chem. Eng. J. 256,93–100.

Liu, Y.X., Pan, J.F., Wang, Q., 2014a. Removal of Hg^0 from Containing-SO_2/NO Flue Gas by Ultraviolet/H_2O_2 Process in a Novel Photochemical Reactor. AIChE Journal 6,2275–565.

Liu, Y.X., Qian, W., 2014b. Removal of Elemental Mercury from Flue Gas by Thermally Activated Ammonium Persulfate in A Bubble Column Reactor. Environ. Sci. Technol. 48,12181−12189.

Lu, D., Anthony, E.J., Tan, Y.W., Dureau, R., Ko, V., Douglas, M.A., 2007. Mercury removal from coal combustion by Fenton reactions–Part A, Bench-scale tests. Fuel 86,2789–2797.

Liu, S.Y., Nengzi, L.C., Qu, B., Liu, P., Ye, Z.X.,2010b. Simultaneous Removal of Elemental Mercury in Aqueous Potassium Hypochlorite by Oxidation. Environ. Eng. Sci. 4,323–327.

Liu, Y.X., Zhang, J., Sheng, C.D., Zhang, Y.C., Yuan, S.J., 2008. New research progress in sorbents for removal of mercury in coal-fired flue gas. Modern. Chem. Ind.11,19−25.

Liu, Y.X., Zhang, J., Pan, J.F., 2014c. Photochemical Oxidation Removal of Hg^0 from Flue Gas Containing SO_2/NO by an Ultraviolet Irradiation/Hydrogen Peroxide (UV/H_2O_2) Process. Energy Fuels 28,2135−2143.

Liu, Y.X., 2011a. Study on integrated desulfurization and denitrification by UV/H_2O_2 advanced oxidation process. Nanjing, Southeast University 1, 6–15.

Liu, Y.X., Zhang, J., Sheng, C.D., Zhang, Y.C., Zhao, L., 2010a. Simultaneous removal of NO and SO_2 from coal-fired flue gas by UV/H_2O_2 advanced oxidation process. Chem. Eng. J. 3,1006–1011.

Lin, T.S., Hong, M., Lei, J., Ping, N., 2008. Purification of H_2S-containing gas stream by aqueous oxidation with Fenton agent. China Environ. Sci. 28,1052–1056.

Li, S.R., Huang, Y.F., Wang, F.F., Liu, J., Feng, F.D., Shen, X.J., Yan, K.P., 2014b. Multi-pollutants Emission from Coal-Fired Flue Gas. Fundamentals and Environmental Applications of Non-thermal Plasmas, Multi-pollutants Emission Control from Coal-Fired Flue Gas. Plasma Chem. Plasma Process 34,579–603.

Licki, J., Chmielewski, A.G., Zimek, E., Mazurek, Z.J., Sobolewski, L., 2003. Electron-beam flue-gas treatment for multicomponent air-pollution control. App. Energ. 3–4,145–154.

Liang, X.H., Looy, P.C., Jayaram, S., 2002. Mercury and Other Trace Elements Removal Characteristics of DC and Pulse-Energized Electrostatic Precipitator. IEEE T Ind. Appl. 1,69–76.

Lin, W.F., Zhang, B., Hou, W.H., Zhou, Q., Yang, H.M., 2010. Enhanced Oxidation of Elemental Mercury in Simulated Flue gas by Non-Thermal Plasma. Proceedings of the CSEE 2010;2,72–76

Li, L.C., Deng, P., Tian, A.M., Xu, M.H., Zheng, C.G., Wong, N.B., 2003. A study on the reaction mechanism and kinetic of

mercury oxidation by chlorine species. J. Mol. Struc-Theochem. 625,277–281.

Lin, H., 2002. Experimental and theoretical study on flue gas denitrification with radical shower induced by DC Corona discharge. Hang Zhou, Zhejiang University.

Lin, W.F., Zhang, B., Yang, H.M., 2009. Characteristics of emissive spectrum and the removal of nitric oxide in N_2/O_2/NO plasma with argon additive. J. Environ. Sci. 21,790–794.

Lee, T.G., 2010. Photocatalytic Removal of Gas-Phase Elemental Mercury Using TiO_2. Environmentally Benign Photocatalysts-Nanostructure Science and Technology 437–449.

Lee, T.G., Biswas, P., 2001. Comparison of Hg^0 Capture Efficiencies of Three in situ Generated Sorbents. AIChE Journal 4,954–961.

Linsebigler, A.L., Lu, G.Q., Yates, J.T., 1995. Photocatalysis on TiO_2 Surfaces, Principles, Mechanisms, and Selected Results. Chem. Rev. 95,735–758.

Lee, Y.G., Park, J.W., Kim, J.H., Min, B.R., Jurng, J., Kim, J., Lee, T.G., 2004. Comparison of Mercury Removal Efficiency from a Simulated Exhaust Gas by Several Types of TiO_2 under Various Light Sources. Chem. Let. 1,36–37.

Lee, Y.G., Lee, T.G., Kim, W.S., 2005. Comparison of the Mercury Removal Efficiency using TiO_2 Powder under Various Light Sources. Korean. Chem. Eng. Res. 43, 65–69.

Lo, S.F., Lin, C.F., Wu, C.H., Hsieh, P.H., 2004. Capability of coupled CdSe/TiO_2 for photocatalytic degradation of 4-chlorophenol. J. Hazard. Mater. B114,183−190.

Li, Y., Wu, C.Y., 2006. Role of Moisture in Adsorption, Photocatalytic Oxidation, and Reemission of Elemental Mercury on a SiO_2-TiO_2 Nanocomposite. Environ. Sci. Technol. 40,6444–6448.

Li, Y., 2007a. Removal of elemental mercury from flue gas using nanostructured silica/titania/vanadia composites. Florida, University of Florida.

Li, Y., Murphy, P., Wu, C.Y., 2008. Removal of elemental mercury from simulated coal-combustion flue gas using a SiO_2-TiO_2 nanocomposite. Fuel Process. Technol. 89,567–573

Lee, T.G., Hyun, J.E., 2006. Structural effect of the in situ generated titania on its ability to oxidize and capture the gas-phase elemental mercury. Chemosphere 62,26–33.

Lee, T.G., Biswas, P., Hedrick, E., 2004. Overall Kinetics of Heterogeneous Elemental Mercury Reactions on TiO_2 Sorbent Particles with UV Irradiation. Ind. Eng. Chem. Res. 43,1411–1417.

Li, Y., Wu, C.Y., 2007b. Kinetic Study for Photocatalytic Oxidation of Elemental Mercury on a SiO_2–TiO_2 Nanocomposite. Environ. Eng. Sci. 1,3–12.

Li, X.T., Grace, J.R., Lim, C.J., Watkinson, A.P., Chen, H.P., Kimc, J.R., 2004. Biomass gasification in a circulating fluidized bed. Biomass and Bioenerg 2,171–193.

Lim, T.H., Kim, S.D., 2005. Photocatalytic degradation of trichloroethylene (TCE) over TiO_2/silica gel in a circulating fluidized bed (CFB) photoreactor. Chem Eng Process 2,327–334.

Li, D.Z., Chen, Z.X., Chen, Y.L., Li, W.J., Huang, H.J., He, Y.H., Fu, X.Z.,2008. A New Route for Degradation of Volatile Organic Compounds under Visible Light, Using the Bifunctional Photocatalyst $Pt/TiO_{2-x}N_x$ in H_2−O_2 Atmosphere. Environ. Sci. Technol. 6,2130–2135.

Liu, Y.X, Zhang, J, Pan, J.F., 2013a. A mercury removal method and system basing on UV irradiation with flue gas cooling unit. China Patent, CN201310684668.

Liu, Y.X., Pan, J.F., Tang, A.K.,2013b. A method and system for flue gas mercury removal basing on coupling flue and UV lamp. China Patent, CN201310683054.

Liu, Y.X., Zhang, J., Yin, Y.S., 2014d. Study on Absorption of Elemental Mercury from Flue Gas by UV/H_2O_2, Process Parameters and Reaction Mechanism. Chem. Eng. J.191,482–494.

Liu, Y.X., Zhang, J., Yin, Y.S., 2015a. Removal of Hg^0 from flue gas Using Two Homogeneous Photo- Fenton-Like Reactions. AIChE Joural, 2015, 61, 1322–1333.

Liu, Y.X., Pan, J.F., Du, M., Tang, A.K., Wang, Q., 2013c. Advanced Oxidative Removal of Nitric Oxide from Flue Gas by

Homogeneous Photo-Fenton in a Photochemical Reactor.Chem. Eng. Technol. 10,1879–1884.

Liu, Y.X., Zhang, J., Pan, J.F., Tang, A.K., 2012a. Investigation on Removal of NO from SO_2-Containing Simulated Flue Gas by UV/Fenton-Like Reaction. Energ Fuels 26,5430−5436.

Liu, Y.X., Zhang, J., 2011b. Photochemical Oxidation Removal of Nitric Oxide and Sulfur Dioxide from Simulated Flue Gas of Coal-fired Power Plants by Wet Scrubbing using UV/H_2O_2 Advanced Oxidation Process. Ind. Eng. Chem. Res. 50, 3836–3841.

Liu, Y.X., Zhang, J., Sheng, C.D., Zhang, Y.C., Zhao, L., 2010a. Simultaneous removal of NO and SO_2 from coal-fired flue gas by UV/H_2O_2 advanced oxidation process. Chem. Eng. J. 162,1006–1011.

Liu, Y.X., Zhang, J., 2010b. A flue gas mercury removal system basing on photochemical advanced oxidation process. China Patent, CN201010296592.

Liu, Y.X., Zhang, J., 2010c. A flue gas simultaneous desulfurization and denitrification system basing on photochemical advanced oxidation process. China Patent, CN201010296492.

Liu, Y.X., Pan, J.F., Tang, A.K., Wang, Q., 2013d. A Study on Mass Transfer-Reaction Kinetics of NO Absorption by Using UV/H_2O_2/NaOH Process. Fuel 108,254–260.

Liu, Y.X., Zhang, J., Wang, Z.L., 2012b. A Study on Kinetics of NO Absorption from Flue Gas by Using UV/Fenton Wet Scrubbing. Chem. Eng. J. 197,468–474.

Liu, Y.X., Pan, J.F., Zhang, J., Tang, A.K., Liu, Y.,2012c. Study on Mass Transfer-Reaction Kinetics of NO Removal from Flue Gas by Using UV/Fenton-Like Reaction. Ind. Eng. Chem. Res. 51,12065−12072.

Liu, Y.X., Zhang, J., Sheng, C.D., 2011c. Study on Kinetics of NO Removal from Simulated Flue Gas by Wet UV/H_2O_2 Advanced Oxidation Process. Energ Fuels 6,1102–1107.

Liu, Y.X., Zhou, J.F., Zhang, Y.C., Pan, J.F., Wang, Q., Zhang, J., 2015b. Oxidation Removal of Elemental Mercury from Flue Gas Using Two Fenton-Like Reagents in a Spray Reactor. Fuel 2015;1,2275–2285.

Liu, Y.X., Wang, Y., Wang, Q., Pan, J.F., Zhang,Y.C., Zhang, J., 2015c. A Study on Removal of Elemental Mercury in Flue Gasusing Fenton Solution. J. Hazard. Mater. 292, 164–172.

Liu, L., Zheng, C.G., Chen, J.H., Zhou, J.S., Gao, X., Ni, M.J., Cen, K.F., 2015d. Plasma-induced adsorption of elemental mercury on TiO_2 supported metal oxide catalyst at low temperatures. Fuel Process. Technol. 138, 14–20.

Lin, Y.T., Liang, C.J., Chen, J.H., 2011. Feasibility study of ultraviolet activated persulfate oxidation of phenol. Chemosphere 82, 1168–1172.

Liang, H.Y., Zhang, Y.Q., Huang, S.B., Hussain, I., 2013. Oxidative degradation of p-chloroaniline by copper oxidate activated persulfate. Chem. Eng. J. 218,384–391.

Lee, Y.C., Lo, S.L., Kuo, J., Huang, C.P., 2013. Promoted degradation of perfluorooctanic acid by persulfate when adding activated carbon. J. Hazard. Mater. 261,463–469.

Li, H., Wan, J.Q., Ma, Y.W., Wang, Y., Huang, M.Z., 2014c. Influence of particle size of zero-valent iron and dissolved silica on the reactivity of activated persulfate for degradation of acid orange 7. Chem. Eng. J. 237,487–496.

Li, H., Guo, J., Yang, L.J., Lan, Y.Q., 2014d. Degradation of methyl orange by sodium persulfate activated with zero-valent zinc. Sep. Purif. Technol. 132,168–173.

Liu, Y., Bisson, T.M., Yang, H.Q., Xu, Z.H., 2010d. Recent developments in novel sorbents for flue gas clean up. Fuel Process. Technol. 10,1175–1197.

Lucas, M.S., Peres, J.A., Puma, G.L., Treatment of winery wastewater by ozone-based advanced oxidation processes (O_3, O_3/UV and O_3/UV/H_2O_2) in a pilot-scale bubble column reactor and process economics. Sep. Purif. Technol. 72,235–241.

Martinezm A.I., Deshpande, B.K., 2007. Kinetic modeling of H_2O_2-enhanced oxidation of flue gas elemental mercury. Fuel Process. Technol. 88,982–987.

Matilainena, A., Sillanpää, M., 2010. Removal of natural organic matter from drinking water by advanced oxidation processes. Chemosphere 80,351–365.

McAdams, R., 2001. Prospects for non-thermal atmospheric plasmas for pollution abatement. J. Phys. D, Appl. Phys. 34, 2810–2821.

Ma, H.B., Chen, P., Zhang, M.L., Lin, X.Y., Ruan, R.,2002. Study of SO_2 Removal Using Non-thermal Plasma Induced by Dielectric Barrier Discharge (DBD). Plasma Chem. Plasma Process 2,239–254.

Mok, Y.S., Nam, C.M., Cho, M.H., Nam, I.S., 2002. Decomposition of volatile organic compounds and nitric oxide by nonthermal plasma discharge processes. Plasma Sci. IEEE Transaction 7,408–416.

Mok, Y.S., Nam, I.S., 1998. Positive pulsed corona discharge process for simultaneous removal of SO_2 and NO_x from iron-ore sintering flue gas. Plasma Sci. IEEE Transaction 8,1188–1196.

Mok, Y.S., Nam, I.S., 1999. Positive pulsed corona discharge process for simultaneous removal of SO_2 and NO_x from iron-ore sintering flue gas. Plasma Sci. IEEE Transaction 8,1188–1196.

Masuda, S., Wu, Y., Urabe, T., Ono, M., 1987. DeNO_x and control of mercury vapor combustion gas by pulse corona induced plasma chemical process, in, Proc. 8th Int. Symp. Plasma Chemistry, Tokyo.

Mannava, P.C.D, 2004. Mercury Remediation by Dielectric Barrier Discharge. Master's Thesis, University of New Hampshire, Durham, NH.

Malik, M.A., Kolb, J.F., Sun, Y., Schoenbach, K.H., 2011. Comparative study of NO removal in surface-plasma and volume-plasma reactors based on pulsed corona discharges. J. hazard. mater.197,220–228.

Meng, N., Leung, M.K.H., Leung, D.Y.C., 2007. Sumathy K. A review and recent developments in photocatalytic water-splitting using TiO_2 for hydrogen production. Renew. Sust. Energ. Rev. 11,401–425.

McCullagh, C., Skillen, N., Adams, M., Robertson, P.K.J.,2011. Photocatalytic reactors for environmental remediation, a review. J. Chem. Technol. Biotechnol. 8,1002–1017.

Maggos, T., Bartzis, J.G., Liakou, M., Gobin, C.,2007. Photocatalytic degradation of NO_x gases using TiO_2-containing paint, A real scale study. J. Hazard. Mater. 146,668–673.

Medellin-Castillo, N.A., Ocampo-Pérez, R., Leyva-Ramos, R., Sanchez-Polo, M., Rivera-Utrilla, J., Méndez-Díaz, J. D., 2013.

Removal of diethyl phthalate from water solution by adsorption, photo-oxidation, ozonation and advanced oxidation process (UV/H_2O_2, O_3/H_2O_2 and O_3/activated carbon). Sci. Total Environ. 442,26–35.

Moussavi, G., Yazdanbakhsh, A., Heidarizad, M., 2009. The removal of formaldehyde from concentrated synthetic wastewater using $O_3/MgO/H_2O_2$ process integrated with the biological treatment. J. Hazard. Mater. 171,907–913.

Niksa, S., Naik, C.V., Berry, M.S., Monroe, L., 2009. Interpreting enhanced Hg oxidation with Br addition at Plant Miller. Fuel Process. Technol. 90,1372–1377.

Nelson, R.J., Flakker, C.L., Muggli, DS., 2007. Photocatalytic oxidation of methanol using titania-based fluidized beds. App. Catal. B Environ. 69,189–195.

Ntampegliotis, K., Riga, A., Karayannis, V., Bontozoglou, V., Papapolymerou, G., 2006. Decolorization kinetics of Procion H-exl dyes from textile dyeing using Fenton-like reactions. J. Hazard. Mater. 1,75–84.

Oller, I., Malato, S., Sánchez-Pérez, J.A., 2011. Combination of Advanced Oxidation Processes and biological treatments for wastewater decontamination—A review. Sci. Total. Environ. 409,4141–4166.

Obradović, B.M., Sretenović, G.B., Kuraica, M.M., 2011. A dual-use of DBD plasma for simultaneous NO_x and SO_2 removal from coal-combustion flue gas. J. Hazard. Mater. 2–3, 1280–1286.

Ohno, T., Mitsui, T., Matsumura, M., 2003. Photocatalytic activity of S-doped TiO_2 photocatalyst under visible light. Chem. Lett. 32,364−365.

Oncu, N.B., Mercan, N., Balcioglu, I.A., 2015. The impact of ferrous iron/heat-activated persulfate treatment on waste sewage sludge constituents and sorbed antimicrobial micropollutants. Chem. Eng. J. 259,972–980.

Oh, B.T., Seo, Y.S., Sudhakar, D., Choe, J.H., Lee, S.M., Park, Y.J., Cho, M., 2014. Oxidative degradation of endotoxin by advanced oxidation process (O_3/H_2O_2 & UV/H_2O_2). J. Hazard. Mater. 279,105–110.

Pavlish, J.H., Sondreal, E.A., Mann, M.D., Olson, E.S., Galbreath, K.C., 2003. Status review of mercury control options for coal-fired power plants. Fuel Process. Technol. 82,89–165.

2559 Presto, A., Granite, E. J., 2006. Survey of Catalysts for Oxidation of Mercury in Flue Gas. Environ. sci. technol. 18,5601–5609.

2560 Portland's Handbook of Chemistry (15th Edition), Section 8, 8,124−8.139.

2561 Park, J.Y., Tomicic, I., Round, G.F., Chang, J.S., 1999. Simultaneous removal of NO_x and SO_2 from NO-SO_2-CO_2-N_2-O_2 gas

2562 mixtures by corona radical shower systems. J. Phy. D App. Phy. 32,1006–1013.

2563 Penetrante, B.M., Hsiao, M.C., Merrit, B.T., Vogtlin, G.E., 1996. Pulsed corona and dielectric-barrier discharge processing of NO in

2564 N_2. App. Phy. Let. 6,3719–3781.

2565 Pitoniak, E.R., 2004. Evaluation of nanostructured silica-titania composites in an adsorption/photocatalytic oxidation system for

2566 elemental mercury vapor control. Florida, University of Florida.

2567 Pitoniak, E., Wu, C.Y., Londeree, D., Mazyck, D., Bonzongo, J.C., Powers, K., Sigmund, W., 2003. Nanostructured silica-gel doped

2568 with TiO_2 for mercury vapor control. J. Nanopart. Res. 3–4, 281–292.

2569 Pitoniak, E., Wu, C.Y., Mazyck, D., Powers, K., Sigmund, W. Adsorption Enhancement Mechanisms of Silica-Titania

2570 Nanocomposites for Elemental Mercury Vapor Removal. Environ. Sci. Technol. 39,1269–1274.

2571 Paola, D., Garcia-Lopez, A., Ikeda, E., Marc, S., Ohtani, G., Palmisano, B.L.,2002. Photocatalytic degradation of organic compounds

2572 in aqueous systems by transition metal-doped polycristalline TiO_2. Catal. Today 75,87−93.

2573 Portela, R., Suárez, S., Rasmussen, S.B., Arconada, N., Castro, Y., 2010. Photocatalytic-based strategies for H_2S elimination. Catal.

2574 Today 151, 64–70.

2575 Portela, R., Sánchez, B., Coronado, J.M., Candal, R., Suárez, S., 2012. A parametric study of the UV-A photocatalytic oxidation of

2576 H_2S over TiO_2. App. Catal. B Environ.115–116,209–218.

2577 Pouran, S.R., Abdul, A.A.R., Daud, W.M.A.W., 2014. Review on the main advances in photo-Fenton oxidation system for

2578 recalcitrant wastewaters. J Ind Eng Chem 2014;xxx,xxx–xxx.

2579 Pouran, S.R., Raman, A.A.A., Daud, W.M.A.W., 2014. Review on the application of modified iron oxides as heterogeneous catalysts

2580 in Fenton reactions. J. Clea. Prod. 64,24–35.

Qi, C.D., Liu, X.T., Lin, C.Y., Zhang, X.H., Ma, J., Tan, H.B., Ye, W., 2014. Degradation of sulfamethoxazole by microwave-activated persulfate, Kinetics, mechanism and acute toxicity. Chem. Eng. J. 49,6–14.

Qi, X.M., Gu, M.L., Zhu, X.Y., Wu, J., 2016. Fabrication of $BiOIO_3$ nanosheets with remarkable photocatalytic oxidation removal for gaseous elemental mercury. Chemical Engineering Journal 285, 11–19.

Reddy, B.M., Durgasri, N., Kumar, T.V., Bhargava, S.K., 2012. Abatement of Gas-Phase Mercury-Recent Developments. 3,344–398.

Rodríguez-Pérez, J., López-Antón, M.A., Díaz-Somoano, M., García, R., Martínez-Tarazona, M.R., 2013. Regenerable sorbents for mercury capture in simulated coal combustion flue gas. J. Hazard. Mater. 260,869–877.

Rupp, E.C., Wilcox, J., 2014. Mercury chemistry of brominated activated carbons-Packed-bed breakthrough experiments. Fuel 117, 351–353.

Ren, J.L., Zhou, J.S., Luo, Z.Y., Xu, Z., Zhang, X.M., 2006. Ca-based sorbents for mercury vapor removal from flue gas. J. Fuel Chem. Technol. 5,558–561.

Ribeiroa, A.R., Nunes, O.C., Pereira, M.F.R., Silva, A.M.T., 2015. An overview on the advanced oxidation processes applied for the treatment of water pollutants defined in the recently launched Directive 2013/39/EU. Environ. Int. 75,33–51.

Ren, W., Ai, Z., Jia, F., Zhang, L., Fan, X., Zou, Z., 2007. Low temperature preparation and visible light photocatalytic activity of mesoporous carbon-doped crystalline TiO_2. Appl. Catal. B 69,138−144.

Robert, D., 2007. Photosensitization of TiO_2 by M_xO_y and M_xS_y nanoparticles for heterogeneous photocatalysis applications. Catal. Today122,20−26.

Rodrı´guez, S., Almquist, C., Lee, T.G., 2044. Masami Furuuchi, Elizabeth Hedrick, Pratim Biswas. J. Air & Waste Manage 54,149–156.

Stolle, R., Koeser, H., Gutberlet, H., 2014. Oxidation and reduction of mercury by SCR $DeNO_x$ catalysts underflue gas conditions in

2603 coal fired power plants. App. Catal. B Environ. 144,486–497.

2604 Shu, T., Lu, P., He, N., 2013. Mercury adsorption of modifiedmulberry twig chars inasimulated flue gas. Bioresource Technol. 136,

2605 182–187.

2606 Shen, B.X., Cai, J., Chen, J.H., Li, Z., He, C., 2014. Removal of element mercury from simulated flue gas by clay modified with KBr

2607 and KI. CIESC Jorunal 2,711–717.

2608 Shan, Y., 2009. Investigation of Nano TiO_2 Composites for Photocatalytic Oxidation Removal of Mercury Vapor. Wu Han,

2609 Huazhong University of Science and Technology.

2610 Stergaršek, A., Horvat, M., Frkal, P., Stergaršek, J., 2010. Removal of Hg^0 from flue gases in wet FGD by catalytic oxidation with air

2611 –An experimental study. Fuel 89,3167–3177.

2612 Serpone, N., Horikoshi, S., Emeline, A.V., 2010. Microwaves in advanced oxidation processes for environmental applications. A

2613 brief review. J. Photochem. Photobiolo. C 11,114–131.

2614 Sharma, V.K., Triantis, T.M., Hiskia, A., Dionysiou, D.D., 2012. Destruction of microcystins by conventional and advanced

2615 oxidation processes, A review. Sep. Puri. Technol. 91,3–17

2616 Sillanpääa, M.E.T., Kurniawan, T.A., Lo, W.H., 2011. Degradation of chelating agents in aqueous solution using advanced oxidation

2617 process (AOP). Chemosphere 83,1443–1460.

2618 Su, C.Y., Ran, X., Hu, J.L., Shao, C.L., 2013. Photocatalytic Process of Simultaneous Desulfurization and Denitrification of Flue

2619 Gas by TiO_2−Polyacrylonitrile Nanofibers. Environ. Sci. Technol. 47,11562−11568.

2620 Sun, W., Pashaie, B.J., Dhali, S.K., Honea, F.I., 1996. Non-thermal plasma remediation of SO_2/NO using a dielectric-barrier

2621 discharge. J. Appl. Phys. 79,3438–3445.

2622 Suriyawong, A., Smallwood, M., Li, Y., Zhuang, Y., Biswas, P., 2009. Mercury Capture by Nano-structured Titanium Dioxide

2623 Sorbent during Coal Combustion, Lab-scale to Pilot-scale Studies. Aerosol Air Qual Res. 9,394–403.

2624 Seery, M.K., George, R., Floris, P., Pillai, S.C., 2007. Silver-doped titanium dioxide nanomaterials for enhanced visible light

2625 photocatalysis. J. Photochem. Photobiol. A 189,258−263.

2626 Sui, R., Young, J.L., Berlinguette, C.P., 2010. Sol-gel synthesis of linear Sn-doped TiO_2 nanostructures. J. Mater. Chem. 20,

2627 498−503.

2628 Stengl, V., Bakardjieva, S., Murafa, N., 2009 Preparation and photocatalytic activity of rare earth-doped TiO_2 nanoparticles. Mater.

2629 Chem. Phys. 114,217−226.

2630 Shi, J.W., Zheng, J.T., Wu, P., 2009. Preparation, characterization and photocatalytic activities of holmium-doped titanium dioxide

2631 nanoparticles. J. Hazard. Mater. 161,416−422.

2632 Sun, L., Li, J., Wang, C.L., Li, S.F., Chen, H.B., Lin, C.J., 2009. An electrochemical strategy of doping Fe^{3+} into TiO_2 nanotube

2633 array films for enhancement in photocatalytic activity. Sol. Energy Mater. Sol. Cells 93,1875−1880.

2634 Shang, J., Yao, W., Zhu, Y., Wu, N., 2004. Structure and photocatalytic performance of glass/SnO_2/TiO_2 interface composite film.

2635 Appl. Catal. A 257,25−32.

2636 Snider, G., Ariya, P., 2010. Photo-catalytic oxidation reaction of gaseous mercury over titanium dioxide nanoparticle surfaces. Chem.

2637 Phy. Lett. 491,23–28.

2638 Snider, G., Ariya, P., 2012. Kinetic and Product Studies of the Reactions of NO_2, with Hg^0 in the Gas Phase in the Presence of

2639 Titania Micro-Particle Surfaces. Water Air Soil Pollut. 223,4397–4406.

2640 Matsuda, S.; Hatano, H., 2005. Photocatalytic removal of NO_x in a circulating fluidized bed system. Powder Technol.

2641 1–3,61–67.

2642 Sommar, J., Katarina, G., Feng, X.B., 2001. A kinetic study of the gas-phase reaction between the hydroxyl radical and atomic

2643 mercury. Atmosp. Environ. 35,3049–3054.

2644 Scala, F., 2001. Simulation of Mercury Capture by Activated Carbon Injection in Incinerator Flue Gas. 1. In-Duct Removal. Environ.

2645 Sci. Technol. 35, 4367–4372

2646 Sun, W.Y., Wang, Q.Y., Ding, S.L., Su, S.J., 2013. Simultaneous absorption of SO_2 and NO_x with pyrolusite slurry combined with

gas-phase oxidation of NO using ozone, Effect of molar ratio of $O_2/(SO_2 + 0.5NO_x)$ in flue gas. Chem. Eng. J. 228,700–707.

Sun, W.Y., Ding, S.L., Zeng, S.S., Su, S.J., Jiang, W.J., 2011. Simultaneous absorption of NO_x and SO_2 from flue gas with pyrolusite slurry combined with gas-phase oxidation of NO using ozone. J. Hazard. Mater. 192,124–130.

Song, S., He, Z.Q., Chen, J.M., 2007. US/O_3 combination degradation of aniline in aqueous solution. Ultrason. Sonochem. 14,84–88.

Shen, H.Z., Ie, I.R., Yuan, C.S., Hung, C.H., 2016. The enhancement of photo-oxidation efficiency of elemental mercuryby immobilized WO_3/TiO_2 at high temperatures. Applied Catalysis B: Environmental 195, 90–103.

Tan, Z.Q., Sun, L.S., Xiang, J., Zeng, H.C., Liu, Z.H., Hu, S., Qiu, J.R., 2012. Gas-phase elemental mercury removal by novel carbon-based sorbents. Carbon 50,362–371.

Tan, Z.Q., Qiu, J.R., Zeng, H.C., Liu, H., Xiang, J., 2011. Removal of elemental mercury by bamboo charcoal impregnated with H_2O_2. Fuel 90,1471–1475.

Tan, Z.Q., Liu, H., Qiu, J.R., Zeng, H.C., Liu, Z.H., 2010. Preparation of Elm Char/Nano-TiO_2 Photocatalyst and Experimental Studies on the Removal of Elemental Mercury. Proceedings of the CSEE. 29,37–41.

Tisa, F., Raman, A.A.A., Daud, W.M.A.W., 2014. Applicability of fluidized bed reactor in recalcitrant compound degradation through advanced oxidation processes, A review. J. Environ. Manage. 146,60–275.

Tokumura, M., Wada, Y., Usami, Y., Yamaki, T., Mizukoshi, A., Noguchi, M., Yanagisawa, Y., 2012. Method of removal of volatile organic compounds by using wet scrubber coupled with photo-Fenton reaction–Preventing emission of by-products. Chemosphere 10,1238–1242.

Tendero, C., Tixier, C., Tristant, P., Desmaison, J., Leprince, P., 2006. Atmospheric pressure plasmas, A review. Spectrochim. Acta B 61,2–30.

Tas, M.A., Hardeveld, R.V., Veldhuizen, E.M.V., 1997. Reactions of NO in a Positive Streamer Corona Plasma. Plasma Chem. Plasma Process 4,371–391.

Takaki K, Jani, M.A., Fujiwara, T., 1999. Removal of nitric oxide in flue gases by multi-point to plane dielectric barrier discharge.

Plasma Sci. IEEE Transaction 6,1716–1723.

Tang, P., Zhu, T.L., Li, H., Luo, H.J., Li, J., 2008. Effects of Gas Compositions on the Oxidation of Gas Phase Elementary Mercury by Non- thermal Plasma. Environ. Sci. 6,1749–1753.

Thiruvenkatachari, R., Vigneswaran, S., Moon, S., 2008. A review on UV/TiO_2 photocatalytic oxidation process. Korean J. Chem. Eng. 25,64–72.

Tsai, C.Y., His, H.C., Bai, H., Fan, K.S., Chen, C., 2011. TiO_{2-x} nanoparticles synthesized using He/Ar thermal plasma and their effectiveness on low-concentration mercury vapor removal. J. Nanopart. Res. 2011, DOI 10.1007/s11051-011-0442-8.

Tsai, C.Y., His, H.C., Kuo, T.H., Chang, Y.M., Liou, J.H., 2013. Preparation of Cu-Doped TiO_2 Photocatalyst with Thermal Plasma Torch for Low-Concentration Mercury Removal. Aerosol Air Qual Res.13,639–648.

Tsai, C.Y., Kuo, T.H., His, H.C., 2012. Fabrication of Al-Doped TiO_2 Visible-Light Photocatalyst for Low-Concentration Mercury Removal. Int. J. Photoenergy 12,1–8.

Todorova, N., Giannakopoulou, T., Karapati, S., Petridis, D., Vaimakis, T., Trapalis, C., 2014. Composite TiO_2/clays materials for photocatalytic NO_x oxidation. App. Surf. Sci. 319,113–120.

Tokumura, M., Wada, Y., Usami, Y., Yamaki, T., Mizukoshi, A., 2012. Method of removal of volatile organic compounds by using wet scrubber coupled with photo-Fenton reaction-Preventing emission of by-products. Chemosphere 89,1238–1242.

Tony, M.A., Zhao, Y.Q., Taye, A.M.,2009. Exploitation of Fenton and Fenton-like reagents as alternative conditioners for alum sludge conditioning. J. Environ. Sci. 1,101–105.

Tan, Y.W., Lu, D., Anthony, E.J., Dureau, R., Mortazavi, R., Douglas, M.A., 2007. Mercury removal from coal combustion by Fenton reactions. Paper B, Pilot-scale tests. Fuel 86,2798–2805.

Tan, C.Q., Gao, N.Y., Deng, Y., Rong, W.L., Zhou, S.D., 2013. Degradation of antipyrine by heat activated persulfate. Sep. Purif. Technol. 109,122–128.

Urashima, K., Chang, J.S., 2000. Removal of volatile organic compounds from air streams and industrial flue gases by non-thermal

plasma technology. IEEE T Dielect El In. 5, 602–614.

Urabe, T., Wu, Y., Nagawa, T., 1998. Study on Hg, NO_x, SO_x behavior in municipal refuse incinerator furnace and removal of those by pulse corona discharge. Seiso. Giho. 13,12–29.

Umebayashi, T., Yamaki, T., Itoh, H., Asai, K., 2002. Analysis of electronic structures of 3d transition metal-doped TiO_2 based on band calculations. J. Phys. Chem. Solids 63,1909−1920.

Umebayashi, T., Yamaki, T., Tanaka, S., Asai, K., 2003. Visible light induced degradation of methylene blue on S-doped TiO_2. Chem. Lett. 32, 330−331.

Usman, M., Faure, P., Ruby, C., Hann, K., 2012. Application of magnetite-activated persulfate oxidation for the degradation of PAHs in contaminated soils. Chemosphere 87,234–240.

Umar, M., Roddick, F., Fan, L.H., Aziz, H.A., 2013. Application of ozone for the removal of bisphenol A from water and wastewater–A review. Chemosphere 90, 2197–2207.

Vaart, R.V.D., Akkerhuis, J., Feron, P., Jansen, B., 2001. Removal of mercury from gas streams by oxidative membrane gas absorption. J. Membrane Sci. 187,151–157.

Vallejo, M., Román, M.F.S., Ortiz, I., Irabien, A., 2015. Overview of the PCDD/Fs degradation potential and formation risk in the application of advanced oxidation processes (AOPs) to wastewater treatment. Chemosphere 118,44–56.

Wang, P.Y., Su, S., Xiang, J., You, H.W., Cao, F., Sun, L.S., Hu, S., Zhang, Y., 2014a. Catalytic oxidation of Hg^0 by MnOx–CeO_2/γ-Al_2O_3 catalyst at low temperatures. Chemosphere 101,49–54.

Wiatros-Motyka, M.M., Sun, C.G., Stevens, L.A., Snape, C.E., 2013. High capacity co-precipitated manganese oxides sorbents for oxidative mercury capture. Fuel 109,559–562.

Wang, Z.H., Jiang, S.D., Zhu, Y.Q., Zhou, J.S., Zhou, J.H., Li, Z.S., Cen, K.F., 2010. Investigation on elemental mercury oxidation mechanism by non-thermal plasma treatment. Fuel Process. Technol. 91,1395–1400.

Wang, Z.H., Zhou, J.H., Zhu, Y.Q., Wen, Z.H., 2007. Simultaneous Removal of NO_x, SO_2 and Hg in Nitrogen Flow in a Narrow

2713 Reactor by Ozone Injection, Experimental Results. Fuel Process Technol. 88,817–823.

2714 Wilcox, J., Rupp, E., Ying, S.C., Lim, D.H., 2011. Negreira AS. Mercury adsorption and oxidation in coal combustion and

2715 gasification processes. Int. J. Coal Geol. 90–91,4–20.

2716 Wols, B.A., Hofman-Caris, C.H.M., 2012. Review of photochemical reaction constants of organic micropollutants required for UV

2717 advanced oxidation processes in water. Water Res. 46,2815–2827.

2718 Wang, M.Y., Zhu, T.L., Luo, H.J., Tang, P., Li, H., 2009. Oxidation of gaseous elemental mercury in a high voltage discharge reactor.

2719 J. Environ. Sci. 21,1652–1657.

2720 Wang, M.Y., Zhu, T.L., Luo, H.J., Wang, H., Fan, W.Y., 2011. Effects of Reaction Conditions on Elemental Mercury Oxidation in

2721 Simulated Flue Gas by DC Nonthermal Plasma. Ind. Eng. Chem. Res. 50,5914–5919

2722 Wang, N.N., Zheng, T., Zhang, G.S., Wang, P., 2016. A review on Fenton-like processes for organic wastewater treatment. J.

2723 Environ.Chem. Eng. 1, 762–787.

2724 Wu, Y., 1996. Experimental study of mercury vapor removal using pulse discharge method. J. Environ. Sci. 2, 221–225.

2725 Wu, Z.L., 2006.Study on removal mechanism of multi-pollutants in flue gas using DC corona radical shower. Hang Zhou, Zhejiang

2726 University.

2727 Wu, C.Y., Lee, T.G., Tyree, G., Arar, E., Biswas, P., 1998. Capture of Mercury in Combustion Systems by In Situ-Generated Titania

2728 Particles with UV Irradiation. Environ. Eng. Sci. 15,137–148.

2729 Worathanakul, P., Kongkachuichay, P., Noel, J.D., Suriyawong, A., Giammar, D.E., Biswas, P., 2008. Evaluation of Nanostructured

2730 Sorbents in Differential Bed Reactors for Elemental Mercury Capture. Environ. Eng. Sci. 7,1061–1070.

2731 Wang, H.Q., Zhou, S.Y., Xiao, L., Wang, Y.J., Liu, Y., Wu, Z.B., 2011. Titania nanotubes-A unique photocatalyst and adsorbent for

2732 elemental mercury removal. Catal. Today 175,202–208.

2733 Wang, X., Wang, L.G., Li, J.B., Qiu, J.J., Cai, C., Zhang, H., 2014b. Degradation of Acid Orange 7 by persulfate activated with zero

2734 valent iron in the presence of ultrasonic irradiation. Sep. Purif. Technol.122,41–46.

Wang, C.W., Liang, C.J., 2014c. Oxidative degradation of TMAH solution with UV persulfate activation. Chem. Eng. J. 254, 472–478.

Wang, Z.H., 2005. Mechanism study on multi-pollution control simultaneously during coal combustion and direct numerical simulation of reaction jets flow. Hangzhou, Zhejiang University.

Wang, Z.H., Zhou, J.L., Zhu, Y.Q., Wen, Z.C., Liu, J.Z., Cen, K.F., 2007. Simultaneous removal of NO_x, SO_2 and Hg in nitrogen flow in a narrow reactor by ozone injection, Experimental results. Fuel Process. Technol. 88, 817–823.

Wen, Z.C., Wang, Z.H., Yang, W.J., Zhou, J.H., Cen, K.F., 2009. Mechanism investigation on oxidization of Hg^0 by ozone in flue gas. J Zhejiang University (Eng Sci) 9,1626–1631.

Wen, Z.C., Zhou, J.H., Wang, Z.H., Cen, K.F., 2008. Quantum Chemical Study on Elemental Mercury Oxidation in Flue Gases by Ozone. J. Combust. Sci. Technol. 5,417–422.

Wu, J., Li, C., Zhao, X., Wu, Q.; Qi, X.M., Chen, X.T., Hu, T., Cao, Y., 2015a. Photocatalytic oxidation of gas-phase Hg^0 by CuO/TiO_2. Applied Catalysis B: Environmental 176–177, 559–569.

Wu, J., Li, X., Ren, J.X., Qi, X. M., 2015b. Experimental study of TiO_2 hollow microspheres removal on elemental mercury in simulated flue gas. Journal of Industrial and Engineering Chemistry 32, 49–57.

Xu, W.Q., Wang, H.R., Zhou, X., Zhu, T.Y., 2014. CuO/TiO_2 catalysts for gas-phase Hg^0 catalytic oxidation. Chem. Eng. J. 243, 380–385.

Xu, Y.L., Zhong, Q., Liu, X.Y., 2015. Elemental mercury oxidation and adsorption on magnesite powdermodified by Mn at low temperature. J. Hazard. Mater. 283,252–259.

Xu, X.H., Ye, Q.F., Tang, T.M., Wang, D.H., 2008. Hg^0 oxidative absorption by $K_2S_2O_8$ solution catalyzed by Ag^+ and Cu^{2+}. J. Hazard. Mater. 158,410–416.

Xu, J.H., Li, C.L., Liu, P., He, D., Wang, J.F., Zhang, Q., 2014. Photolysis of low concentration H_2S under UV/VUV irradiation emitted from high frequency discharge electrodeless lamps. Chemosphere 109,202–207.

Xu, F., Luo, Z.Y., Cao, W., Wang, P., Wei, B., Gao, X., 2009. Simultaneous oxidation of NO, SO_2 and Hg^0 from flue gas by pulsed corona discharge. J. Environ. Sci. 3,328–332.

Yang, S.J., Yan, N.Q., Guo, Y.F., Wu, D.Q., He, H.P., Qu, Z., Li, J.F., Zhou, Q., Jia, J.P., 2011. Gaseous Elemental Mercury Capture from Flue Gas Using Magnetic Nanosized $(Fe_3\text{-}xMn_x)1\text{-}\delta O_4$. Environ. Sci. Technol. 45,1540–1546.

Yang, H.Q., Xu, Z.H., Fan, M.H., Bland, A.E., Judkins, R.R., 2007. Adsorbents for capturing mercury in coal-fired boiler flue gas. J. Hazard. Mater.146,1–11.

Yu, Y., Zhang, T.T., Zheng, L.Q., Yu, J., 2013. Photocatalytic degradation of hydrogen sulfide using TiO_2 film under microwave electrodeless discharge lamp irradiation. Chem. Eng. J. 1,9–15.

Ye, J.H., Shang, J., Li, Q., Xu, W.W., Liu, J., Feng, X., Zhu, T., 2014. The use of vacuum ultraviolet irradiation to oxidize SO_2 and NO_x for simultaneous desulfurization and denitrification. J. Hazard. Mater.30,89–97.

Yan, K., Kanazawa, S., Ohkubo, T., Nomoto, Y., 1999. Oxidation and Reduction Processes During NO_x Removal with Corona-Induced Nonthermal Plasma. Plasma Chem. Plasma Process 3,421–443.

Yoshida, K., Yamamoto, T., Kuroki, T., Okubo, M., 2009. Pilot-Scale Experiment for Simultaneous Dioxin and NO_x Removal from Garbage Incinerator Emissions Using the Pulse Corona Induced Plasma Chemical Process. Plasma Chem. Plasma Process 5,373–386.

Yang, H.M., Hou, W.H., Zhang, H.R., Zhou, L.Y., 2012a. Oxidation of Elemental Mercury with Non-Thermal Plasma Coupled with Photocatalyst. J. Adv. Oxid. Technol. 2,321–327.

Yang, H.M., Liu, H., Wu, H., Wang, M., 2012b. Photochemical Removal of Gaseous Elemental Mercury in a Dielectric Barrier Discharge Plasma Reactor. Plasma Chem. Plasma Process 32,969–977.

Yuan, Y., Zhao, Y.C., Zhang, J.Y., Wang, Y.X., Chen, Y.M., Zheng, C.G., 2011. Study on Photocatalytic Experiments of Desulfurization, Denitrification and Mercury Removal Using a TiO_2-aluminum Silicate Fiber Nanocomposite. Proceedings of the CSEE 11,79–85.

Yuan, Y., Zhang, J.Y., Zhao, Y.C., Wang, Y.X, Zheng, C.G., 2012a. Effects of SO_2 and NO on removal of elemental mercury using a TiO_2-aluminum silicate fiber. J. Fuel Chem. Technol. 5,630–635.

Yuan, Y., Zhang, J.J., Fan, G.X., Zhao, Y.C., Zheng, C.G., 2012b. Electrospun TiO_2-WO_3 Nanofibers for Photocatalytic Removal of Mercury. Proceedings of the CSEE 32,44–49.

Yuan, Y., Zhao, Y.C., Li, H.L., Gao, X., Zheng, C.G., Zhang, J.Y., 2012c. Electrospun metal oxide-TiO_2 nanofibers for elemental mercury removal from flue gas. J. Hazard. Mater. 227–228,427– 435.

Yuan, Y., 2012d. Removal of multiple pollutants from coal combustion flue gas over novel TiO_2-based nanomaterials. Wu Han, Huazhong University of Science and Technology.

Yuan, Y., Zhang, J.Y., Li, H.L., Li, Y., Zhao, Y.C., 2012e. Simultaneous removal of SO_2, NO and mercury using TiO_2-aluminum silicate fiber by photocatalysis. Chem. Eng. J. 192,21–28.

Ye, Q.F., 2006. Gaseous Mercury Absorption from Simulated Flue Gas. Hangzhou, Zhejiang university.

Yan, J.C., Han, L., Gao, W.G., Xue, S., Chen, M.F., 2015. Biochar supported nanoscale zerovalent iron composite used as persulfate activator for removing trichloroethylene. Bioresource Technol. 175,269–274.

Yang, S.Y., Yang, X., Shao, X.T., Niu, R., Wang, L.L., 2011. Activated carbon catalyzed persulfate oxidation of Azo dye acid orange 7 at ambient temperature. J. Hazard. Mater. 186,659–666.

Zheng, Y.J., Jensen, A.D., Windelin, C., Jensen, F., 2012. Dynamic measurement of mercury adsorption and oxidation on activated carbon in simulated cement kiln flue gas. Fuel 93,649–657.

Zhao, P.F., Guo, X., Zheng, C.G., 2010. Removal of elemental mercury by iodine-modified rice husk ash sorbents. J. Environ. Sci. 22,1629–1636.

Zhao, B., Liu, X.W., Zhou, Z.J., Shao, H.Z., Wang, C., Si, J.P., Xu, M.H., 2014a. Effect of molybdenum on mercury oxidized by V_2O_5–MoO_3/TiO_2 catalysts. Chem. Eng. J. 253,508–517.

Zhang, A,C,, Zheng, W.W., Song, J., Hu, S., Liu, Z.C., Xiang, J.,2014a. Cobalt manganese oxides modified titania catalysts for

oxidation of elemental mercury at low flue gas temperature. Chem. Eng. J. 236,29–38.

Zhang, B.K., Liu, J., Zheng, C.G., Chang, M., 2014b. Theoretical study of mercury species adsorption mechanism on MnO_2(110) surface. Chem. Eng. J. 256,93–100.

Zhou, S.Y., 2011. Adsorption-Photocatalytic Oxidation performance of TiO_2 based nanotubes in elemental mercury removal. HangZhou, Zhejiang University.

Zhao, Y., Hao, R.L., Zhang, P., Zhou, S.H., 2014b. An integrative process for Hg^0 removal using vaporized $H_2O_2/Na_2S_2O_8$. Fuel 136,113–121.

Zhao, Y., Hao, R.L., Guo, Q., 2014c. A novel pre-oxidation method for elemental mercury removalutilizing a complex vaporized absorbent. J. Hazard. Mater. 280,118–126.

Zhao, Y., Xue, F.M., Zhao, X.C., Guo, T.X., Li, X.L., 2013a. Experimental study on elemental mercury removal by diperiodatonickelate (IV) solution. J. Hazard. Mater. 260,383–388.

Zhao, Y., Xue, F.M., Ma, T.Z., 2013b. Experimental study on Hg^0 removal by diperiodatocuprate (III) coordination ion solution. Fuel Process. Technol. 106,468–47.

Zheng, Y.J., Jensen, A.D., Windelin, C., Jensen, F., 2012. Review of technologies for mercury removal from flue gas from cement production processes. Prog. Energ. Combust. 5,599–629.

Zhong, Y., 2008. Experimental and theory study on synergy removal of sulfur, nitrogen, mercury contaminants using WFGD system. Hang Zhou, Zhejiang University.

Zhao, Y., Chen, Z.Y., Wang, L.D., Zhang, S.W., 2008. Study on simultaneous removal of SO_2 and Hg in wet flue gas desulfurization. 1, 64–68.

Zhao, Y., Wen, X.Y., Guo, T.X., Zhou, J.H., 2014d. Desulfurization and denitrogenation from flue gas using Fenton reagent. Fuel Process. Technol. 128,54–60.

Zhou, Q., 2013. The research of reactor structural optimization as well as influence of power parameters and gas conditions on

plasma denitrification. Wu Han, Wuhan Textile University.

Zhou, L.M., Wang, Y.P., Huang, Q.W., Liu, Z.R., 2008. Preparation and visible light activity of silver, sulfur, and carbon co-doped nano-TiO_2. Semiconduct. Optoelect 29,365−369.

Zhuang, Z.K., Yang, Z.M., Zhou, S.Y., Wang, H.Q., Sun, C.L, Wu, Z.B., 2014. Synergistic photocatalytic oxidation and adsorption of elemental mercury by carbon modified titanium dioxide nanotubes under visible light LED irradiation. Chem. Eng. J. 253,16–23.

Zhang, D., Zeng. F., 2011a. Photocatalytic oxidation of organic dyes with visible light driven codoped TiO_2 photocatalysts. Russ. J. Phys. Chem. A 85,1077−1083.

Zhang, H.; Chen, G.; Behnemann, D. W., 2009. Photo-electrocatalytic materials for environmental applications. J. Mater. Chem. 19, 5089−5121.

Zhao, Y., Zhao, L., Han, J., Xu, Y.Y., Wang, S.Q., 2008. Study on method and mechanism for simultaneous desulfurization and denitrification of flue gas based on the TiO_2 photocatalysis. Sci. China Ser. E 3,268–276.

Zuo, G.M., Cheng, Z.X., Chen, H., Li, G.W., Miao, T., 2006. Study on photocatalytic degradation of several volatile organic compounds. J. Hazard. Mater. 2–3,158–163.

Zhan, F., Li, C.T., Zeng, G.M., Tao, S.S., Xiao, Y.J., 2013. Experimental study on oxidation of elemental mercury by UV/Fenton system. Chem. Eng. J. 232,81–88.

Zhang, J., Liu, Y.X., Sheng, C.D., 2011b. An integrated flue gas purification system basing on heterogeneous UV/Fenton-like. China Patent, CN201110045887.

Zhao, Y., Hao, R.L., 2014d. Macrokinetics of Hg^0 Removal by a Vaporized Multicomponent Oxidant. Ind. Eng. Chem. Res. 53,10899−10905.

Zhang, C. F., 1985. Gas-Liquid Reaction and Reactor. Beijing, Chemical Industry Press.

Zhu, K.H., 2003. Analysis introduction of industry reaction process. Beijing, China Petrochemical Press, 2003.

Zhuang, Y., 2011. Martin, C., Pavlisha, J., Botha, F., 2011. Cobenefit of SO_3 reduction on mercury capture with activated carbon in coal flue gas. Fuel 90,2998–3006.

Zhou C.S., Sun, L.S., Zhang, A.C., Wu, X.F., Ma, C., Su, S., 2015a. $Fe_{3-x}Cu_xO_4$ as highly active heterogeneous Fenton-like catalysts toward elemental mercury removal. Chemosphere 125, 16–24.

Zhou, C.S., Wang, B., Ma, C., Song, Z.J., Zeng, Z., Xiang, J., Hu, S., Su, S., Sun, L.S., 2015b. Gaseous elemental mercury removal through heterogeneous Fenton-like processes using novel magnetically separable $Cu_{0.3}Fe_{2.7-x}Ti_xO_4$ catalysts. Fuel 161, 254–261.

Zhou, C.S., Sun, L.S., Zhang, A.C., Ma, C., 2015c. Elemental mercury (Hg^0) removal from containing SO_2/NO flue gas by magnetically separable $Fe_{2.45}Ti_{0.55}O_4/H_2O_2$ advanced oxidation processes. Chemical Engineering Journal 273, 381–389.